Report: Project Fi 441/10-1 and 10-2
DFG/BMZ Program

Prof. Mohamed Belhaq & Prof. Bernold Fiedler

18. Februar, 2008

Contents

1 Allgemeine Angaben

1.1 Antragsteller

DFG/GTZ

- a)Dieses Projekt Fi 441/10-2
- b)Voriges Projekt Fi 441/10-1
- c)Vorbereitungsreise 445 MAR-111/2/00

Prof. Dr. Bernold Fiedler
Universitätprofessor, C4
Geb. 15.05.1956, Deutsch

Institut für Mathematik I
FU Berlin
Arnimallee 2-6
D- 14 195 Berlin

Tel: 030-838 75 411
Fax: 030-838 75 409
Email: fiedler@math.fu-berlin.de

Oeynhauser Str. 4
D- 14 199 Berlin
Tel: 030-823 9814
Fax: 030-8972 3242

Prof. Dr. Mohamed Belhaq
University Hassan II, Ain Chock
Laboratory of Mechanics, Faculty of Sciences
BP. 5366 Maârif, Casablanca, Morocco
Tel: +212 22 230682/84
Fax: +212 22 230674
Email : mbelhaq@hotmail.com

Hay Lissasfa, Lot Al Khawarizmy, N31
Casablanca, Morocco

Tel: +212 64821885
Fax: +212 22 230674

1.2 Thema

Nonlinear Dissipative Vibrations: Rational Suppression of Chaos and Stabilization

1.3 Kennwort

Nonlinear Dissipative Vibrations

1.4 Fachgebiet und Arbeitsrichtung

Mathematics and Mechanics, Nonlinear Dynamics

1.5 Gesamtdauer

June 2002 - December 2007

1.6 Berichtszeitraum

June 2002 - December 2007

1.7 Förderungsbeginn

June 2002

1.8 Publikationen des Projekts

1.8.1 Wissenschaftliche Zeitschriften

1. K. Guennoun, M. Houssni and M. Belhaq "Quasi-periodic solutions and stability for a weakly damped nonlinear quasi-periodic Mathieu equation", Nonlinear Dynamics, Vol. 27(3), p. 211-236 (2002).

2. M. Belhaq, K. Guennoun and M. Houssni "Asymptotic solutions for a damped non-linear quasi-periodic Mathieu equation", Int. J. of Non-Linear Mechanics, Vol. 37(3), p. 445-460 (2002).

3. M. Belhaq and F. Lakrad "Analytic of homoclinic bifurcations in three dimensional systems", Int. J. Bifurcation and Chaos, Vol. 12 (11), p. 2479-2486 (2002).

4. F. Lakrad and M. Belhaq "Periodic solutions of strongly nonlinear oscillators" , Journal of Sound and Vibration, Vol. 258(4), p. 677-700 (2002).

5. R. Rand, K. Guennoun and M. Belhaq "2:2:1 resonance in the quasiperiodic Mathieu equation, "Nonlinear Dynamics, Vol. 31(4), p. 367-374 (2003).

6. R. Rand, K. Guennoun and M. Belhaq: "2:2:1 Resonance in the Quasiperiodic Mathieu Equation" , Proceedings of the 2003 ASME Design Engineering Technical Conferences, 19th Biennial Conference on Mechanical Vibrations and Noise, Chicago, IL, Sept. 2-6 (2003).

7. A. Azouani, M. Belhaq: "Effects of different nonlinear Parametric Resonant Perturbations on suppression of chaos", Progress in Analysis, Proceedings of the 3rd International ISAAC Congress, World Scientific, Vol. 1, p. 519-524 (2003).

8. F. Lakrad and W. Schiehlen "Effect of low frequency parametric excitation" Chaos, Solitons and Fractals 22 (2004), p. 1149-1164.

9. F. Lakrad and W. Schiehlen " Dynamical systems with slow parametric excitation", EUROMECH 452: Advances in Simulation Techniques for Applied Dynamics, March 1-4, Halle (Saale), Germany (2004).

10. F. Lakrad, M. M. Charafi "Perturbation methods and the Melnikov functions for slowly varying oscillators." Chaos, Solitons & Fractals, 25, p. 675-680 (2005).

11. F. Lakrad, M. Belhaq, "Solutions of a shallow arch under fast and slow excitation", IUTAM Symposium on Chaotic Dynamics and Control of Systems and Processes in Mechanics. (Ed. G. Rega, F. Vestroni) The Netherlands: Springer, p. 233-240 2005).

12. N. Abouhazim, M. Belhaq, F. Lakrad "Quasi-periodic solutions and bursters in a self-excited quasi-periodic Mathieu oscillator", 8^{th} Int. Conf. on Condensed Matter and Statistical Physics, September 21-24, Marrakech, Morocco (2004).

13. S. Aniss, M. Belhaq, M. Souhar and M. G. Velarde, "Effect of the surface temperature modulation on the onset of Rayleigh-Bénard convection in Hele-Shaw cell", Physica Scripta, vol. 71, p. 1-7 (2005).

14. N. Abouhazim, M. Belhaq and F. Lakrad, "Three-Period quasi-periodic oscillations in a self-excited quasi-periodic Mathieu equation", Nonlinear Dynamics, vol. 39, p. 395-409 (2005).

15. F. Lakrad, A Azouani, N. Abouhazim and M. Belhaq, "Bursters and quasi-periodic solutions of a self-excited quasi-periodic Mathieu equation", Chaos, Solitons & Fractals, vol. 24(3), p. 813-824 (2005).

16. M. Belhaq, B. Fiedler and F. Lakrad, "Experiment on nonlinear dynamics of a harmonically excited cantilever beam", Proceeding of the 7th Congress of Mechanics, pages 24-26, Casablanca, April 2005.

17. M. Belhaq , S.M. Sah, Horizontal fast excitation in delayed van der Pol oscillator, Commun Nonlinear Sci Numer Simul (2007), doi:10.1016/j.cnsns.2007.02.007

18. S.M. Sah, M. Belhaq, Effect of vertical high-frequency parametric excitation on on self-excited motion in a delayed van der Pol oscillator, Chaos, Solitons & Fractals (2006), doi:10.1016/j.chaos.2006.10.040

19. N. Abouhazim, R.H. Rand, and M. Belhaq, The Damped Nonlinear Quasiperiodic Mathieu Equation Near 2:2:1 Resonance, Nonlinear Dynamics, vol. 45, p. 237-247 (2006),

20. R. Bourkha, M. Belhaq, Effect of fast harmonic excitation on a self-excited motion in Van der Pol oscillator, Chaos, Solitons & Fractals, vol. 34, p. 621-627, (2007)

21. M. Rougui, A. Karimine, M. Belhaq, Nonlinear flexural vibration of a circular ring. A single mode approach, Chaos, Solitons & Fractals (2007), doi:10.1016/j.chaos.2006.10.006,

22. N. Abouhazim, M. Belhaq, R. H. Rand, Two models for the parametric forcing of a nonlinear oscillator , Nonlinear Dynamics 50:147-160 (2007).

23. A. Fahsi, M. Belhaq, Effect of horizontal fast harmonic excitation on frequency-locking in van der Pol-Mathieu-Duffing oscillator, Comm. Nonlinear Science Numerical Simulation, doi:10.1016/j.cnsns.2007.07.010, 2007.

24. M. Belhaq, A. Fahsi, 2:1 and 1:1 frequency-locking in fast excited van der Pol-Mathieu-Duffing oscillator, Nonlinear Dynamics, doi:10.1007/s11071-007-9302-6, 2007.

1.8.2 Dissertationen und Habilitationen

1. K. Guennoun, "Quasi-periodic solutions in a two degree of freedom model arch subjected to quasi-periodic parametric and external excitations " Ph.D. University Hassan II-Ain Chock (November 2003).

2. A. Azouani, "Suppression of chaos in an asymmetrical mechanical system and computation of Melnikov functions of second order autonomous equations" Ph.D. University Hassan II-Ain Chock (November 2004).

3. N. Abouhazim, "Three-Period quasi-periodic oscillations in a self-excited quasi-periodic Mathieu equation" Ph.D. University Hassan II-Ain Chock (November 2005).

4. R. Bourkha "Effect of fast harmonic excitation on a self-excited motion in Van der Pol oscillator" Ph.D. University Hassan II-Ain Chock (2007).

5. A. Fahsi, "Frequency-locking in the fast excited van der Pol-Mathieu-Duffing oscillator" Habilitation University Hassan II-Ain Chock (June 2008).

6. M. Hamdi "Self-excitation vibration Control for axially fast excited beam by a time delay state feedback" Ph.D. University Hassan II-Ain Chock (June 2008).

7. S.M. Sah "Effect of horizontal and vertical high-frequency parametric excitation on self-excited motion in a delayed van der Pol oscillator" Ph.D. University Hassan II-Ain Chock (Dec 2008).

2 Introduction

Physical systems are inherently nonlinear. The sources of nonlinearity may be geometric, inertial, material, damping, or a combination of them. Nonlinearities generate a whole range of nontrivial phenomena. For instance, in the case of a single degree of freedom system, we may have multiple solutions, jumps, limit cycles, subharmonic and superharmonic resonances, period-doubling bifurcations and chaos.
The behavior of continuous systems is richer since it theoretically includes the contribution of an infinite number of degrees-of-freedom. From a practical point of view, only a few number of modes contribute to the dynamics due to the existence of dissipation. Thus, in addition to the above mentioned nontrivial phenomena, the exchange of energy in the response of multi-degree-of-freedom systems can be achieved through internal resonances of the natural modes and through Hopf bifurcations of the directly excited mode. For a review, see the book by A. H. Nayfeh [*Nonlinear interactions: analytical, computational and experimental methods*, Wiley Interscience, 2000].

In what follows, we investigate experimentally and theoretically the dynamics of a cantilevered beam subject to a periodic motion of its support. The natural frequencies and modal damping are determined experimentally. Nonlinear phenomena related to a one mode model are explored. The energy exchange between the third or the fourth mode and the first mode are investigated. A theoretical model is proposed and numerical simulations are shown.

In the first part of the present project we have embarked on a careful detailed analysis of an actual vibrating block, as described in section 3, with or without the presence of magnetic fields. As we describe in the following sections, we have observed chaotic dynamic behavior which clearly and visibly involves more than one spatial mode. The third mode and the fourth mode experiment has also been investigated in a second experimental model. Furthermore, we study the flexural vibration modes of a cantilever beam governed by a one-dimensional version of the mathematical model for the linear elastic system with structural damping. We discuss the mode shapes for different values of the damping coefficient. In section 4, we present a theoretical model which describes the in-plane vibrations of a cantilevered beam subject to periodic support motions. A single mode is considered and softening effects of nonlinearities are shown through a perturbation method. Then, a multi-modes model is investigated and the transfer of energy from the third mode to the first mode is shown. In section 5, we analyze the effect of an axial rapid harmonic

forcing on the stabilization of flexible beams in a single mode approximation. In addition, we assume that the system is controlled by a proportional position feedback with a time delay. Then we examine the spectrum of natural frequencies and the stability chart of the trivial equilibrium of the structure. In the second part of this section, we study the effect of a rapid temporal excitation on the existence of periodic motions. The control with time delay is also discussed. The last part deals with the effect of rapid excitation on the frequency-locking (entrainment) area in a self-excited system. In particular, we have shown that a rapid temporal forcing can change the nonlinear characteristic stiffness of the material by shifting the behavior from hardening to softening and vice versa. This control strategy in homogenous systems can play an important role to understand the effect due to layering in materials. In section 6 we present some results on the suppression of chaos in different situations and give results on the homoclinic criterion in the case of a three-dimensional system. Section 7 presents the development relevance of the project. In the two last sections 1.8 and 1.8.2, we give the publication and the dissertation lists, respectively, of the Casablanca group since 2002.

3 Experimental work

The experimental system investigated in this research project is the cantilevered elastic beam. This system is an experimental apparatus for studying nonlinear dynamics and testing new ideas like interaction phenomena, transfer of energy from high modes to lower modes, or controlling and suppressing resonant vibrations and chaotic dynamics.
In this section the experimental set up is presented. The flexural vibrational behaviors of two types of beams are investigated. The first type is subject to the support motion and to a magnetic field effect, and the second model is softer and is subject only to the periodic base excitation.

3.1 Experimental set up

The following equipment was used to perform the modal analysis experiment

- Elastic beams mounted on a rigid support
- Two magnets
- Electromagnetic shaker
- Power amplifier

- Accelerometers
- Power supply
- Digital oscilloscope
- AC driving function generator.

These elements as well as the set-up experiment may be visualized in the following files on the CD-ROM:

- "key_elements/oscillo.JPG",
- "key_elements/power_gener.JPG",
- "key_elements/power_sup.JPG",
- "key_elements/shaker_acc.JPG",
- "key_elements/vue_exp.JPG".

For the first beam, near the free end, two magnets are used to produce a nonlinear, time independent magnetic field, alias potential, with at most two stable equilibria. The beam is subjected to the harmonic signal produced by the function generator. The signal is then amplified towards the shaker. The data are obtained using two devices: an accelerometer and an inductance coil. The digital oscilloscope records time series and Lissajous curves.
For the second beam, the experiments are done in the presence of a base displacement and in the absence of magnetic field.

3.2 First experimental model

To investigate the effect of a magnetic force and the motion of the base, we consider a steel beam with dimensions 238 mm $\times$ 10 mm $\times$ 0.5 mm and a density of $7800 kg/m^3$, (see Fig.1). Experimental investigations of the response of this beam allowed us the observation of linear and nonlinear phenomena.
In the first stage we have measured resonance frequencies corresponding to the first six resonance modes in the linear free case without the magnets. Comparisons with the analytical predictions in the undamped case were carried out, without any satisfactory agreement. For an analysis which includes damping, see section 3.2.1.

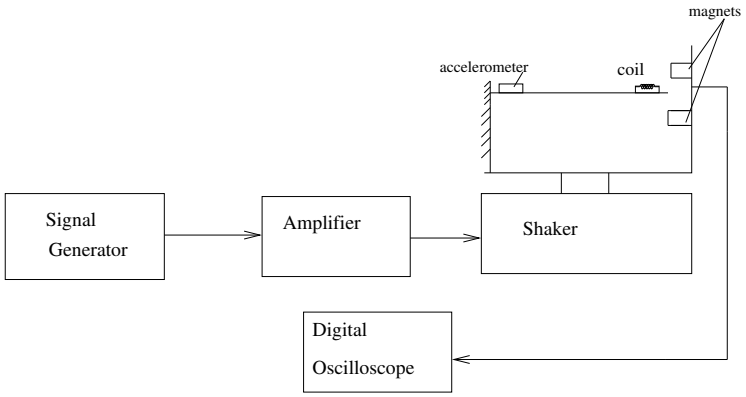

Figure 1: Experimental set-up

In the second step we have studied the response of the beam near the first and the second spatial mode. The investigation of the first mode (with the magnets) shows breather phenomena of this mode and chaotic responses of the beam; see the corresponding files in the enclosed CD-ROM:

- "mode1/breathers_plain040327.MOV",
- "mode1/chaos_ind_040331.MOV",
- "mode1/chaos_plain_030404.MOV".

For the second spatial mode, we have observed transition phenomena between the bottom, the top, and the central position; see in CD-ROM:

- "mode12/trans_bot_cent_plain030404.MOV",
- "mode12/trans_bot_top_cent_plain030404.MOV",
- "mode12/trans_bot_top_plain030404.MOV",
- "mode12/trans_top_to_cent_plain030404.MOV",
- "mode12/trans_torus_top_plain040327a.MOV",
- "mode12/trans_torus_top_plain040327b.MOV".

In other words, the beam vibrating in the second mode around the top magnet position can experience transitions to vibrations around the bottom position and around the central position between the two magnets. The transitions involve first mode components, and hence require an

ordinary differential equation analysis involving at least two degrees of freedom. We have also observed toroïdal subharmonics, chaotic motions, and bi-stability phenomena of the beam; see in CD-ROM:

- "mode12/hand_bistab_plain030404.MOV",
- "mode12/hand_chaos_plain030404.MOV".

Other observations show that in the presence of the second mode Hopf bifurcation can take place towards a periodic motion around the top magnet position, around the bottom one, or between them; see in CD-ROM:

- "mode12/Hopf_bot_plain040327.MOV",
- "mode12/Hopf_cent_plain040327a.MOV",
- "mode12/Hopf_cent_plain040327b.MOV",
- "mode12/Hopf_cent_plain040327Detail.MOV",
- "mode12/Hopf_top_plain040327.MOV".

For this phenomenon, the stable respective position of the vibrating second mode becomes unstable, and periodic oscillation set in. It was observed that the periodic motions persist when we increase the distance between the magnets by a factor three; see in CD-ROM:

- "mode12/Still_1to3_040401a.JPG",
- "mode12/Still_1to3_040401b.JPG",
- "mode12/Still_1to3_040401c.JPG",
- "mode12/Still_1to3_040401d.JPG".

A physical explanation of this phenomenon is that the amplitude of the second mode, which is being directly excited through a resonance, saturates and the extra energy that it receives is passed on to the first mode, which is indirectly excited through the second mode. This two-mode vibration corresponds to a nonlinear periodic motion of the beam. The saturation phenomenon can play a vital role to control or suppress the resonant vibrations of thin layer material elastic beam, which is of central interest in this project.

Moreover, the chaotic energy transport from higher to lower spatial modes, which we observe in the elastic beam, is just the opposite of conventional wisdom in fluid mechanics. There, the paradigm of the Kolmogorov cascade is supposed to describe energy dissipation from lower to higher frequency modes in the spatial Fourier spectra, due to turbulence. We are therefore led to speak of reverse energy cascades in the chaotic elastic beam.

Experimental observations of the excited beam with the magnets also show the existence of 1:7 sub-harmonic resonance; see in CD-ROM:

- "Subh7/Subh1to7_acc_040401a.JPG",
- "Subh7/Subh1to7_acc_040401a_detail.JPG",
- "Subh7/Subh1to7_acc_040401b.JPG",
- "Subh7/Subh1to7_acc_040401c.JPG",
- "Subh7/Subh1to7_acc_040401c_detail.JPG",

and toroïdal 1:6 and 1:7 motions of the beam; see in CD-ROM:

- "Subh6/Torus_1to6_fix_ind040330.MOV",
- "Subh6/Torus_1to6_scan_ind040330a.MOV",
- "Subh6/Torus_1to6_scan_ind040330b.MOV",
- "Subh6/Torus_1to6_scan_ind040330c.MOV",
- "Subh7/Torus_1to7_fix_blade040.MOV",
- "Subh7/Torus_1to7_scan_acc_040330a.MOV",
- "Subh7/Torus_1to7_scan_acc_040330b.MOV".

Using the coil near the free end of the beam, we have recorded resonance phenomena and two sub-harmonic resonances of the second mode around the respective magnet position, and around the central position between the magnets; see in CD-ROM:

- "mode2/res_2har_ind040330.MOV",
- "mode2/res_2har_ind040330b.MOV",

- "mode2/res_bot_ind040330.MOV",
- "mode2/res_cent_ind040330.MOV",
- "mode2/res_top_ind040330.MOV",
- "mode2/stable_top_ind040330.MOV".

3.2.1 Linear damping

For the linear damped oscillator

$$\ddot{u} + \alpha\dot{u} + \omega^2 u = 0 \tag{1}$$

the general solution is

$$u(t) = \exp\left(-\frac{\alpha}{2}t\right)\left[A\sin\left(\omega_d t\right) + B\cos\left(\omega_d t\right)\right] \tag{2}$$

where A and B are constant and $\omega_d = \sqrt{\omega^2 - (\frac{\alpha}{2})^2}$. The damped period and frequency are given by $T_d = 2\pi/\omega_d$ and $f_d = \omega_d/2\pi$.
To calculate the linear proper frequencies of the beam we can use the formula $\omega_k = n_k^2\sqrt{EI/(\rho S)}$ where $n_1\,L = 1.8751\,; n_2\,L = 4.69409\,; n_3\,L = 7.85476\,; n_4\,L = 10.9955\,; n_k\,L \approx (2k-1)\pi/2$.
In the experiment we have directly measured the damping coefficient α_k of the three first modes $k = 1, 2, 3$ of the linear beam modelled by the linear damped oscillator

$$\ddot{u} + \alpha_k\dot{u} + \omega_k^2 u = 0 \tag{3}$$

Experimentally the damping coefficients α_k were determined by the logarithmic decrement δ_k

$$\delta_k = \ln(\frac{u(t)}{u(t+T_d)}) = \frac{\alpha_k}{2}T_d \tag{4}$$

Table 1 gives experimental damping coefficients of the first three modes of flexion of the clamped/free beam.

A second approach to measure damping α_k proceeds via the expansion of solutions $u(t,x)$ into Galerkin modes $u(t,x) = \sum_{k=1}^{\infty} u_k(t)\varphi_k(x)$. Thus we obtain the linear damped pendulum equations of the form (3) above

$$\ddot{u}_k + \alpha_k\dot{u}_k + \omega_k^2 u_k = A_k\cos(\Omega t) \tag{5}$$

with $A_k = A\int_0^L \varphi_k / \int_0^L \varphi_k^2$ and undamped reference frequencies

$$\omega_k := \lambda_k^2 \tag{6}$$

Modes k	α_k test1	α_k test2	α_k test3	α_k average
1	0.001129	0.001434	0.0018	0.001454
2	0.008145	0.008106	0.008317	0.008189
3	0.0218	0.0193	0.0236	0.02156

Table 1: Experimental damping coefficients

with λ_k is a solution of

$$\cos(\lambda_k L)\cosh(\lambda_k L) + 1 = 0 \tag{7}$$

More generally, we test our measured resonance frequencies

$$\tilde{\omega}_k = \sqrt{\omega_k^2 - (\frac{\alpha_k}{2})^2} \tag{8}$$

for a power law dependence of the form

$$\alpha_k = \alpha\omega_k^\beta \tag{9}$$

See Figure 2 for a least squares log-log plot from which we derive $\beta = 1$, to whithin one per cent accuracy.

Moreover, we note that this remarkable proportionality

$$\alpha_k = \alpha\omega_k \tag{10}$$

causes all resonances frequencies ω_k of the beam to be multiplied by the *same* constant factor $\gamma < 1$. The measured frequencies $\tilde{\omega}_k$ are thus given by

$$\tilde{\omega}_k = \gamma\omega_k = \gamma\lambda_k^2 \tag{11}$$

with zeros λ_k of (7). The same multicative frequency shift can be effected by adjusting the length L of the beam, or its elasticity constant, and ignoring the obvious damping effects, altogether. Nonlinearities, however, will not forgive such sloppiness. For sample tables of $\tilde{\omega_k}/\omega_k$ see Table 2.

3.2.2 Nonlinear magnetic effects

The two magnets placed near the free end of the beam create a strong nonlinearity with respect to the distance from the magnetic pole. This nonlinear magnetic field consists of a potential with two stable equilibria producing a destabilization of the center position of the beam.

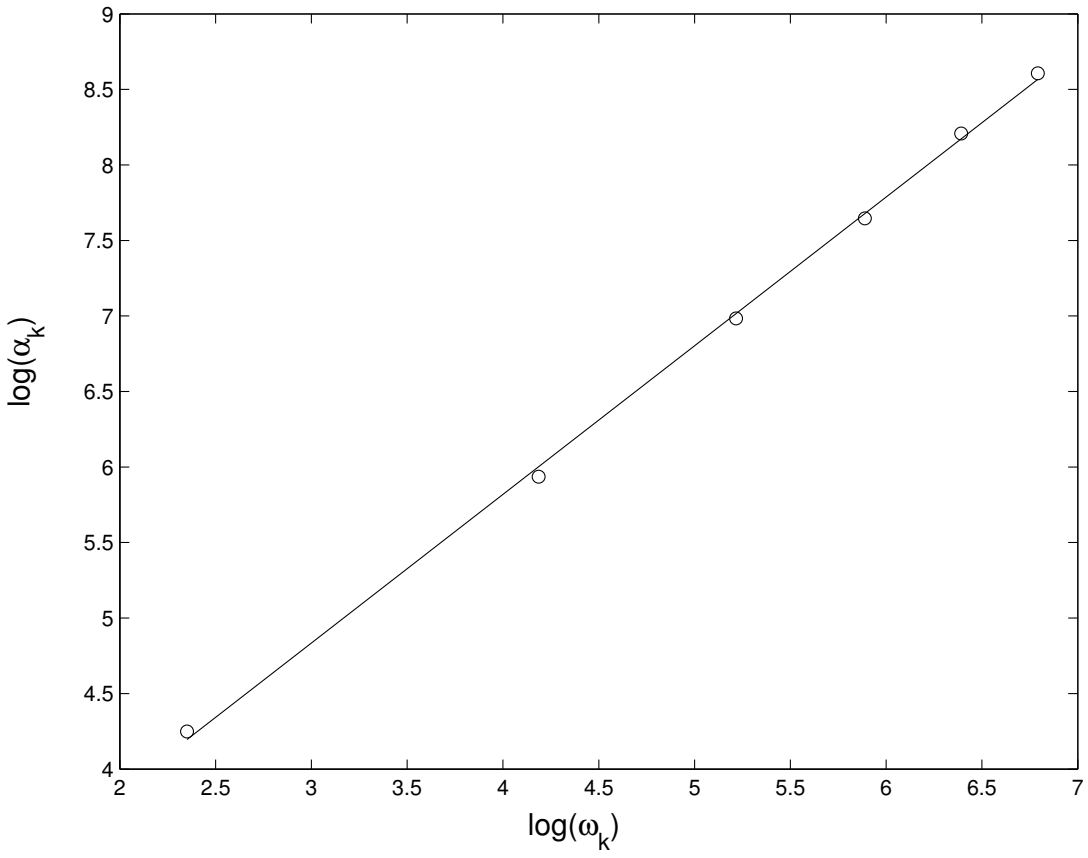

Figure 2: $\log\alpha_k$-$\log\omega_k$ plot

The interaction between elastic beam and magnetic forces usually leads to nonlinear differential equations. The harmonic external excitation together with the nonlinear magnetic field produce interaction phenomena, harmonic, subharmonic, quasiperiodic and chaotic responses of the beam. Experimental observations of the beam motion in presence of the magnetic field clearly show the existence of such responses. In section 3.2 we have discussed the interaction between the two-mode and the one-mode motions and the transfer of energy from higher to low order and shown transition phenomenon of the response between different positions of the system. A careful inspection of the beam response, using the accelerometer, allowed us the detection of 1:7 subharmonic resonance; see in CD-ROM:

- "Subh7/Subh1to7_acc_040401a.JPG",
- "Subh7/Subh1to7_acc_040401a_detail.JPG",
- "Subh7/Subh1to7_acc_040401b.JPG",

Modes	ω_k theory	$\tilde{\omega_k}$ experiment	Relative errors
mode 1	9.17	8.90	0.02
mode 2	57.5	58.5	0.017
mode 3	161	163	0.012
mode 4	315.5	320.40	0.015
mode 5	521.5	520.6	0.001

Table 2: Comparison of the frequencies of the first five modes, in Hz

- "Subh7/Subh1to7_acc_040401c.JPG",
- "Subh7/Subh1to7_acc_040401c_detail.JPG".

Another nonlinear effect observed in the experiment are Hopf bifurcations produced by the destabilization of the second mode of vibration. This destabilization produces periodic oscillations of the second mode around the three equilibria (top, center and bottom); see in CD-ROM:

- "mode12/Hopf_bot_plain040327.MOV",
- "mode12/Hopf_cent_plain040327a.MOV",
- "mode12/Hopf_cent_plain040327b.MOV",
- "mode12/Hopf_cent_plain040327Detail.MOV",
- "mode12/Hopf_top_plain040327.MOV".

Using a coil near the free end of the beam, we have observed resonance phenomena, toroïdal 1:6 response; see in CD-ROM:

- "Subh6/torus_1to6_fix_ind040330.Mov",
- "Subh6/torus_1to6_scan_ind040330a.Mov",
- "Subh6/torus_1to6_scan_ind040330b.Mov",
- "Subh6/torus_1to6_scan_ind040330c.Mov",

and chaotic response of the beam; see in CD-ROM:

- "mode1/chaos_ind_040331.MOV".

Modes	Analytical	Experimental
mode 1	4.60	4.5
mode 2	28.84	28.85
mode 3	80.76	68.95
mode 4	158.26	127
mode 5	261.62	208.4
mode 6	390.82	302.7

Table 3: The in-plane natural frequencies of the first six flexural modes. Experimental and analytical values

The difficulty to adequately model the magnetic field term from a physical point of view suggests to center interest on measuring it directly from the experiment using the acceleration component, known from the accelerometer, ω_k^2, φ_k, A_k and ω. This topic will be investigated in the future.

3.3 Second experimental model

To investigate the transfer of energy from a directly excited third-mode or fourth-mode to the first mode, we consider a steel beam with the dimensions $300mm \times 13mm \times 0.506mm$, the density and Young´s modulus of the beam are $7800Kg/m^3$ and $200GPa$, respectively.
In Table 3, the experimental and analytical values of the in-plane natural frequencies of the first six flexural modes are given. In addition, the first and the second out-of-plane (i.e. in the plane perpendicular to the plane of excitation) flexural natural frequencies of the beam were also determined using the finite element method (FEM) model and are found to be equal to 118.057 Hz and 727.65 Hz respectively. The first and the second torsional frequencies are respectively 205.719 Hz and 586.195 Hz.
The damping coefficients of the first four in-plane flexural modes are found using the logarithmic decrement method as $\xi_1 = 0.0094$, $\xi_2 = 0.0039$, $\xi_3 = 0.0017$ and $\xi_4 = 0.0035$.

3.3.1 Third-mode and fourth-mode experiments

The frequency- and force-response curves illustrate various characteristics of a nonlinear system like the presence of multiple stable response, jumps, bifurcation, type of nonlinearity (softening or hardening), etc.
For the frequency-response curve, the excitation amplitude a_b was held constant at 24 (in mV) for the third-mode and 309 (in mV) for the fourth-mode, and the excitation frequency Ω was

varied in the neighborhood of the third and the fourth natural frequency. For the force-response curve, the excitation frequency Ω was held constant at 68 Hz and 122.5 Hz, and the excitation amplitude a_b was varied between 70 mV and 200 mV, and 333 mV and 604 mV for the third- and the fourth-mode, respectively. Changes in the control parameters (excitation frequency or amplitude) were made very gradually, and, at each value of the control parameter, transients were allowed to die out before the amplitude of the response was recorded. Data are given by accelerometer placed near the clamped part of the beam. Data are given by an acceloremeter placed near the part of the beam. Data obtained from both forward and backward sweeps of the control parameter are used to plot the curves. For certain frequency ranges, a small out-of-plane motion was also observed, which seemed to increase with an increase in the amplitude of the beam response.

The frequency-response curves of the third- and the fourth-mode are shown in Fig.3. and Fig.4., respectively. They show the softening effect of the nonlinearities since the maximum response is shifted to the left with respect to the linear curves of resonances.

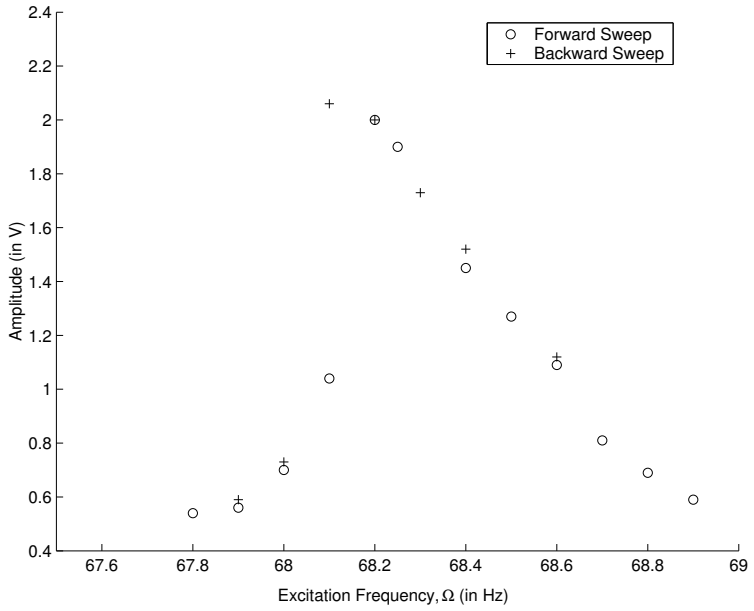

Figure 3: Frequency-response curve of the third-mode when $a_b = 24$mV

Well away from the third and the fourth natural frequencies, the only modes present in the beam responses are the third and the fourth mode. This can be easily confirmed by a visual inspection of the beam motion. As the frequency of excitation is swept downward from well above the third and the fourth natural frequencies, the third-mode and the fourth-mode responses become modulated

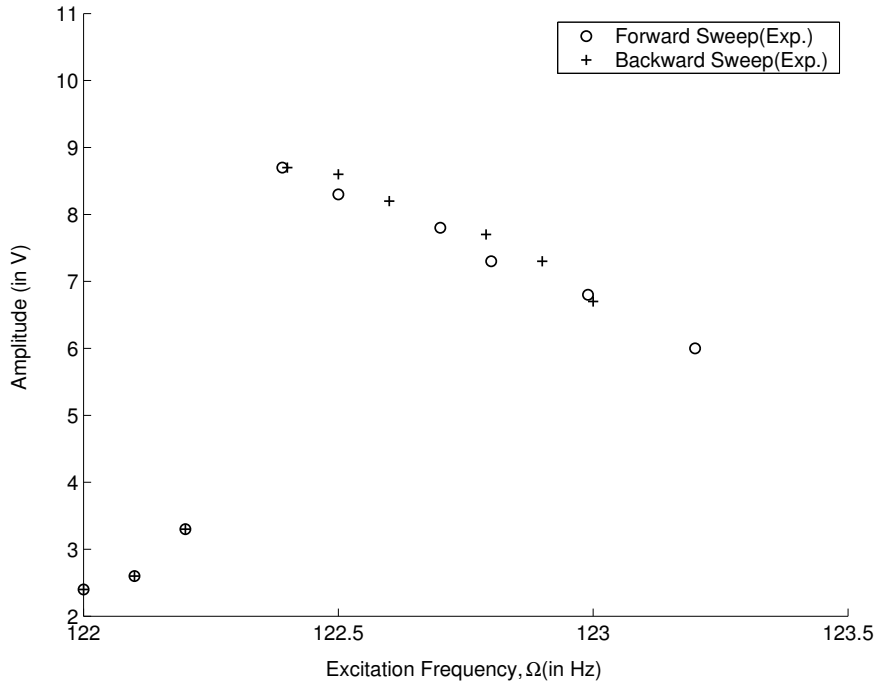

Figure 4: Frequency-response curve of the fourth-mode when $a_b = 309$mV: Experiment

and a growing contribution of the low-frequency first mode is observed; see the following files in CD-ROM:

- "mode3_4/mode3_1interaction.MOV": showing the modulation of the third-mode by the first mode. The corresponding frequency as well as the signal response are illustrated by the generator and the oscilloscope.
- "mode3_4/mode3_1birth.MOV": showing clearly the birth of this third mode and its modulation by the low-frequency first mode.
- "mode3_4/mode4_Hopf.MOV": illustrating the destabilization of the fourth-mode by a Hopf bifurcation.

These observations are the signature of energy transfer between widely spaced modes. Visually we can see the amplitude of the third-mode and the fourth-mode being modulated, along with a large swaying (i.e. the first-response). Typical responses time traces are illustrated in Fig.5 (third-mode) and Fig.6 (fourth-mode).

For $a_b = 336mV$ and $\Omega = 67.95Hz$, the modulation frequency of the third-mode and swaying amplitude increase with time and the beam response eventually gets drawn to chaotic attractor.

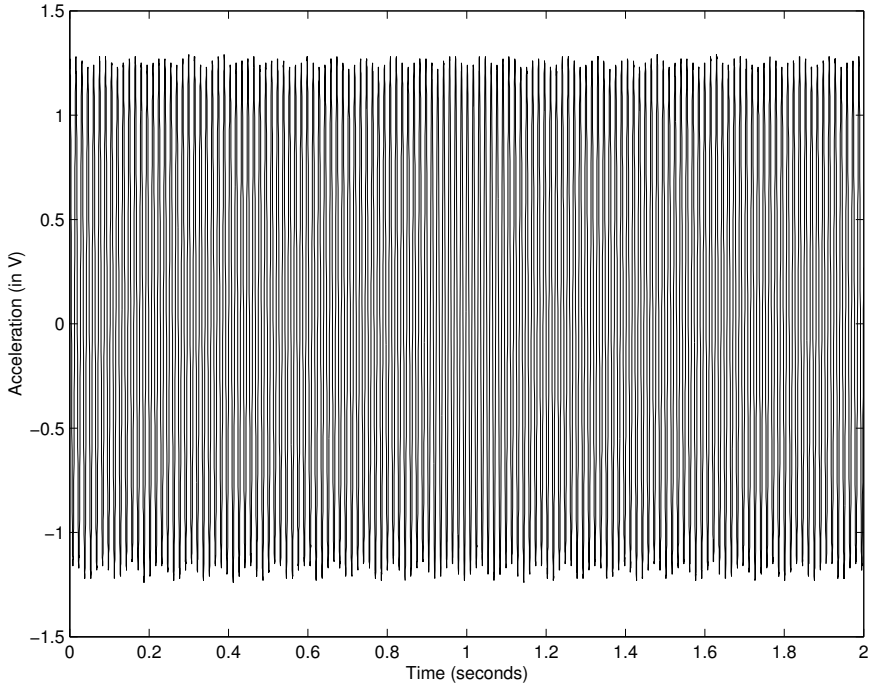

Figure 5: Response time trace for the modulated third-mode at $\Omega = 68$Hz when $a_b = 336$mV.

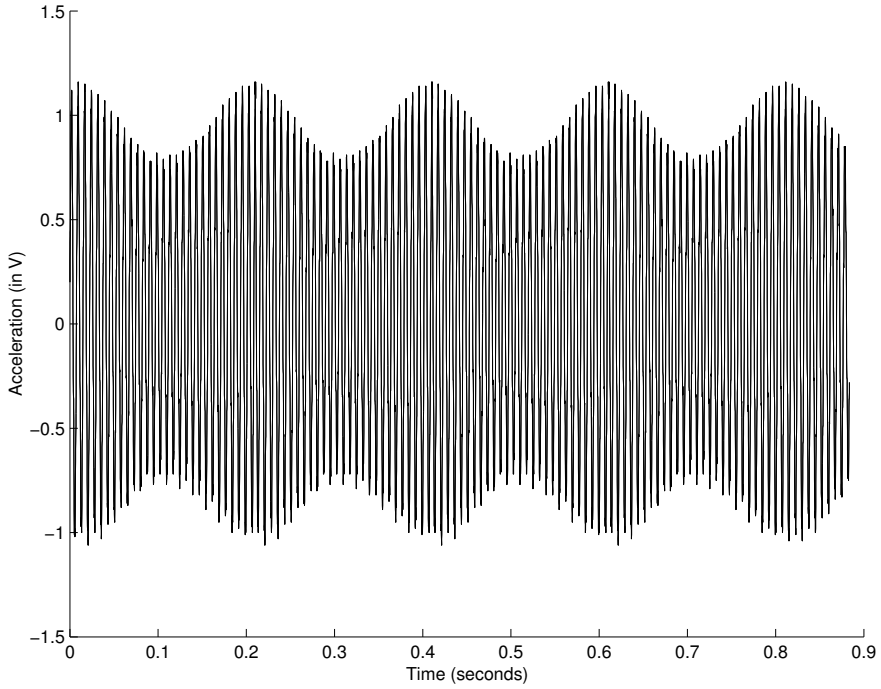

Figure 6: Response time trace for the modulated fourth-mode at $\Omega = 130$Hz when $a_b = 562$mV.

Figures 7(a) and 7(b) show the time trace of a transition to a chaotic motion and of a fully developed chaotic motion, respectively.

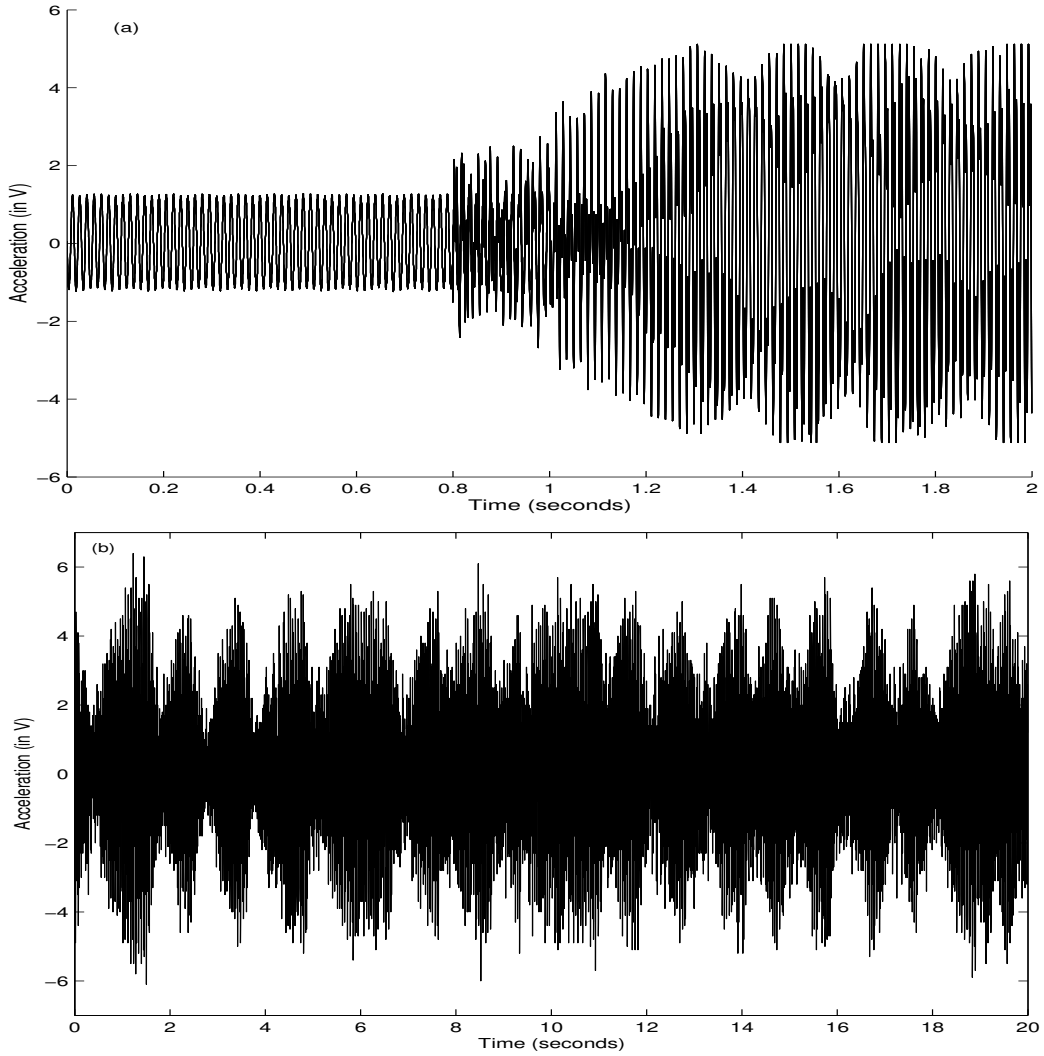

Figure 7: Response time trace for the third-mode at $\Omega = 67.95$Hz when $a_b = 336$mV.

The force-response curves of the third- and the fourth-mode are shown in Fig. 8 and Fig. 9. As the excitation amplitude is increased, the amplitude of the beam's response increases till reaching a threshold where chaotic motion appears. To study the influence of the excitation amplitude on the transfer of energy between widely spaced modes, we repeated the above experiments at higher amplitudes of excitation.

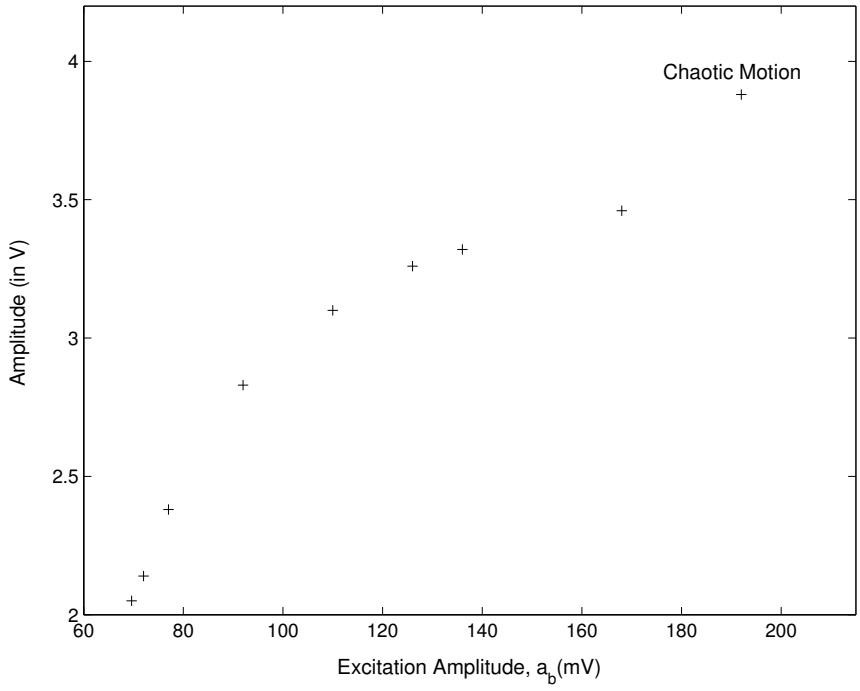

Figure 8: Force-response curve of the third-mode when $\Omega = 68$Hz

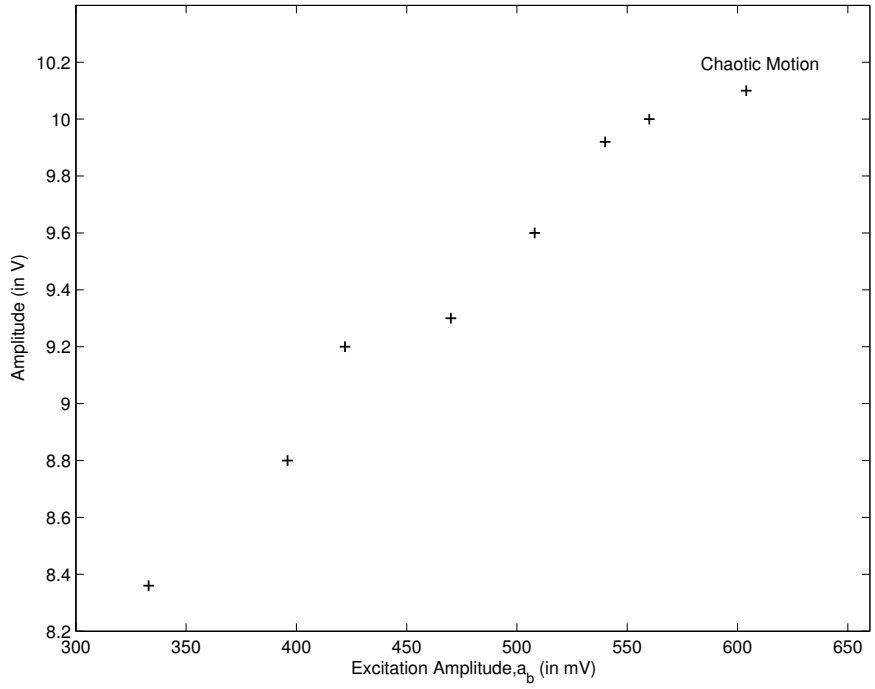

Figure 9: Frequency-response curve of the fourth-mode when $\Omega = 122.5$Hz

3.3.2 Out-of-plane mode

The first out-of-plane (i.e. in the plane perpendicular to the plane of excitation) flexural natural frequencies of the beam were also observed from experiment and is found to be equal approximately to 103 Hz; see the following files in the CD-ROM:

- "Out_of_plane/mode1_out_of_plane_a.MOV",
- "Out_of_plane/mode1_out_of_plane_b.MOV".

They show the variation of amplitude of the first flexural out-of-plane mode on the oscilloscope. The amplitude increases to a maximum and then decreases.

Other observations showed the interaction between the third-mode, the first in-plane flexural mode and the first out-of-plane flexural mode, see the following files in CD-ROM:

- "Out_of_plane/mode3_1_1out_of_plane_a.MOV", showing the interaction between the third mode and the first in-plane flexural mode,
- "Out_of_plane/mode3_1_1out_of_plane_b.MOV", illustrating the small vibrations of the out-of-plane flexural mode in the presence of the third mode, view from top.

3.4 Third model with structural damping

3.4.1 Abstract

In this part we study the flexural vibration modes of a cantilevered beam governed by the following nondimensional equation

$$v'' - \delta v'_{xx} + v_{xxxx} = 0, \tag{12}$$

with the boundary conditions

$$v(0,t) = 0, \qquad v_x(0,t) = 0, \tag{13}$$

$$v_{xx}(1,t) = 0, \qquad v_{xxx}(1,t) = \delta v'_x(1,t) \tag{14}$$

For positive δ we distinguish three regions:

- For $0 < \delta < 2$: All modes are complex. For small δ the shapes of the real part of the complex modes are similar to the modes of the undamped classical cantilevered beam. Using a least square fitting method we find that δ is proportional to the inverse of the natural frequency ω.

- For $\delta = 2$: existence of one real mode and complex modes.
- For $\delta > 2$: coexistence of complex modes and real modes.

3.4.2 Formulation of the problem

We adopt a linear constitutive relation [1] so that the shear force V is given by

$$V = EIu_{xxx} - \alpha u_{tx} \tag{15}$$

where E, I and α are Young's modulus, the moment of inertia of the cross section and viscoelastic damping coefficient respectively. The damping force is proportional to the bending rate of the beam (see Humar [3]). Thus the governing equation of motion is given by

$$mu_{tt} - \alpha u_{txx} + EIu_{xxxx} = 0, \tag{16}$$

with the boundary conditions

$$u(0,t) = 0, \qquad u_x(0,t) = 0, \tag{17}$$

$$u_{xx}(L,t) = 0, \qquad EIu_{xxx}(L,t) = \alpha \dot{u}_x(L,t) \tag{18}$$

Here $u(x,t)$ is the transverse displacement of the cantilevered beam, m is a mass per unit length and α is a damping coefficient expressed in [N.s].
Equation (16) is a one-dimensional version of the mathematical model for the linear elastic systems with structural damping introduced by Chen and Russell in [4].
Writing the equations of motion (16-18) in non dimensional form leads to

$$v'' - \delta v'_{xx} + v_{xxxx} = 0, \tag{19}$$

with the boundary conditions

$$v(0,t) = 0, \qquad v_x(0,t) = 0, \tag{20}$$

$$v_{xx}(1,t) = 0, \qquad v_{xxx}(1,t) = \delta v'_x(1,t) \tag{21}$$

where

$$v = \frac{u}{L}, \quad h = \sqrt{\frac{EI}{m}}, \quad \delta = \frac{\alpha}{mh} = \frac{\alpha}{\sqrt{mEI}} \quad \tau = ht, \quad ()' = \frac{d()}{d\tau} \tag{22}$$

Equation (19) was studied by Zarubinskaya and van Horssen [5] with one boundary condition given in π instead of 1 in our case. They showed numerically that dissipation is generated for all

positive δ.

It can be shown that the energy $E(t)$ given by

$$E(t) = \frac{1}{2}\int_0^1 (v'^2(x,\tau) + v_{xx}^2(x,\tau))dx \tag{23}$$

decreases for increasing times i.e.,

$$\frac{dE}{d\tau} = -\delta \int_0^1 v_x'^2 dx \leq 0. \tag{24}$$

Assume that the solution of equation (19) can be sought in the form

$$v(x,\tau) = T(\tau)X(x) \tag{25}$$

Guided by the experimental observations and by the fourth boundary condition given in (21), we take the time dependent solution of the form

$$T(\tau) \;\; = \;\; \exp(\lambda\tau), \qquad \text{with } \lambda = \frac{X'''(1)}{\delta X'(1)} \tag{26}$$

where λ is a complexe valued variable that can be written as $\lambda = \lambda_r + i\omega$, with λ_r and ω are real. Physically, they reflect the exponential decreasing of the amplitude and the frequency of vibration of natural modes, respectively.

The space dependent solution $X(x)$ satisfies consequently the following boundary value problem

$$X'''' - \delta\lambda X'' + \lambda^2 X = 0, \qquad 0 < x < 1, \tag{27}$$

$$X(0) = X'(0) = X''(1) = 0, \qquad X'''(1) = \delta\lambda X'(1) \tag{28}$$

Let us briefly collect a few facts about (27). First, it is a Hamiltonian dynamical system with (constant) Hamiltonian 'energy' given by

$$H = X'X''' - \frac{\delta\lambda}{2}X'^2 + \frac{\lambda}{2}X^2 - \frac{X''^2}{2} \tag{29}$$

Second, the dynamical system is also reversible, that is (29) is invariant under

$$\mathcal{R} : (X', X''') \to (-X', -X''') \tag{30}$$

The spectral problem corresponding to equation (27) is

$$k^4 - \delta\lambda k^2 + \lambda^2 = 0 \tag{31}$$

The analysis of this characteristic equation leads to consider three cases: $\delta = 2$, $\delta > 2$ and $0 < \delta < 2$.

1. <u>for $\delta > 2$</u>

$$k_{1,2}^2 = \frac{\delta\lambda}{2} \pm \frac{1}{2}\sqrt{\lambda^2(\delta^2 - 4)} \tag{32}$$

the general solution of equation (27) can be written as

$$X(x) = C_1 \cosh(k_1 x) + C_2 \sinh(k_1 x) + C_3 \cosh(k_2 x) + C_4 \sinh(k_2 x) \tag{33}$$

2. <u>for $\delta = 2$</u>

$$k^2 = \lambda \tag{34}$$

the general solution of equation (27) can be written as

$$X(x) = (C_1 + C_2 x)\cosh(kx) + (C_3 + C_4 x)\sinh(kx) \tag{35}$$

3. <u>for $\delta < 2$</u>

$$k_{1,2}^2 = \frac{\delta\lambda}{2} \pm \frac{i}{2}\sqrt{\lambda^2(4 - \delta^2)} \tag{36}$$

the general solution of equation (27) can be written as

$$X(x) = C_1 \cosh(k_1 x) + C_2 \sinh(k_1 x) + C_3 \cosh(k_2 x) + C_4 \sinh(k_2 x) \tag{37}$$

In all these expressions, C_1, C_2, C_3 and C_4 are complex valued constants of integration. By substituting the solution $X(x)$ given in equations (33), (35) or (37) into the boundary conditions (28), we obtain a system of four linear homogeneous equations for C_1, C_2, C_3 and C_4. To have a nontrivial solution $X(x)$, the determinant of the coefficient matrix has to be zero. This leads to the following complex equations

1. <u>for $\delta > 2$</u>

$$\begin{aligned} &p^2(1 + a^4) - \delta\lambda(1 + a^2) + \sinh(p)\sinh(pa)[a^3p^2 + ap^2 - 2a\delta\lambda] \\ &+ \cosh(p)\cosh(pa)[a^2(\lambda\delta - 2p^2) + \lambda\delta] = 0 \end{aligned} \tag{38}$$

where $a = k_1^2/\lambda$ and $p^2 = \lambda/a$.

2. <u>for $\delta = 2$</u>

$$k^2 + 1 + 3\cosh^2(k) = 0 \tag{39}$$

3. <u>for $0 < \delta < 2$</u>

$$p^2(1+a^4) - \delta\lambda(1+a^2) + \sinh(p)\sinh(pa)[a^3p^2 + ap^2 - 2a\delta\lambda]$$
$$+ \cosh(p)\cosh(pa)[a^2(\lambda\delta - 2p^2) + \delta\lambda] = 0 \tag{40}$$

where $a = k_1^2/\lambda$ and $p^2 = \lambda/a$.

We have three unknowns λ_r, ω and δ, and two equations relating them: through the spectral equation (31). This means that through the physical model we should have an additional equation.
This additional equation can be obtained through experiment by measuring either λ_r which is the decaying of the amplitude due to the damping, or the frequency of the mode ω.

3.4.3 Application

In this section, we discuss the mode shapes for different values of the damping coefficient δ.

3.4.4 For $\delta = 2$

For real λ i.e., $\omega = 0$ the solution of equation (39) is a pure imaginary $k = \pm i1.1896165$ and consequently $\lambda = -1.4151$. The general solution (35) (mode shape) is a <u>real</u> function of x and it is given by

$$\begin{aligned} X(x) &= x\cos(1.189616503x) - .8406070338\sin(1.189616503x) \\ &- 3.805597616x\sin(1.189616503x) \end{aligned} \tag{41}$$

which has a similar shape as the first undamped linear mode (see figure 10). This case can be seen as a critical mode i.e., separating the vibrating and non-vibrating modes.
On the other hand, for complex λ i.e., $\lambda = \lambda_r + i\omega$ (see table 4), the modes are complexes. In figures 11-14 are shown the ten first complex modes corresponding to $\delta = 2$ for increasing ω.

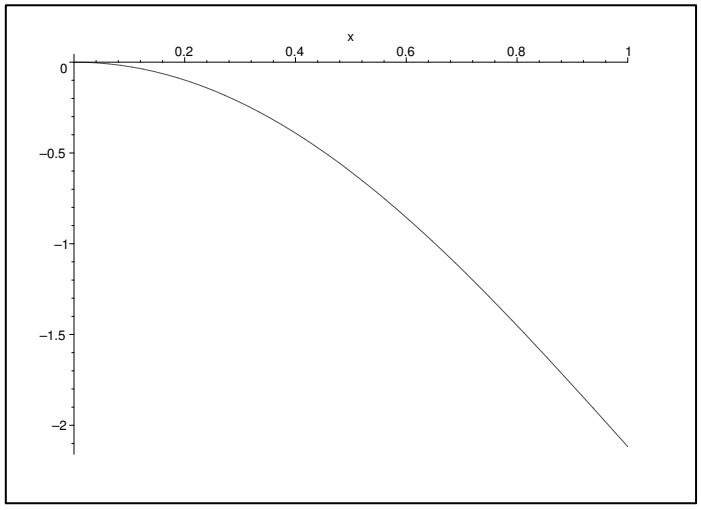

Figure 10: Real mode shape corresponding to $\delta = 2$

Modes	ω	λ_r
mode 1	5.611598842	-5.622187119
mode 2	23.20877682	-31.54474193
mode 3	66.02776524	-145.3742493
mode 4	89.97854232	-232.5161838
mode 5	115.1617249	-339.6314969
mode 6	141.3757272	-466.6580262
mode 7	168.4756217	-613.5561166
mode 8	196.3522015	-780.2987755
mode 9	224.9202213	-966.8667262
mode 10	254.1112900	-1173.245682

Table 4: Complex valued λ solutions of equation (35) for $\delta = 2$

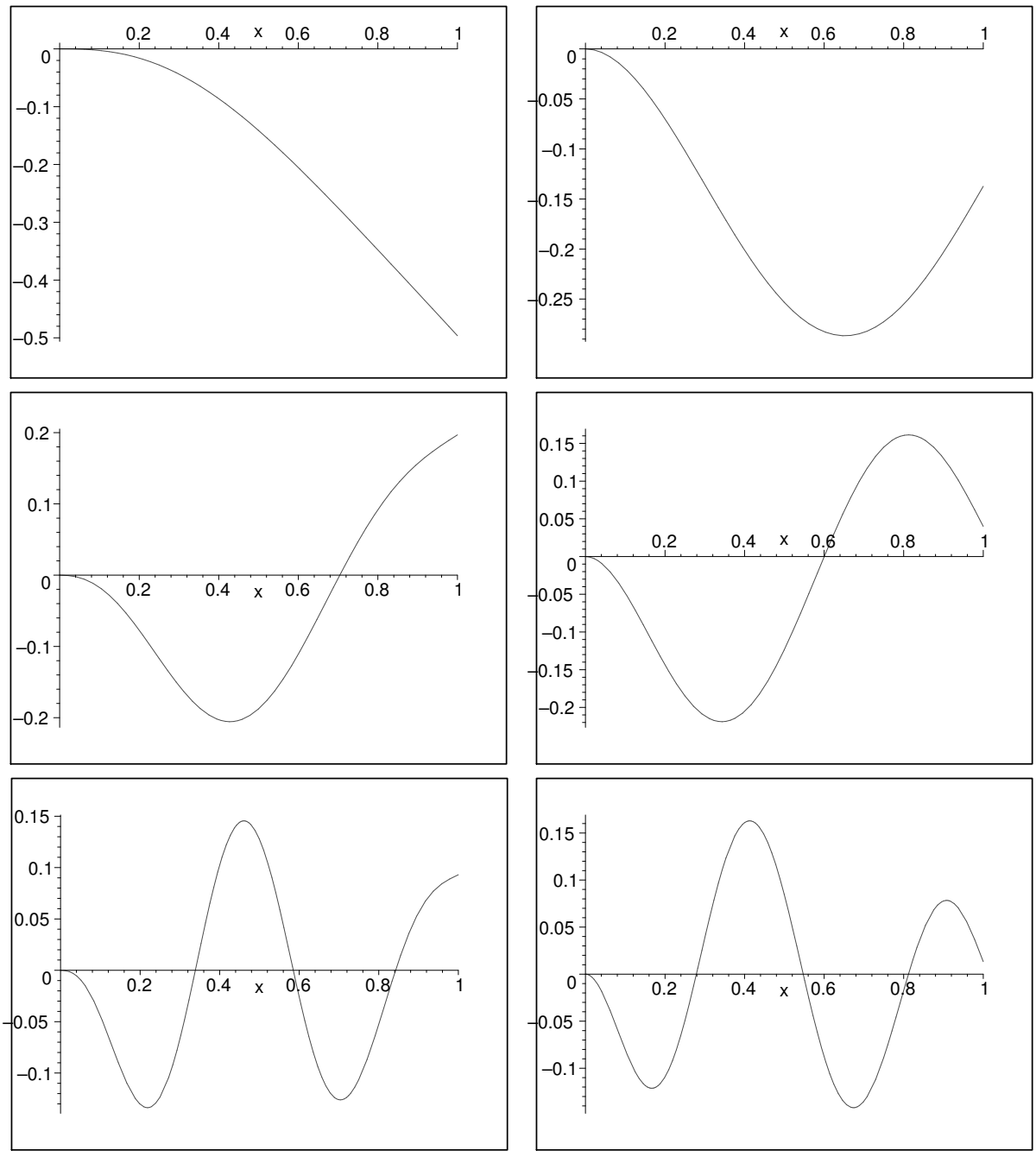

Figure 11: a) Five first complex modes corresponding to $\delta = 2$, the real parts (left) and imaginary parts (right)

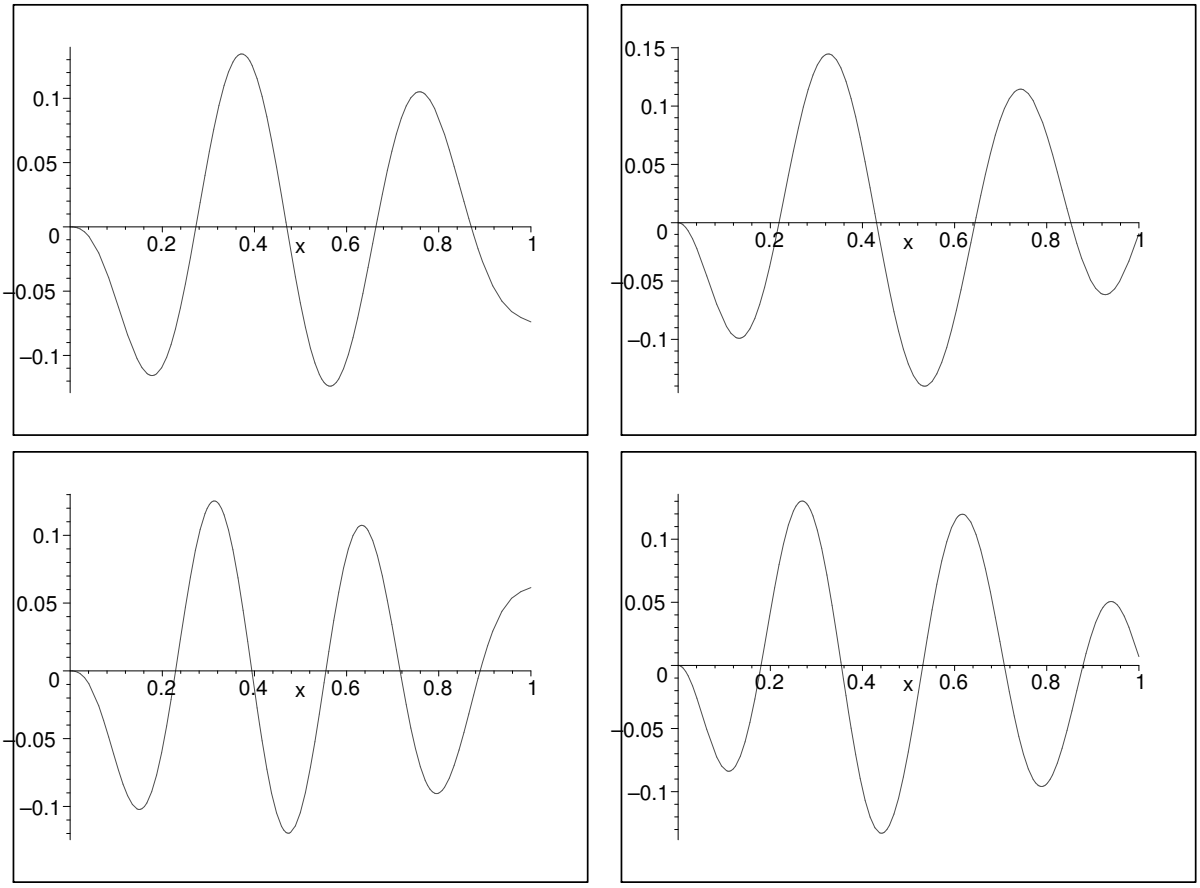

Figure 12: b) Five first complex modes corresponding to $\delta = 2$, the real parts (left) and imaginary parts (right)

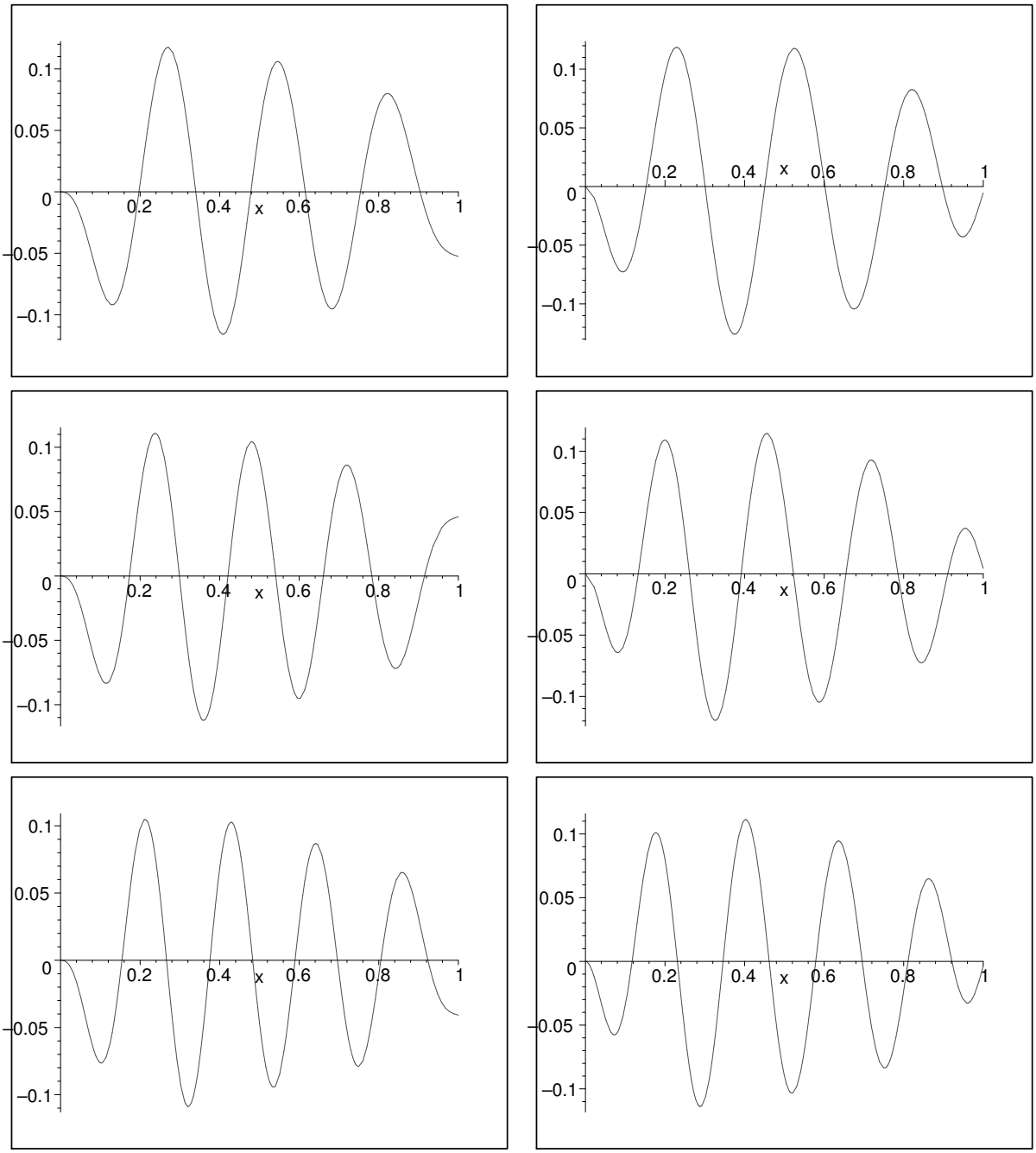

Figure 13: a) Sixth to tenth complex modes corresponding to $\delta = 2$, real modes (left) and imaginary modes (right)

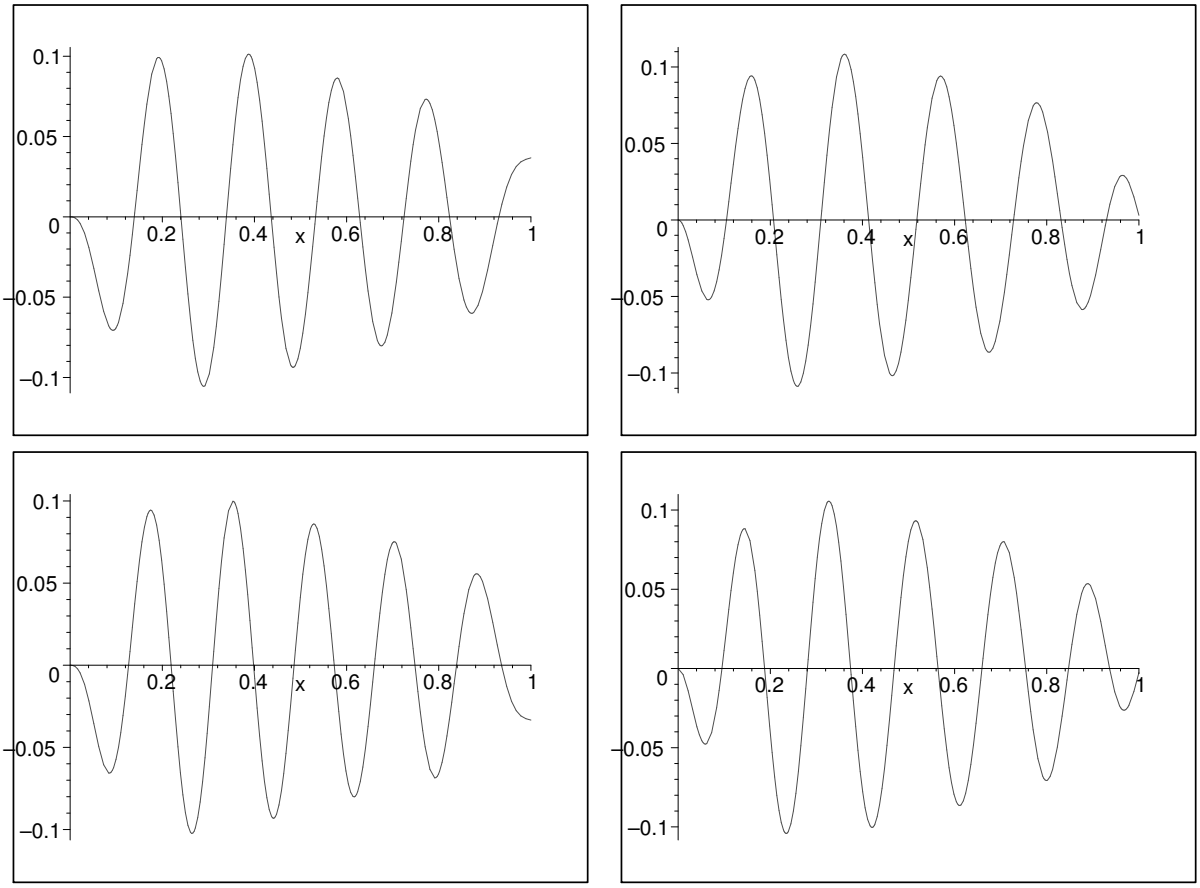

Figure 14: b) Sixth to tenth complex modes corresponding to $\delta = 2$, real modes (left) and imaginary modes (right)

Modes	λ_r
mode 1	-1.405789649
mode 2	-3795.6870874420743812
mode 3	-4093.6414717981212955
mode 4	-15476.141366293485278
mode 5	-16072.905424128655580
mode 6	-35042.54728040902431
mode 7	-35939.949149609889807
mode 8	-62494.777867278649130
mode 9	-63695.889569408146754
mode 10	-97832.782317529792018

Table 5: Real valued λ for $\delta = 2.01$

3.4.5 For $\delta > 2$

In this case we have found the coexistence between real modes (i.e., $\omega = 0$) and complex modes.

For $\delta = 2.01$

In Table 5 are shown the values of λ which are real i.e., corresponding to $\omega = 0$. In this case the mode shapes $X(x)$ are found to be real functions. The ten first modes are shown in figures 15 for decreasing values of λ. It is worth noting that these modes are highly damped since $|\lambda_r|$ are very high.

The system has also complex valued λ given in table 6, and consequently complex modes shown in figures 16 and 17.

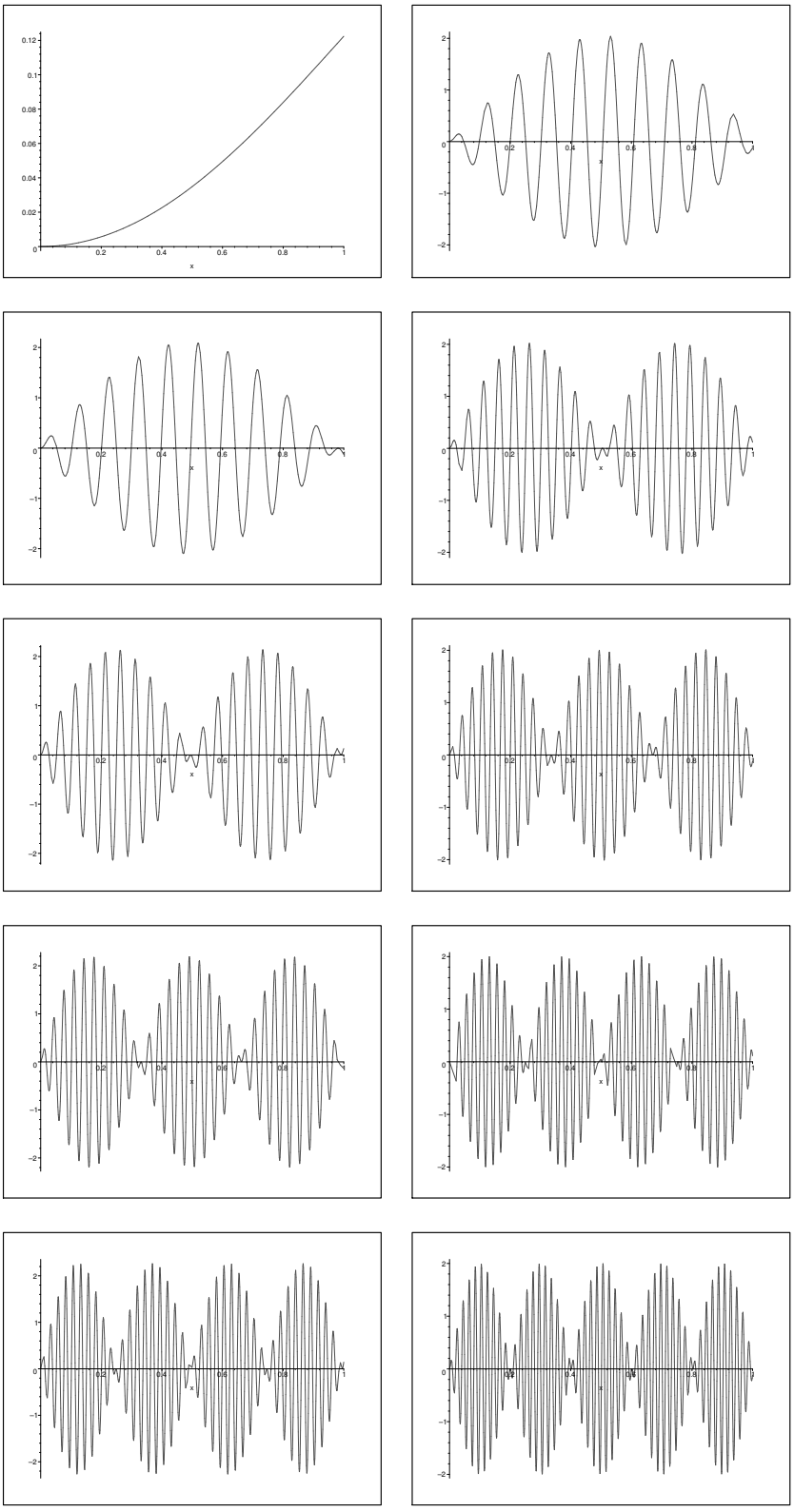

Figure 15: Real modes corresponding to $\delta = 2.01$

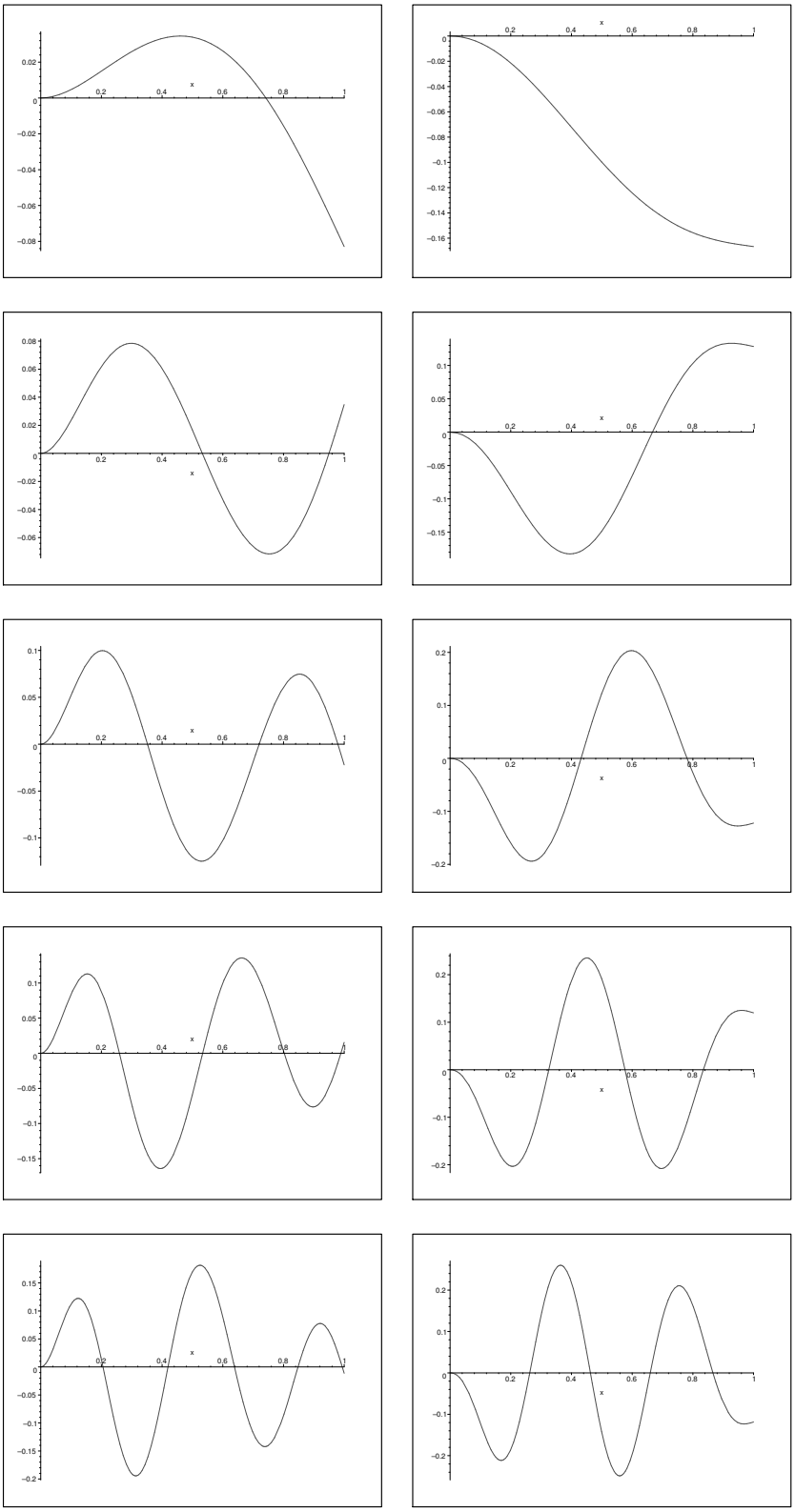

Figure 16: Five first complex modes corresponding to $\delta = 2.01$: Real parts (left) and imaginary parts (right)

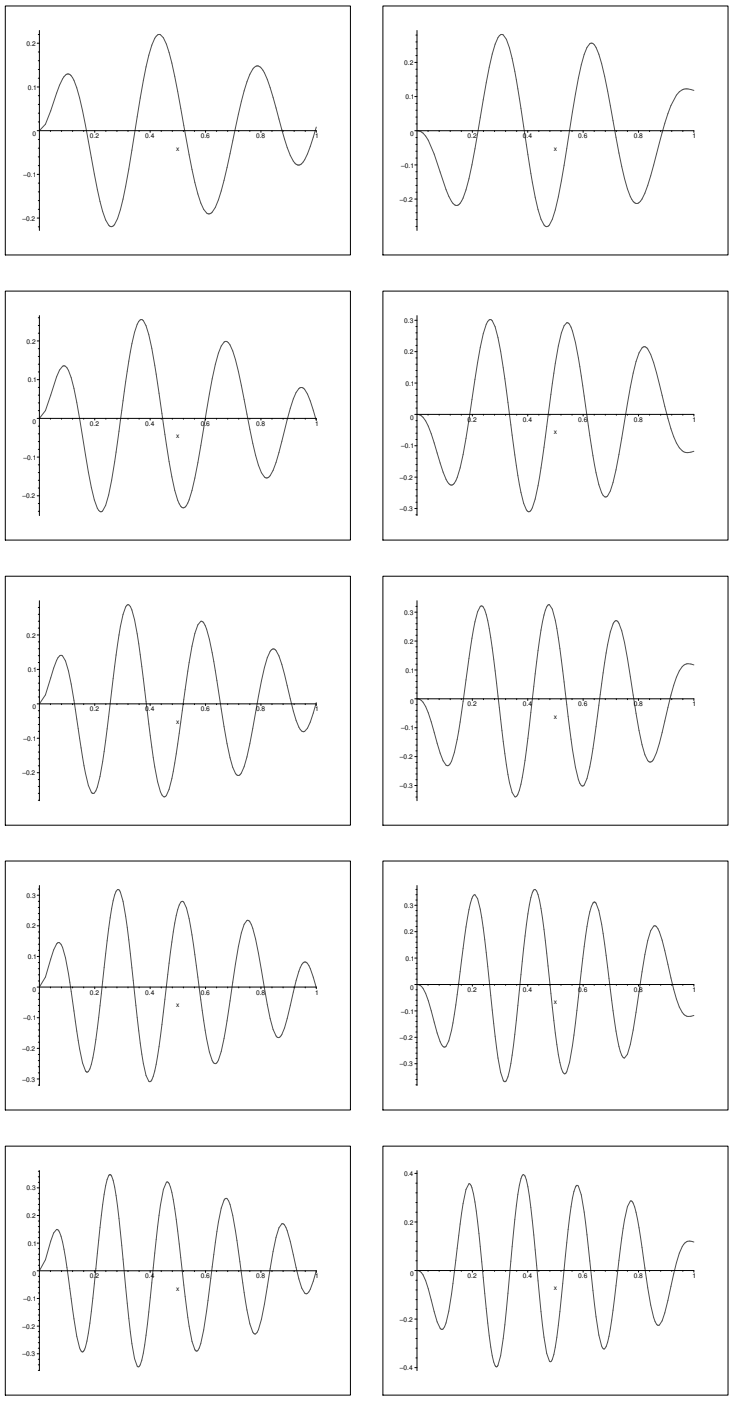

Figure 17: Sixth to tenth complex modes corresponding to $\delta = 2.01$: Real parts (left) and imaginary parts (right)

Modes	ω	λ_r
mode 1	5.616646605706798761192	-5.621921891814156528859
mode 2	23.0851474852	-31.6452365245
mode 3	43.0695665168	-78.6560686107
mode 4	64.6127480003	-146.123747181
mode 5	87.0516847702	-233.852977129
mode 6	109.900641289	-341.754364661
mode 7	132.755241192	-469.784731579
mode 8	155.244791352	-617.926503409
mode 9	177.002496630	-786.179823229
mode 10	197.641149548	-974.560279587

Table 6: Complex values of λ for $\delta = 2.01$, solutions of equation (38)

For $\delta = 2.1$

In table 7 are listed the real values of λ i.e., corresponding to $\omega = 0$ and in figures 18 are shown the corresponding first ten modes which are real.
In table 8 are given the nine first complex values of λ. For increasing ω the decreasing of λ_r is not granted for all modes. See for instance modes 4 and 5 and modes 8 and 9. In figure 19 are shown the shapes of the five first complex modes.

Modes	λ
mode 1	-1.3272416057488207846
mode 2	-328.25996709762212773
mode 3	-475.29633384968554519
mode 4	-1504.8997008869650697
mode 5	-1696.3795933157434893
mode 6	-3379.6501627280319989
mode 7	-3667.0420853353194963
mode 8	-6012.5467814103897986
mode 9	-6594.6656321066948959
mode 10	-9637.5008377941180125

Table 7: Real valued λ corresponding to $\delta = 2.1$

Modes	ω	λ_r
mode 1	5.6504874868488989230	-5.6276837035923778302
mode 2	21.8867308110	-32.5875919894
mode 3	37.5776682582	-81.9293074825
mode 4	47.8043585943	-249.445405638
mode 5	48.8052258966	-153.692217650
mode 6	80.2197665604	-598.752283941
mode 7	110.307798399	-770.298348044
mode 8	120.022814056	-1179.36751667
mode 9	125.032085349	-962.976427957

Table 8: Complex values of λ for $\delta = 2.1$, solutions of equation (35)

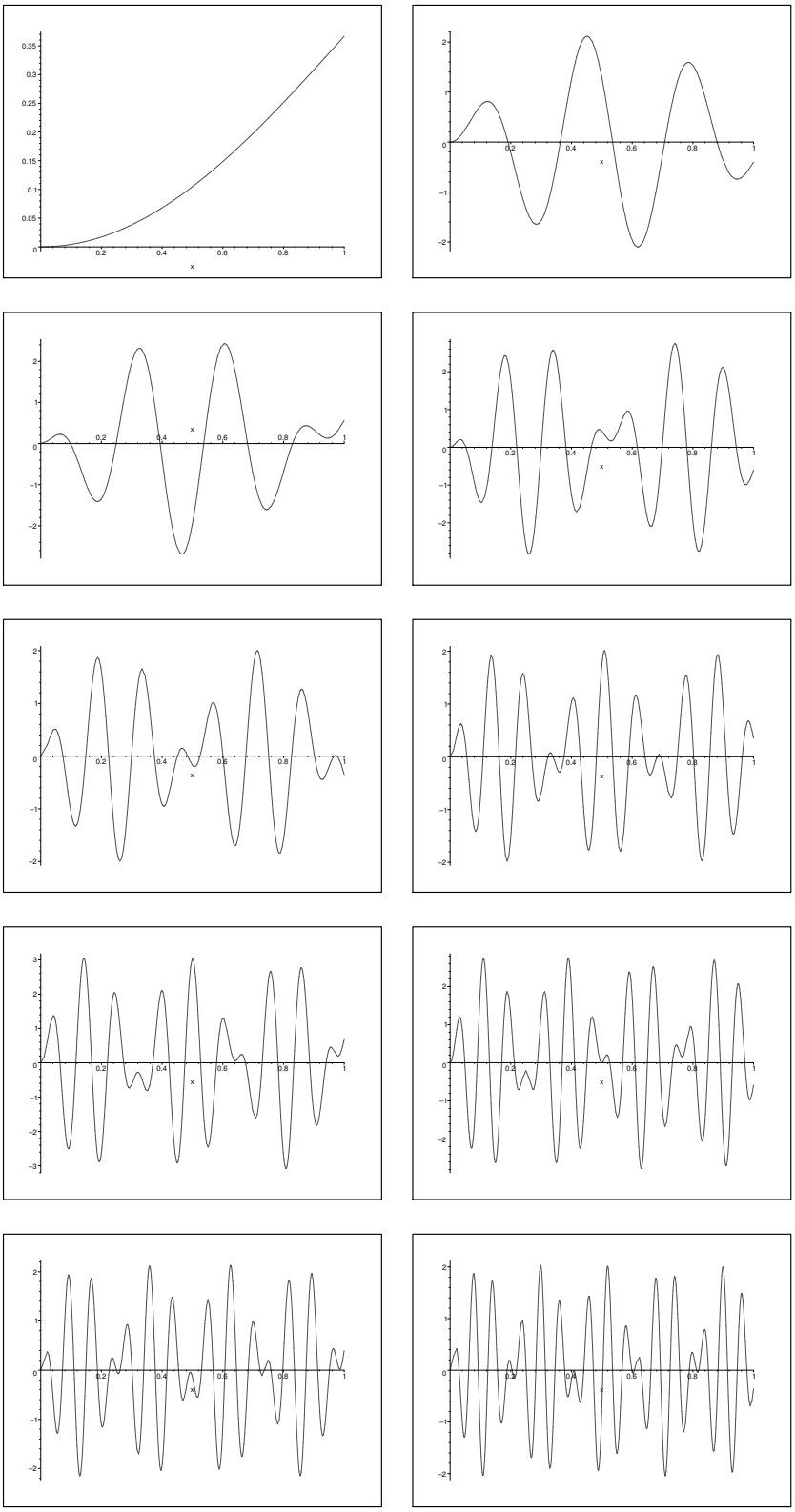

Figure 18: Real modes corresponding to $\delta = 2.1$

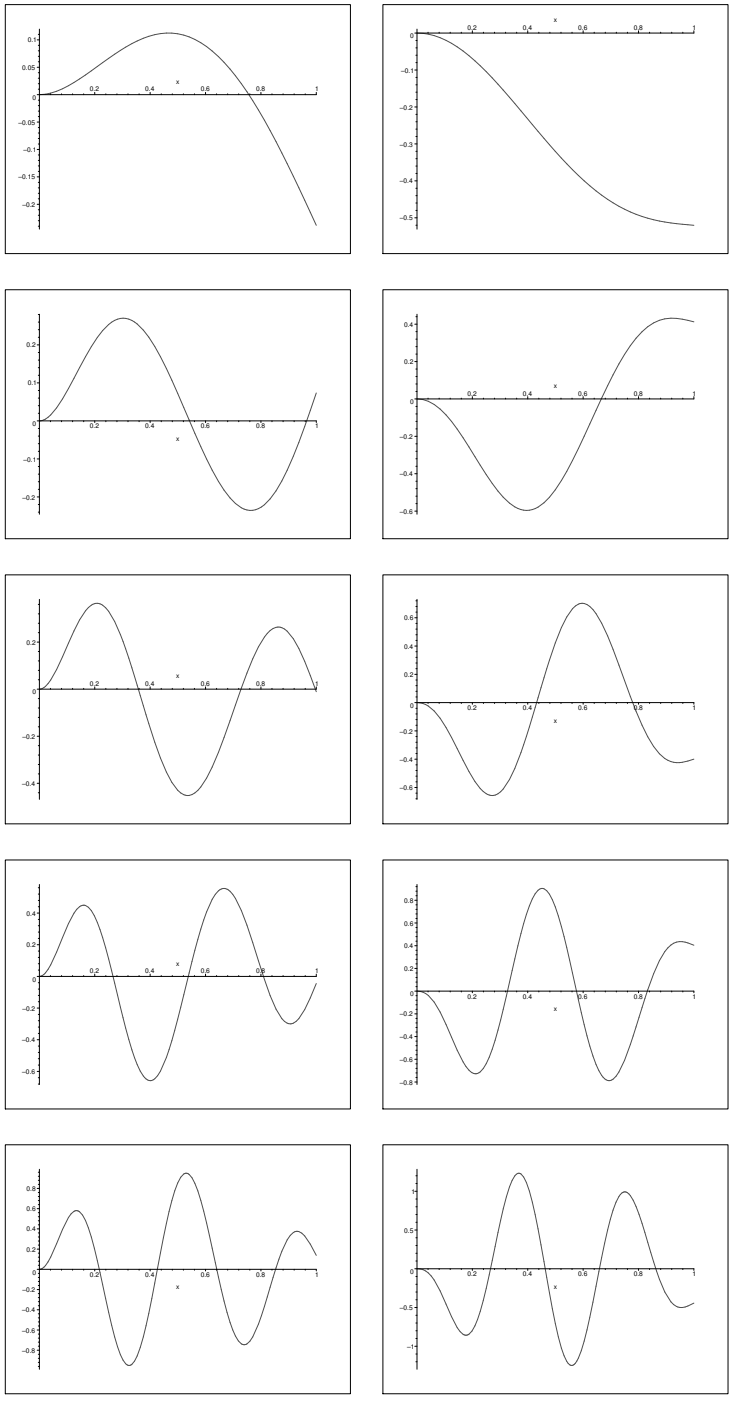

Figure 19: Five first complex modes corresponding to $\delta = 2.1$: the real modes left column, the imaginary modes right column

Modes	λ
mode 1	-.24786890568109528554
mode 2	-2.3168337612119401343
mode 3	-6.3522112439887708407
mode 4	-12.808510727593993108
mode 5	-23.102827352028054393
mode 6	-41.502304663470018043
mode 7	-55.475989863513051771
mode 8	-71.894167693810871866
mode 9	-89.777725995171986294
mode 10	-110.19584006612002298

Table 9: Real eigenvalues for $\delta = 10$

For $\delta = 10$

In table 9 are given the first ten real values of λ and in figure 20 are shown the first ten corresponding real modes.

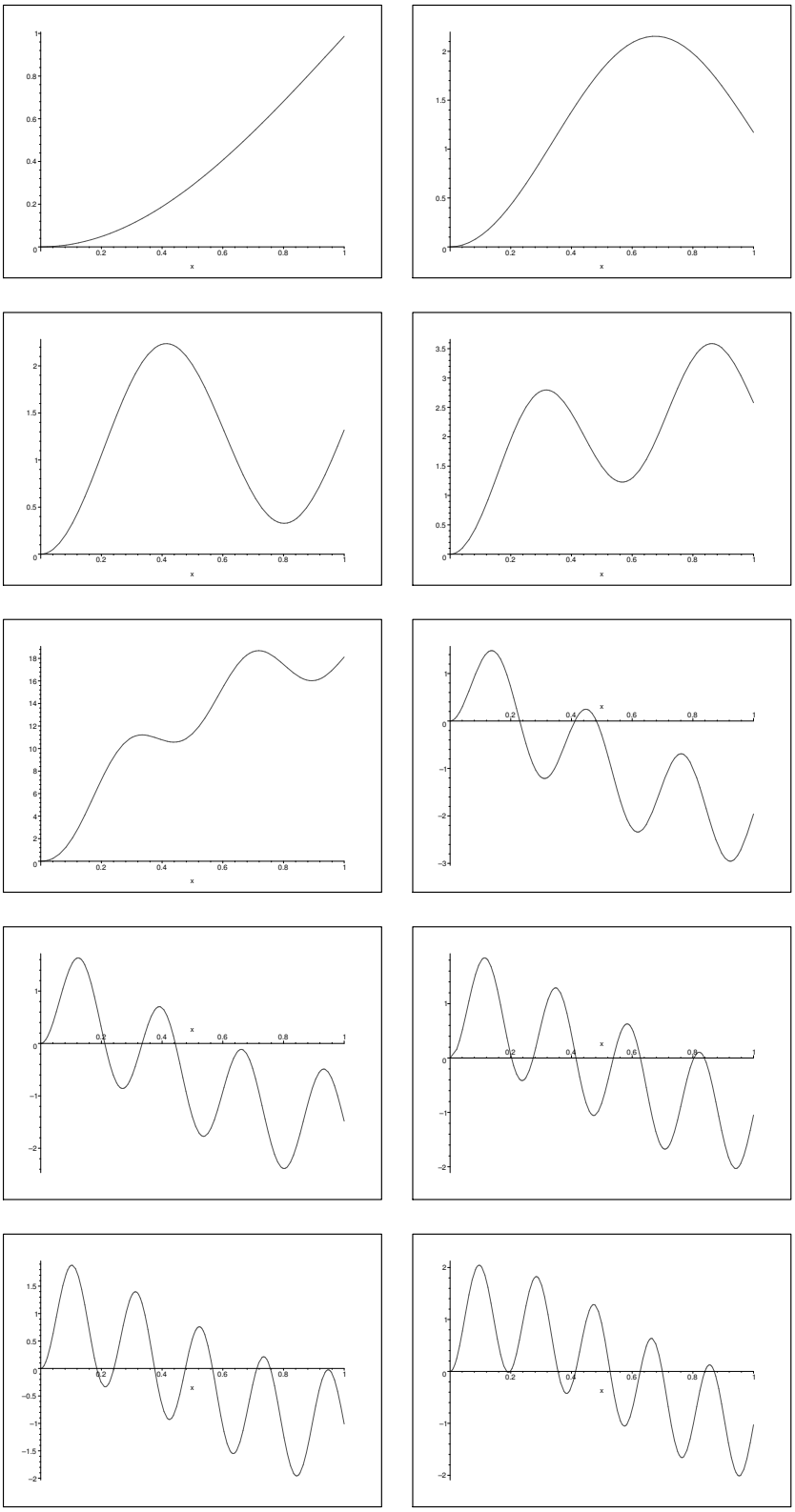

Figure 20: Real Modes corresponding to $\delta = 10$

Modes	ω	λ_r
mode 1	5.544283396	-5.636062820
mode 2	24.35110466	-30.58606088
mode 3	48.42890583	-75.04550690
mode 4	78.08775030	-138.4062280
mode 5	113.566580014	-220.495936464
mode 6	155.0357696	-321.2839952
mode 7	202.5904977	-440.7812792
mode 8	256.2767357	-579.0042969
mode 9	316.114463149	-735.965257536
mode 10	382.1116256	-911.6713836

Table 10: Complex values of λ for $\delta = 1.9$, solutions of equation (40)

3.4.6 For $0 < \delta < 2$

It is found that in this case all values of λ are complex and the modes are all complex.

For $\delta = 1.9$

In table 10 are shown the complex values of λ, and in figures 21 and 22 are shown the ten first complex modes.

For $\delta = 0.1$

In table 11 are shown the complex values of λ, and in figures 23 are shown the five first complex modes. It is worth noting that the real parts are similar to the undamped modes. This is the case for all real modes corresponding to small δ.

3.4.7 Discussion

First, let us take, for instance $\lambda_r = -0.6$. The numerical values of ω and δ are given in table 12. Fitting these values one finds $\delta = 0.8808\omega^{-0.9915}$. In figure 24 we show a comparison between the seven first normalized modes corresponding to the undamped model $\delta = 0$ and the real part of the complex modes given in (37) for $\lambda_r = -0.6$. It is clear that the first mode is the most influenced by the constant decaying λ_r. The higher modes are almost not influenced.

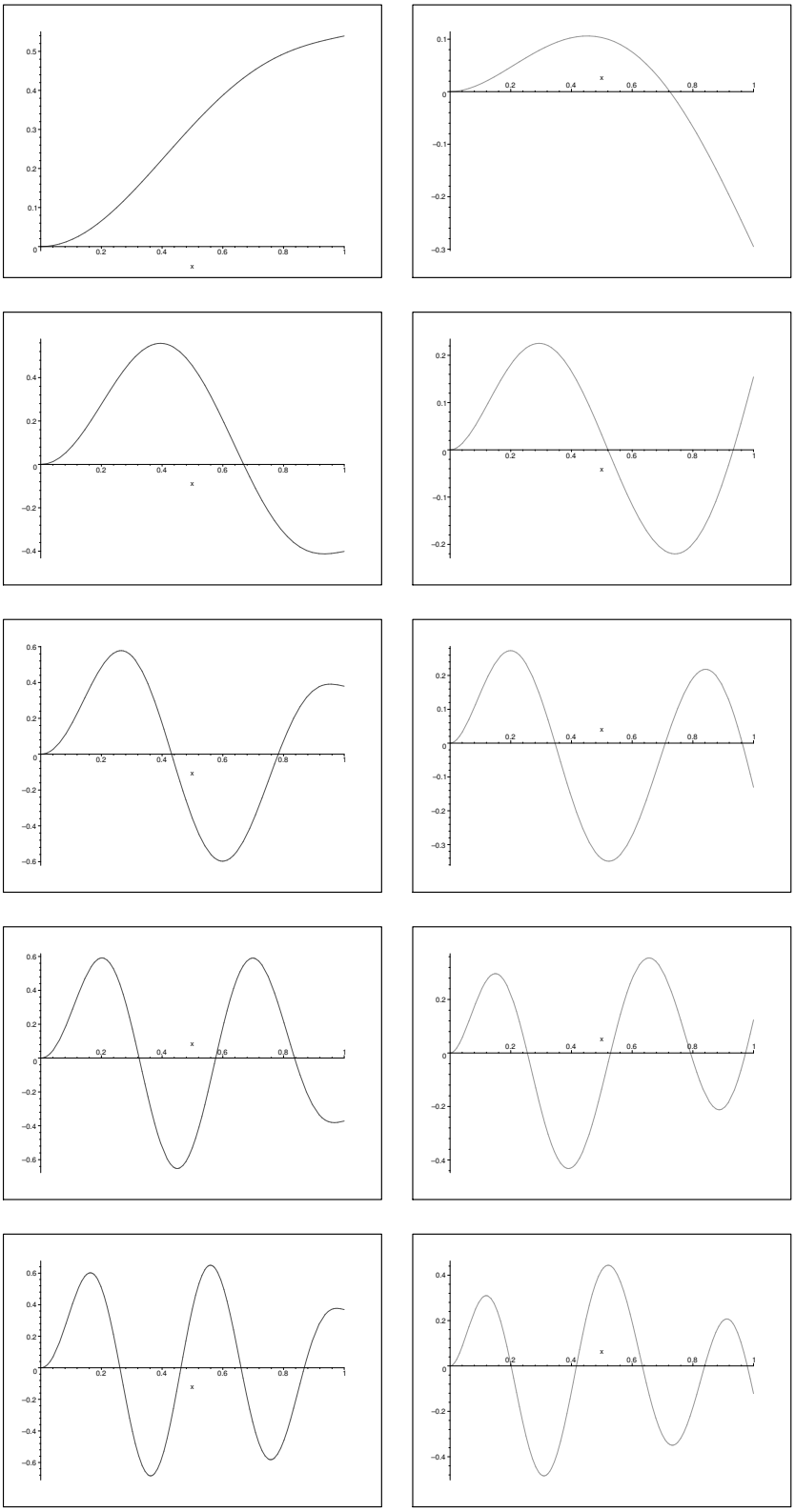

Figure 21: First five complex modes corresponding to $\delta = 1.9$: real parts (left) and imaginary part (right)

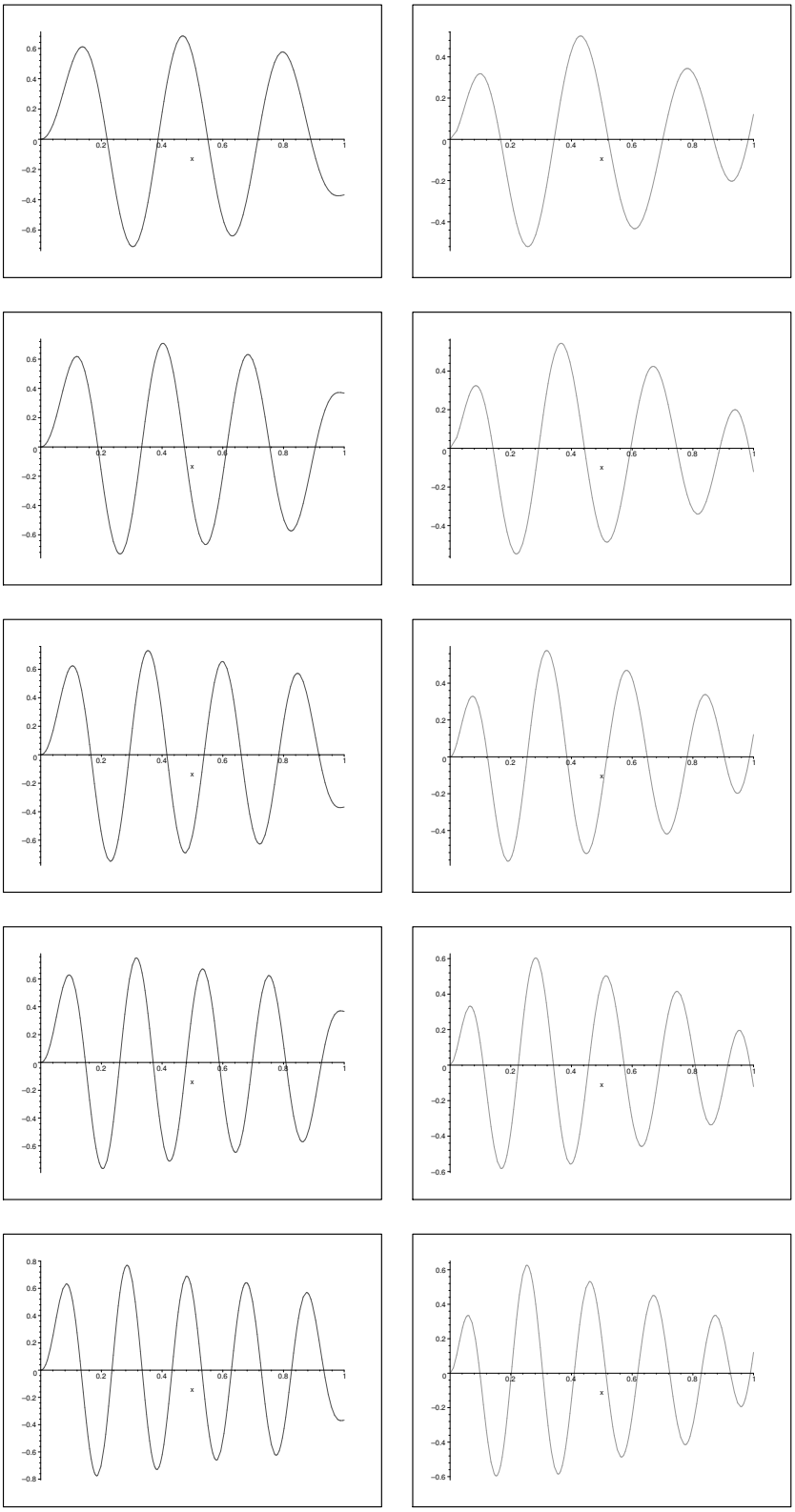

Figure 22: Sixth to tenth complex modes corresponding to $\delta = 1.9$: real parts (left) and imaginary part (right)

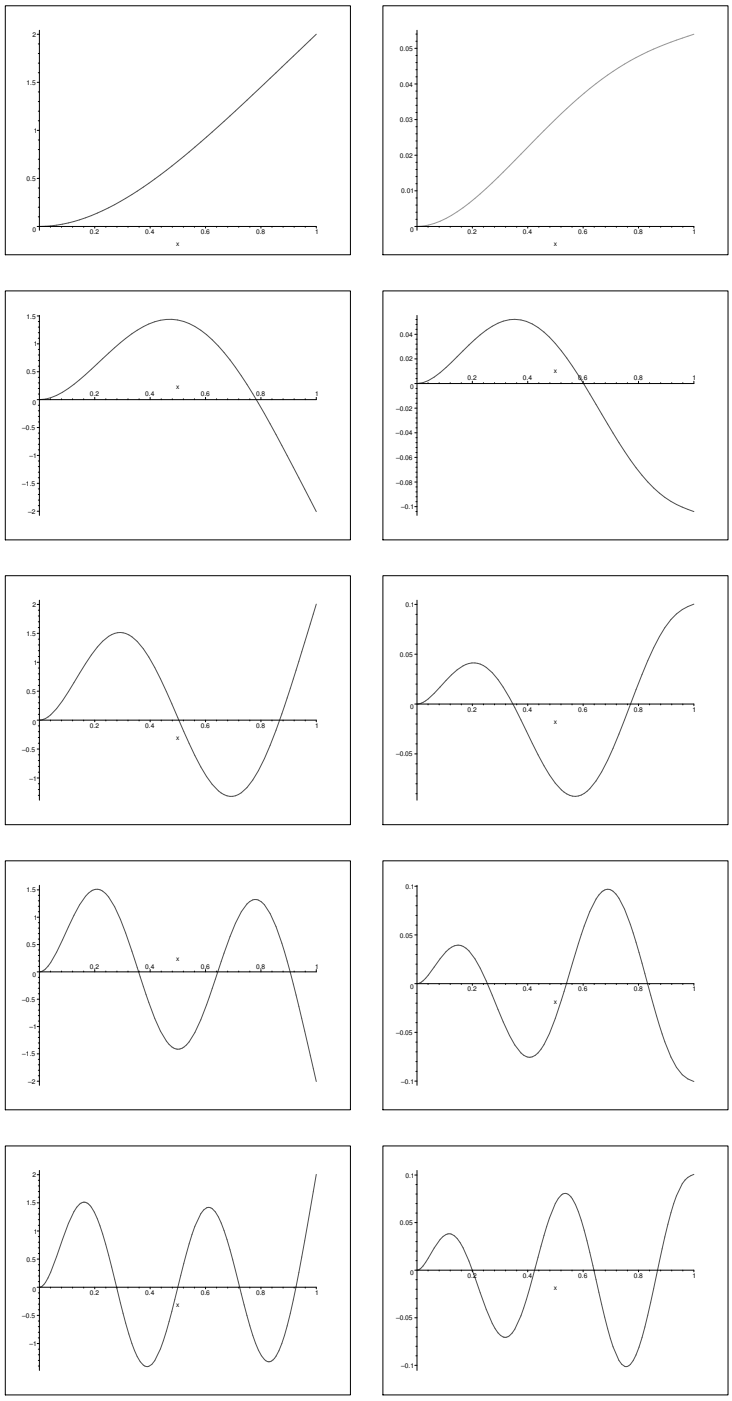

Figure 23: First five complex modes corresponding to $\delta = 0.1$: real parts (left) and imaginary part (right)

Modes	ω	λ_r
mode 1	3.5104962969451496	-.23262744814900117
mode 2	21.982485544604480	-1.6231856047759467
mode 3	61.577348012506420	-3.8684696364915563
mode 4	120.69295882921888	-7.1500287987983971
mode 5	199.535913311	-11.4130606771
mode 6	298.092676306	-16.6635006740
mode 7	416.363993716	-22.9008703963
mode 8	554.349828903	-30.1252024520
mode 9	712.050183503	-38.3364948397
mode 10	889.4650576	-47.53474767

Table 11: Complex values of λ for $\delta = 0.1$, solutions of equation (40)

Now we focus our attention on the first mode, we find that the best fit is given by $\delta \approx -0.4\lambda_r + 0.013$; see Fig.14. For the second mode, we find $\delta \approx -0.061\lambda_r$, see Fig.26. For the third mode, we find $\delta \approx -0.025\lambda_r$, see Fig.27. Thus, $\delta(\lambda_r)$ is a linear function which is decreasing with the order of the mode for increasing ω.

In tables 13 - 21, we show for fixed decreasing values of λ_r the natural frequencies of the ten first flexural modes and the corresponding values of δ. It is obvious that ω_n is decreasing with increasing δ and consequently increasing $|\lambda_r|$. For different $\lambda_r \leq 1$, a least square fit method leads to the following relation

$$\delta \approx \frac{0.01357 - 1.42475\lambda_r}{\omega} \tag{42}$$

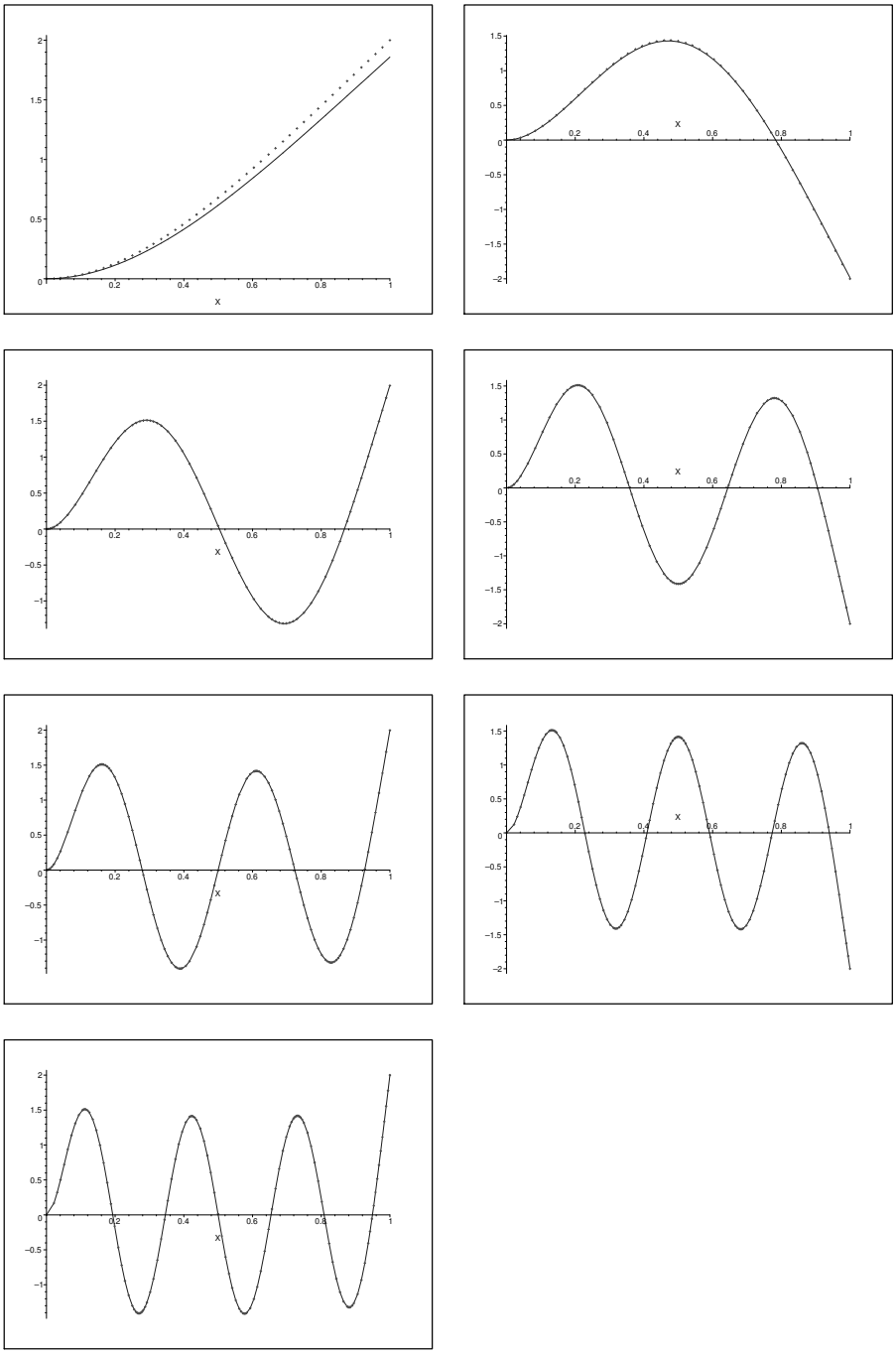

Figure 24: Comparison on the first seven modes corresponding to $\delta = 0$ in dots, and the real normalized modes corresponding to (37) in continuous line

Modes	ω	δ	ω for δ=0
mode 1	3.4792779830753535	0.25642247474261911	3.5160152685001511
mode 2	22.027386303470494	0.037009955897800919	22.034491564666770
mode 3	61.694333032512817	0.015523816467832633	61.697214413549101
mode 4	120.90044569648437	0.0083973314686887331	120.90191605230572
mode 5	199.85863636977717	0.0052600757189864517	199.85953011680345
mode 6	298.55493130963915	0.0036023780172085773	298.55553096773010
mode 7	416.99035610961929	0.0026210509726806063	416.99078605660547
mode 8	555.16492432029990	0.0019923982626406579	555.16524755576268
mode 9	713.07866616522019	0.001565586217957760	713.07891797897610
mode 10	890.73159551578611	0.001262596901892794	....

Table 12: The values of ω and δ for $\lambda_r = -0.6$ and the values of ω for $\delta = 0$ ($\lambda_r = 0$)

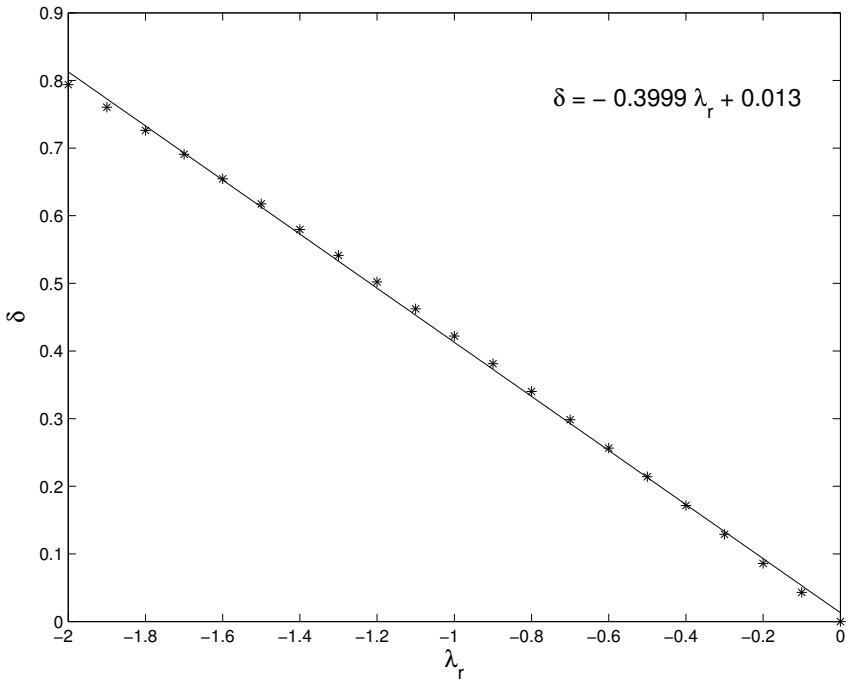

Figure 25: δ versus λ_r for the first mode

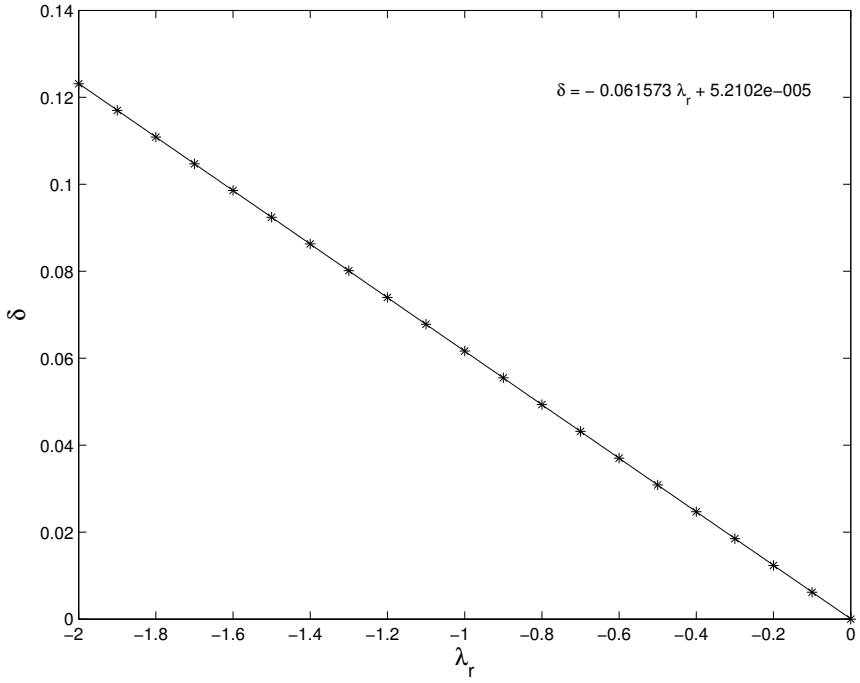

Figure 26: δ versus λ_r for the second mode

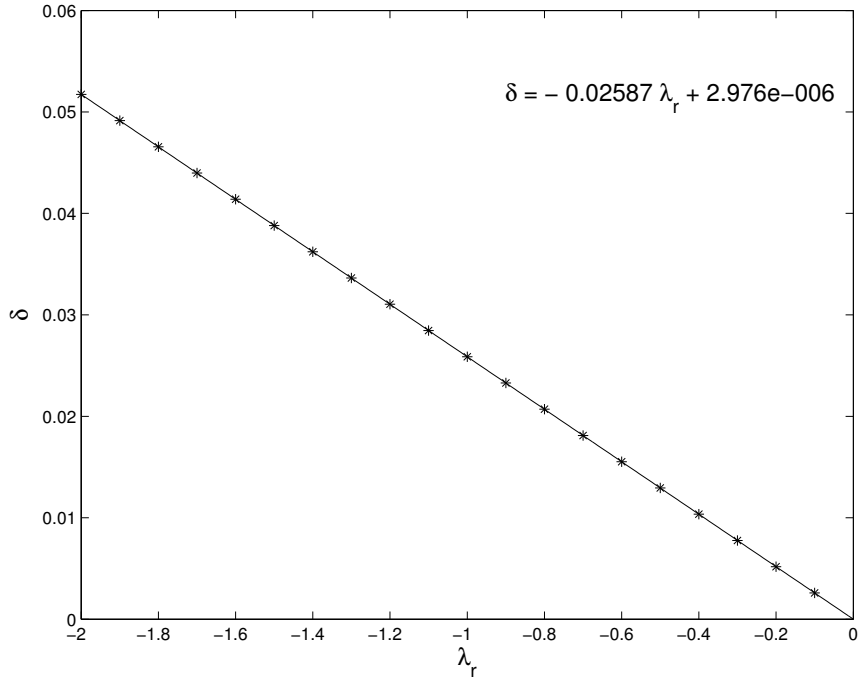

Figure 27: δ versus λ_r for the third mode

Modes	ω	δ
mode 1	3.5149955111983954	0.043023161526641025
mode 2	22.0342941991	0.00616949309073
mode 3	61.697134376604811	0.0025873576788871834
mode 4	120.90187520929713	0.0013995618303243444
mode 5	199.85950529054561	0.00087668060061278631
mode 6	298.55551431057595	0.00060039669068738750
mode 7	416.99077411363928	0.00043684194647919045
mode 8	555.16523857700223	0.00033206642253284966
mode 9	713.07891098415085	0.00026093105598086692
mode 10	890.73179159601005	0.00021043282628443438

Table 13: The values of ω and δ for $\lambda_r = -0.1$. The best fit is given by $\delta = 0.1467\,\omega^{-0.9787}$

Modes	ω	δ
mode 1	3.5119359873280870	0.085997403126576179
mode 2	22.0337021014	0.0123387861551
mode 3	61.696894265285829	0.0051747059412512763
mode 4	120.90175268019979	0.0027991225317304191
mode 5	199.85943081175551	0.0017533609759514461
mode 6	298.55546433910835	0.0012007933206061110
mode 7	416.99073828473846	0.00087368387278144978
mode 8	555.16521164072007	0.00066413283727838467
mode 9	713.07888999967451	0.00052186210859238803
mode 10	890.73177478913534	0.00042086565097419152

Table 14: The values of ω and δ for $\lambda_r = -0.2$. The best fit is given by $\delta = 0.2929\,\omega^{-0.9783}$

Modes	ω	δ
mode 1	3.5068359448803793	0.12887372675364248
mode 2	22.0327152691	0.0185076791414
mode 3	61.696494078133809	0.0077620353700838022
mode 4	120.90154846479909	0.0041986809752799765
mode 5	199.85930668038329	0.0026300409007401047
mode 6	298.55538105331179	0.0018011898289872988
mode 7	416.99067856989811	0.0013105257587298514
mode 8	555.16516674691419	0.00099619923644930495
mode 9	713.07885502554524	0.00078279315446519888
mode 10	890.73174677767686	0.00063129847247458277

Table 15: The values of ω and δ for $\lambda_r = -0.3$. The best fit is given by $\delta = 0.4379\,\omega^{-0.9777}$

Modes	ω	δ
mode 1	3.4996941434346181	0.17160298026892849
mode 2	22.031333696943298	0.024675971923751508
mode 3	61.695933812718198	0.010349336547405532
mode 4	120.90126256273736	0.0055982360319948649
mode 5	199.85913289634590	0.0035067201496995341
mode 6	298.55526445316059	0.0024015861550616194
mode 7	416.99059496910762	0.0017473675841473053
mode 8	555.16510389557910	0.0013282656122582272
mode 9	713.07880606176193	0.0010437241902299456
mode 10	890.73170756163352	0.00084173128919094434

Table 16: The values of ω and δ for $\lambda_r = -0.4$. The best fit is given by $\delta = 0.586\,\omega^{-0.9829}$

Modes	ω	δ
mode 1	3.4905088734517290	0.21413578580447283
mode 2	22.029557377944537	0.030843464290072054
mode 3	61.695213465636195	0.012936600053780950
mode 4	120.90089497300000	0.0069977865730050435
mode 5	199.85890945952701	0.0043833984975453820
mode 6	298.55511453861845	0.0030019822380590177
mode 7	416.99048748235382	0.0021842093288566721
mode 8	555.16502308671027	0.0016603319569178247
mode 9	713.07874310832139	0.0013046552125172582
mode 10	890.73165714100383	0.0010521640995285707

Table 17: The values of ω and δ for $\lambda_r = -0.5$. The best fit is given by $\delta = 0.7355\,\omega^{-0.9891}$

Modes	ω	δ
mode 1	3.4792779830753535	0.25642247474261911
mode 2	22.027386303470494	0.037009955897800919
mode 3	61.694333032512817	0.015523816467832633
mode 4	120.90044569648437	0.0083973314686887331
mode 5	199.85863636977717	0.0052600757189864517
mode 6	298.55493130963915	0.0036023780172085773
mode 7	416.99035610961929	0.0026210509726806063
mode 8	555.16492432029990	0.0019923982626406579
mode 9	713.07866616522019	0.0015565586217957760
mode 10	890.73159551578611	0.0012625969018927940

Table 18: The values of ω and δ for $\lambda_r = -0.6$. The best fit is given by $\delta = 0.8808\,\omega^{-0.9815}$

Modes	ω	δ
mode 1	3.4659989121980860	0.29841303171761134
mode 2	22.024820462867129	0.043175246246465868
mode 3	61.693292508000836	0.018110976365755641
mode 4	120.89991473086235	0.0097968695903321515
mode 5	199.85831362691361	0.0061367515887230485
mode 6	298.55471476616582	0.0042027734317382131
mode 7	416.99020085088270	0.00305789249544157
mode 8	555.16480759633849	0.0023244645216393109
mode 9	713.07857523245399	0.0018265172031820600
mode 10	890.731522687	0.00147302969460

Table 19: The values of ω and δ for $\lambda_r = -0.7$. The best fit is given by $\delta = 1.023\,\omega^{-0.9929}$

Modes	ω	δ
mode 1	3.4506687334331566	0.34005705020901389
mode 2	22.0218598437	0.0493391346449
mode 3	61.692091885780834	0.020698070320831428
mode 4	120.89930207571756	0.01119639980842992
mode 5	199.85794123072034	0.0070134258814452454
mode 6	298.55446490813146	0.0048031684208744760
mode 7	416.99002170611901	0.0034947338769617702
mode 8	555.16467291481561	0.002656530726126241
mode 9	713.07847031001750	0.0020874481648207544
mode 10	890.73143865157680	0.0016834624763222261

Table 20: The values of ω and δ for $\lambda_r = -0.8$. The best fit is given by $\delta = 1.16\,\omega^{-0.9919}$

Modes	ω	δ
mode 1	3.4332841994785980	0.38130370248726898
mode 2	22.018504431461134	0.055501420182576233
mode 3	61.690731158561196	0.023285088902941735
mode 4	120.89860772997685	0.012595920993504853
mode 5	199.85751918094823	0.0078900983718311748
mode 6	298.55418173545866	0.0054035629238423056
mode 7	416.98981867529918	0.0039315750970631078
mode 8	555.16452027571862	0.0029885968683138415
mode 9	713.07835139790485	0.0023483790995044142
mode 10	890.73134341257960	0.0018938952451980353

Table 21: The values of ω and δ for $\lambda_r = -0.9$. The best fit is given by $\delta = 1.292\omega^{-0.9904}$

4 Theoretical modelling

4.1 Partial differential equations modelling

In this subsection, we present the equations of motion and boundary conditions governing the nonlinear vibrations of isotropic and inextensible cantilever beams. A variational approach based on the extended Hamilton principle is used [see Crespo da Silva, *Non-linear flexural-flexural-torsional-extensional dynamics of beams. I: Formulation*, International Journal of Solids and Structures **24**, 1225-1234, 1988].

In nonlinear elastic beams, large deformations give rise to geometric nonlinearities due to nonlinear curvature and/or midplane stretching, leading to nonlinear strain-displacement relations. We use the Euler-Bernoulli beam theory to model the beam, and accordingly neglect the effects of warping and shear deformation. The usually small Poisson effect is also neglected in our case. Hence, knowing the deformation of the neutral axis enables the determination of the deformation of all points on the beam. Neglecting the out-of plane motions, the beam's neutral axis being inextensional leads to the following constraint equation

$$(1 + v')^2 + u'^2 = 1 \tag{43}$$

which gives up to the second order equation

$$v' \approx -\frac{1}{2}u'^2 \tag{44}$$

where $u(s,t)$ is the transverse displacement, $v(s,t)$ is the longitudinal displacement and the prime is the derivative with respect to the arclength s.
Then, substituting the inextensionality condition, given by (44), and applying the boundary condition $u(0,t)=0$, leads to

$$v(s,t) = -\frac{1}{2}\int_0^s u'^2 ds \tag{45}$$

The no-transverse-shear assumption leads to the fact that the cross sections rotations are due to the bending alone. Assuming the rotatory inertia to be negligible compared to the translational inertia, in what follows we develop a nonlinear partial-differential equation of motion describing the flexural motion of an inextensional beam.
The Lagrangian $\mathcal{L}$ of motion is defined as

$$\mathcal{L} = T - V \tag{46}$$

where T is the kinetic energy and V the potential energy. In our case, we are interested to the transverse in-plane motions of the beam. Thus the total kinetic energy is given by

$$T = \frac{m}{2}\int_0^L \left[\dot{u}^2 + \dot{v}^2\right] ds \tag{47}$$

where m is the mass per unit length. Inserting the inextensibility condition (45) into the kinetic energy expression (47) gives

$$T = \frac{m}{2}\int_0^L \left[\dot{u}^2 + \frac{1}{4}\left(\frac{\partial}{\partial t}\int_0^s u'^2 d\sigma\right)^2\right] ds \tag{48}$$

The potential energy for the bending vibrations of inextensional beams is given by

$$V = \frac{EI}{2}\int_0^L \kappa^2(s,t) ds \tag{49}$$

where E is the Young's modulus, I is the moment of inertia, EI is the bending stiffness and κ is the change in curvature due to the bending, which is expressed as

$$\kappa = \frac{u''}{\sqrt{(1-u'^2)}} \tag{50}$$

The Taylor expansion of κ up to the second order is given by

$$\kappa^2 = \frac{u''^2}{1-u'^2} \approx u''^2 + u''^2 u'^2 \tag{51}$$

Thus the potential energy is approximated by

$$V = \frac{EI}{2} \int_0^L \left(u''^2 + u''^2 u'^2 \right) ds \tag{52}$$

Hamilton's principle states that, of all the possible paths satisfying the prescribed initial and final configurations, the true path minimizes the following functional

$$\delta I = \int_{t_1}^{t_2} \left[\delta(\mathcal{L}) + \delta(W_{nc}) \right] dt = 0 \tag{53}$$

where t_1 and t_2 denote the initial and final time instants, and W_{nc} the work done by non-conservative forces such as damping, external forces and moments. In our case the expression for δW_{nc} is

$$\delta W_{nc} = \int_0^L \left(m a_b \cos(\Omega t) - c\dot{u} \right) \delta u \; ds \tag{54}$$

where a_b is the acceleration of the supported end of the beam, Ω is the excitation frequency and c is the linear damping coefficient. Here the damping term is taken into account resorting to the phenomenological linear effect of the dissipation forces.
Using the Hamilton's principle (53), we find the following equation of motion describing the in-plane transverse displacement $u(s,t)$

$$\begin{aligned} m\ddot{u} + c\dot{u} + EIu^{iv} &= -EI[u'(u'u'')']' + ma_b \cos(\Omega t) \\ &- \frac{m}{2} \left[u' \int_L^s \frac{\partial^2}{\partial t^2} \left(\int_0^s u'^2 ds \right) ds \right]' \end{aligned} \tag{55}$$

and the boundary conditions are

$$u(0,t) = 0, \qquad u'(0,t) = 0 \tag{56}$$

$$u''(L,t) = 0, \qquad u'''(L,t) = 0 \tag{57}$$

In the governing equation of motion (55) there are two type of nonlinearities: geometric and inertial. The geometric nonlinearity $[u'(u'u'')']'$ is due to the nonlinear change in curvature (50) and the inertial nonlinearity $\left[u' \int_l^s \frac{\partial^2}{\partial t^2} \left(\int_0^s u'^2 ds \right) ds \right]'$ is due to the inextensionality condition (45). For higher modes, the inertia nonlinearity is the dominant nonlinear term, whereas for the first mode, the geometric nonlinearity is the dominant nonlinear term.
For more details, see [Ph.D. Pramod Malatkar, Virginia Tech. 2003].

4.2 Single-mode response

The steel beam used in the experiment constitutes a lightly damped, weakly nonlinear system, and none of its modes is involved in an internal resonance with other modes. We, therefore, assume that the response of the beam consists essentially of one undamped linear mode whose natural frequency is close to the excitation frequency Ω. We refer to this mode as the nth mode whose natural frequency is ω_n. Other modes, not being directly or indirectly excited, will decay to zero with time due to the presence of damping [A. H. Nayfeh and D. T. Mook, Perturbation Methods, Wiley, New York (1979) and Ali H. Nayfeh, Nonlinear Interactions, Analytical, Computational and Experimental Methods, Wiley, New York, 2000].

The method of multiple scales (A.H. Nayfeh and D.T. Mook, 1979) is used to derive a first-order uniform expansion for the beam response governed by equations (55)-(57) under primary resonance.

Thus we scale the damping coefficient c and the forcing coefficient a_b appearing in Eq.(55) in terms of a small dimensionless parameter $\varepsilon(\leq 1)$ as follows

$$\frac{c_u}{2m} = \zeta\omega_n = \varepsilon^2\mu \tag{58}$$

$$a_b = \epsilon^3\hat{f} \tag{59}$$

where ζ is the dimensionless linear viscous damping factor corresponding to the nth mode. Also, we let

$$u(s,t;\varepsilon) = \varepsilon u_1(s,T_0,T_2) + \varepsilon^3 u_3(s,T_0,T_2) + ... \tag{60}$$

where the $T_n = \varepsilon^n t$ represent different time scales, T_0 being the fast-time scale and T_2 the slow-time scale. The derivatives with respect to t now take the form

$$\frac{d}{dt} = D_0 + \varepsilon\, D_1 + \varepsilon^2 D_2 + ... \tag{61}$$

$$\frac{d^2}{dt^2} = {D_0}^2 + 2\varepsilon D_0 D_1 + \varepsilon^2(2\, D_0 D_2 + {D_1}^2) + ... \tag{62}$$

where $D_n = \partial/\partial T_n$. For the natural frequencies, we use the experimental values instead of the theoretical ones. The model equation becomes after substituting Eqs.(58)-(59) into Eq.(55)

$$\begin{aligned} \ddot{u} + 2\varepsilon^2\mu\dot{u} + \frac{EI}{m}\left[u^{iv} + [u'(u'u'')']'\right] &= \varepsilon^3\hat{f}\cos(\Omega t) \\ &- \frac{1}{2}\left\{u'\int_L^s\left[\frac{\partial^2}{\partial t^2}\int_0^\xi {u'}^2 d\eta\right]d\xi\right\}' \end{aligned} \tag{63}$$

Inserting Eqs. (60)-(62) into Eq. (63) and equating coefficients of equal powers of ε, we obtain

Order $\mathcal{O}(\varepsilon)$:

$$\mathrm{D}_0^2 u_1 + \frac{EI}{m} u_0^{iv} = 0 \tag{64}$$

$$u_1 = 0 \qquad \text{and} \qquad u_1^{'} = 0 \qquad \text{at} \qquad s = 0 \tag{65}$$

$$u_1^{''} = 0 \qquad \text{and} \qquad u_1^{'''} = 0 \qquad \text{at} \qquad s = L \tag{66}$$

Order $\mathcal{O}(\varepsilon^3)$:

$$\begin{aligned} \mathrm{D}_0^2 u_3 + \frac{EI}{m} u_3^{iv} &= -D_0 D_2 u_1 - 2\mu D_0 u_1 - \frac{EI}{m}[u_1^{'}(u_1^{'} u_1^{''})']' \\ &\quad - \frac{1}{2}\left[u_1^{'} \int_L^s D_0^2 \left(\int_0^s u_1^{'2} ds\right) ds\right]' + \hat{f} cos(\Omega T_0) \end{aligned} \tag{67}$$

$$u_3 = 0 \qquad \text{and} \qquad u_3^{'} = 0 \qquad \text{at} \qquad s{=}0 \tag{68}$$

$$u_3^{''} = 0 \qquad \text{and} \qquad u_3^{'''} = 0 \qquad \text{at} \qquad s = L \tag{69}$$

Since we are seeking a single-mode response solution, the solution of the first order problem associated with Eqs. (64)-(66) is taken as

$$u_1(s, T_0, T_2) = (A(T_2) e^{i\omega_n T_0} + \bar{A}(T_2) e^{-i\omega_n T_0}) \Phi_n(s) \tag{70}$$

where $\omega_n = r_n^2 \sqrt{\frac{EI}{ml^4}}$, r_n is the nth root of the characteristic equation $1 + cos(r) cosh(r) = 0$, and $\Phi(s)$ denotes the normalized shape of the nth undamped linear vibration mode, which is given by the following expression

$$\Phi_n(s) = \frac{1}{\sqrt{L}} \left(\cosh \frac{r_n s}{L} - \cos \frac{r_n s}{L} + \frac{\cos r_n + \cosh r_n}{\sin r_n + \sinh r_n} (\sin \frac{r_n s}{L} - \sinh \frac{r_n s}{L})\right) \tag{71}$$

Substituting Eq. (70) into Eq. (67) yields

$$\begin{aligned} \mathrm{D}_0^2 u_3 &+ \frac{EI}{m} u_3^{iv} = -2i\omega_n \Phi_n D_2 A e^{i\omega_n T_0} - 2i\omega_n \Phi_n A e^{i\omega_n T_0} + \frac{1}{2} \hat{f} e^{i\Omega T_0} \\ &- \frac{EI}{m} [\Phi_n^{'}(\Phi_n^{'} \Phi_n^{''})']' (A^3 e^{3i\omega_n T_0} + 3A^2 \bar{A} e^{i\omega_n T_0}) \\ &+ 2\omega_n^2 \left(\Phi_n^{'} \int_L^s \int_0^s \Phi_n^{'2} ds ds\right)' (A^3 e^{3i\omega_n T_0} + A^2 \bar{A} e^{i\omega_n T_0}) + cc \end{aligned} \tag{72}$$

Here we restrict our discussion to the case of primary resonance of the nth mode i.e., $\Omega = \omega_n + \varepsilon^2 \sigma$, where $\varepsilon^2 \sigma$ is measuring the deviation from the exact primary resonance. Since the

homogeneous problem associated with Eq (72) has nontrivial solutions, the nonhomogeneous problem has a solution only if the right-hand side of Eq.(72) is orthogonal to every solution of the adjoint homogeneous problem [Ali H. Nayfeh and P. Frank Pai, *Linear and Nonlinear Structural Mechanics*, Wiley-Interscience, 2004]. Therefore, demanding that the right-hand side of Eq. (72) be orthogonal to $\Phi_n(s)\exp(-i\omega_n T_0)$, we obtain the following solvability condition

$$-2i\omega_n(D_2A+\mu A)-2\alpha A^2\bar{A}+\frac{1}{2}fe^{i\sigma T_2}=0 \tag{73}$$

where

$$\begin{aligned} f &= \hat{f}\int_0^L \Phi_n(s)ds \\ \alpha &= \frac{3EI}{m}\int_0^L \Phi_n^{'}(s)^2\Phi_n^{''}(s)^2ds-\omega_n^2\int_0^L\left(\int_0^s \Phi_n^{'}(s)^2ds\right)^2ds \end{aligned} \tag{74}$$

The first term in the expression of α is due to the contribution of the geometric nonlinearity which is hardening. The second term is due to the inertial nonlinearity which is softening. The effect of inertial nonlinearities is increasing with the increase of the order n of the mode. Substituting the polar form

$$A=\frac{1}{2}ae^{i(\sigma T_2-\gamma)} \tag{75}$$

into the solvability condition (73), and separating real and imaginary parts, we obtain the following autonomous modulation equations of the amplitude a and the phase γ

$$a^{'} = -\mu a+\frac{f}{2\omega_n}\sin\gamma \tag{76}$$

$$a\gamma^{'} = \sigma a-\frac{\alpha}{4\omega_n}a^3+\frac{f}{2\omega_n}\cos\gamma \tag{77}$$

where the prime indicates differentiation with respect to T_2. We set the right-hand sides of Eqs. (76) and (77) equal to zero, which gives the following two equations that will be used to obtain the frequency-response and force-response diagrams, respectively:

$$\sigma_{\mp}=\frac{\alpha}{4\omega_n}a^2\mp\sqrt{\frac{f^2}{4\omega^2a^2}-\mu^2} \tag{78}$$

$$f=2\omega_n a\sqrt{\mu^2+\left(\sigma-\frac{\alpha}{4\omega_n}a^2\right)^2} \tag{79}$$

The beam response is given by

$$u(s,t;\varepsilon)=\varepsilon a(t)\cos(\omega-\gamma)\Phi_n(s)+... \tag{80}$$

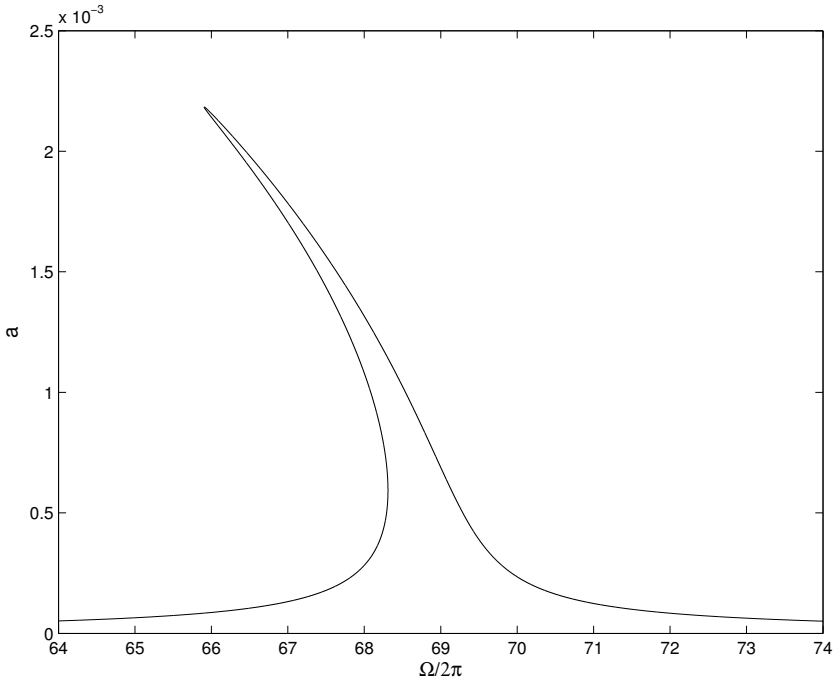

Figure 28: Frequency-response curve of the third-mode using equation (78) when $a_b = 100m/s^2$.

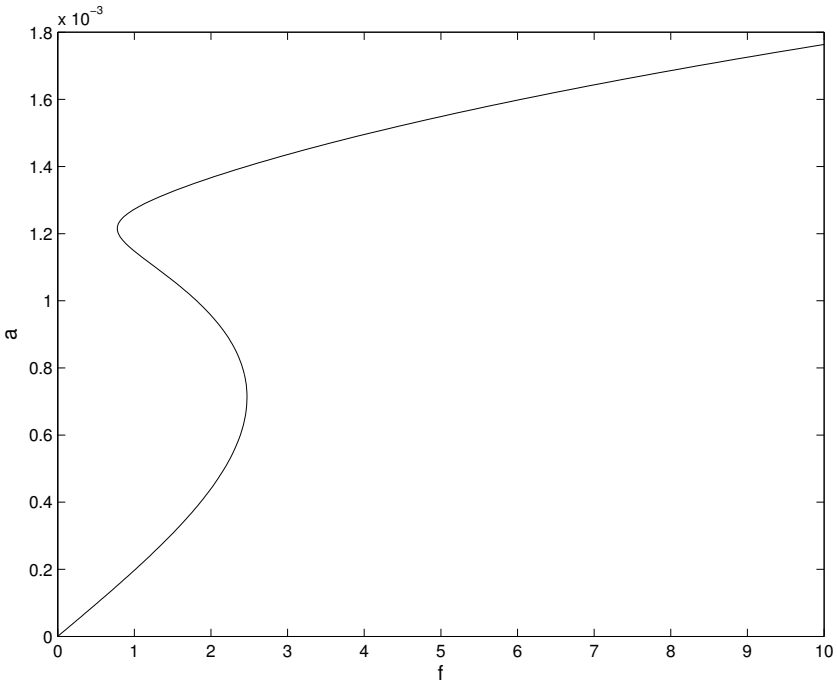

Figure 29: Theoretically obtained third mode force-response curve using equation (79) for $\Omega = 68Hz$.

In figure 28, the softening character of the nonlinearities is shown near the third mode. This effect is also found experimentally see Fig.3.

In figure 29, the force response curve of the third mode given by equation (79) for $\Omega = 68Hz$ is shown. Nonlinear effects are present: coexistence of three solutions and hysteresis phenomenon. The same analysis can be done for all the other modes. Future works will focus on the identification of nonlinear parameters such as damping and stiffness through experiment and theory.

4.3 Multi-modes response

In order to investigate the experimentally observed modal interactions (see section 3.3), the equations of motion (55)-(57) are non-dimensionalized by applying the following scalings:

$$\begin{aligned} s^* &= \frac{s}{L}, \qquad u^* = \frac{u}{L}, \qquad t^* = \omega_n t, \\ \mu &= \frac{cL^2}{r_n^2\sqrt{mEI}}, \qquad F = \frac{ma_bL^3}{EIr_n^4} \end{aligned} \tag{81}$$

Here we have used the length L of the beam as the characteristic length and the inverse of the nth natural frequency $\omega_n = r_n^2\sqrt{EI/mL^4}$ as the characteristic time. The r_n is the nth root of the characteristic equation $1 + \cos(r)cosh(r) = 0$. Then, in nondimensional form, the governing equation and boundary conditions (55)-(57) become after dropping the stars,

$$\begin{aligned} \ddot{u} + \mu\dot{u} + \frac{1}{r_n^4}u^{iv} &= F\cos(\Omega t) - \frac{1}{r_n^4}[u'(u'u'')']' \\ &- \frac{1}{2}\left\{u'\int_1^s [\frac{\partial^2}{\partial t^2}\int_0^\xi u'^2 d\eta]d\xi\right\}' \end{aligned} \tag{82}$$

$$u = 0 \quad \text{and} \quad u' = 0 \quad \text{at} \quad s = 0 \tag{83}$$

$$u'' = 0 \quad \text{and} \quad u''' = 0 \quad \text{at} \quad s = 1 \tag{84}$$

Applying the Galerkin method to equation (82) after expanding the response in terms of a series of the normalized undamped linear mode shapes $\phi_n(s)$, leads to the following system of N ODEs

$$\begin{aligned} \ddot{u}_n + \mu_n\dot{u}_n + \omega_n^2 u_n &= f_n\cos(\Omega t) + \sum_i g_{ni}u_i + \sum_{i,j,k}\Lambda_{nijk}u_iu_ju_k \\ &+ \sum_{i,j,k}\Gamma_{nijk}u_k(\ddot{u}_iu_j + 2\dot{u}_i\dot{u}_j + u_i\ddot{u}_j), \quad n = 1, 2, ..., N \end{aligned} \tag{85}$$

where

$$\Lambda_{nijk} = \frac{1}{r_n^4}\int_0^1 \phi_n'\phi_i'(\phi_j''\phi_k'' + \phi_j'\phi_k''')ds \tag{86}$$

$$\Gamma_{nijk} = -\frac{1}{2}\int_0^1 (\int_0^s \phi_n'\phi_k' ds)(\int_0^s \phi_i'\phi_j' ds)ds \tag{87}$$

are the coefficients of the cubic geometric and inertia nonlinearity terms, respectively, and

$$\mu_n = \int_0^1 \mu\phi_n^2 ds, \quad f_n = \int_0^1 F\phi_n ds, \quad \sum_{i,j,k} = \sum_i \sum_j \sum_k \tag{88}$$

In this section we consider the transfer of energy between the third mode and the first one. Thus, the third natural frequency ω_3 is used as a characteristic time. We retain the first four modes in the expression of $u(s,t)$; that is, $N = 4$. Since the resulting system of ODEs is stiff, as the first mode evolves on a slow scale while the third and fourth modes evolve on a fast scale, the Gear algorithm is used for numerical resolution. The resulting motion is expressed as $u(s,t) = \sum_{i=1}^{4} u_i(t)\phi_i(s)$.

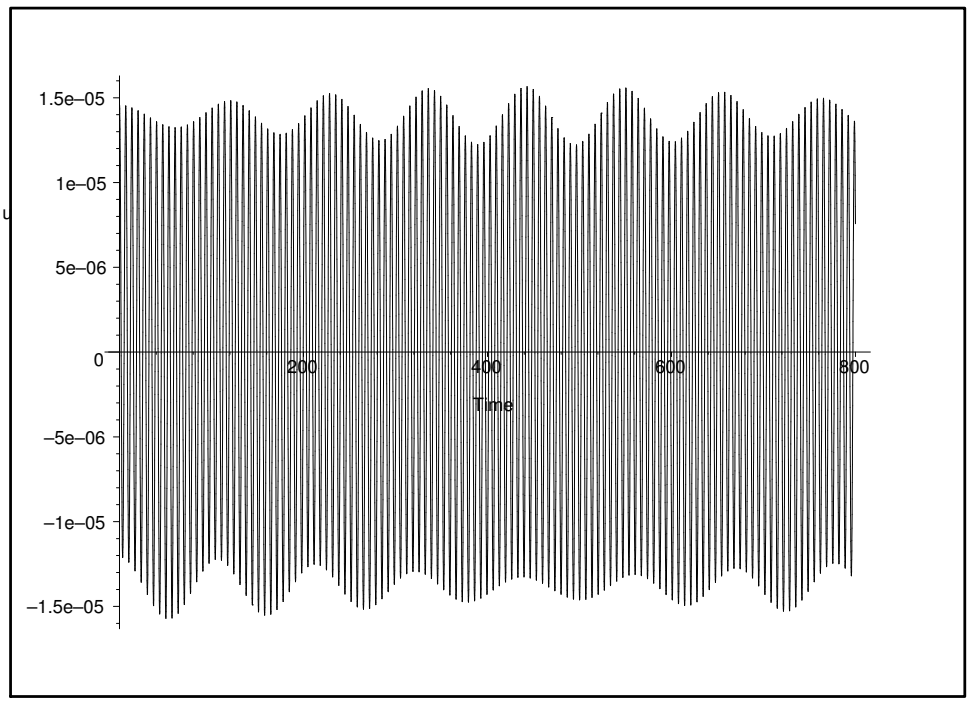

Figure 30: Displacement time trace of Eq. (85) for $a_b = 0.8$ and $\Omega = 0.936$.

In Fig. 30 is shown a coupled motion including the third and the first modes. In Fig. 31 is shown an apparently chaotic motion.

The same procedure can be used to study the transfer of energy from the fourth mode.
Some future perspectives of this research are

1. the study of the coupled system of ODEs (85) using perturbation methods in order to have an insight on possible dynamics and their regions of existence in the space of parameters,

2. the formulation of a theoretical model taking into account the coupled motion of the in-plane and out-of-plane flexural modes observed experimentally in the subsection 3.3.2,

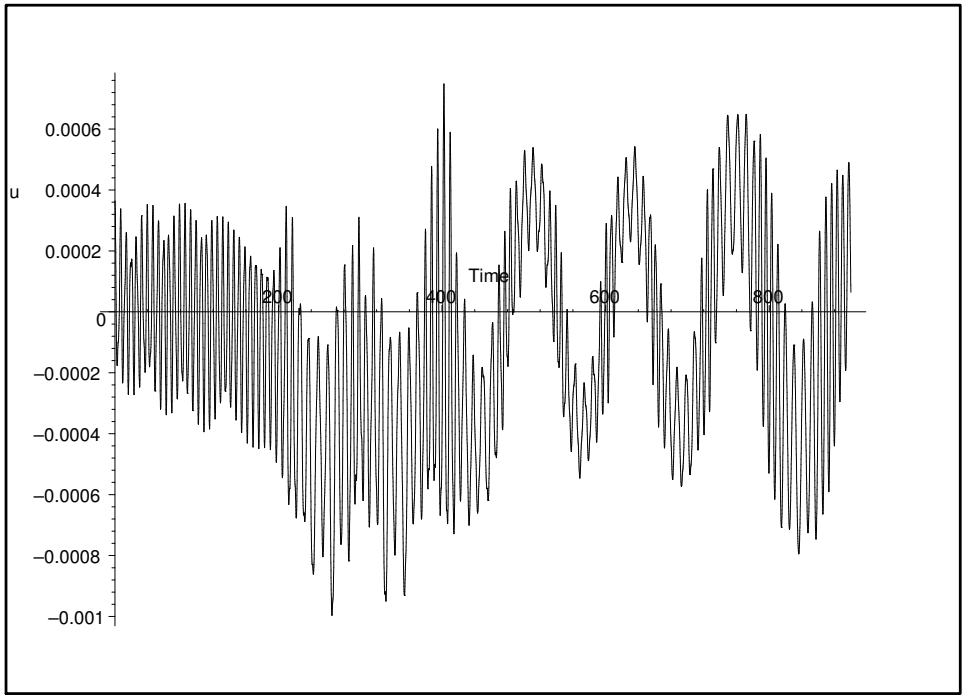

Figure 31: Displacement time trace of Eq. (85) for $a_b = 0.98$ and $\Omega = 1.4$.

5 Rapid forcing of elastic structures and control with time delay

5.1 Effect of rapid forcing and time delay on the dynamics of an elastic beam

Consider a controlled simply-supported beam subjected to an axial high-frequency excitation having the form $a\Omega^2 cos(\Omega t)$ where a is a non-dimensional amplitude of excitation and Ω is the excitation frequency (see Fig. 32). The control consists of a proportional position feedback with a time delay. The equation of motion governing small transverse deflections $w(x,t)$ of the beam

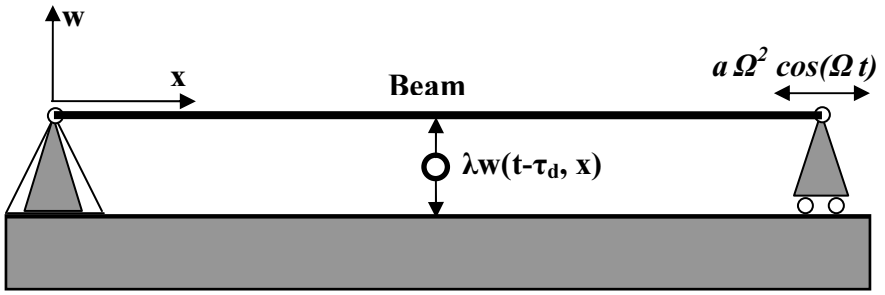

Figure 32: representation of the beam

can be written in the dimensionless form as

$$\ddot{w} + \frac{\eta}{\pi^2}\dot{w}'''' + \frac{1}{\pi^4}w'''' + \lambda w(x, \tau - \tau_d) = w'' a\Omega^2 cos(\Omega\tau) \tag{89}$$

with the boundary conditions

$$w = 0 \ \text{ and } \ w'' = 0 \ \text{ at } \ x = 0 \tag{90a}$$

$$w = 0 \ \text{ and } \ w' = 0 \ \text{ at } \ x = 1 \tag{90b}$$

where η is the internal damping, λ and τ_d represent the gain and time delay, a and Ω denote the amplitude and frequency of the fast excitation, and $\tau = \omega_1 t$ is the dimensionless time. The characteristic frequency corresponding to the first natural frequency of the structure is $\omega_1 = (\frac{\pi}{l})^2\sqrt{\frac{EI}{m}}$, where l, EI and m are the length, the constant bending stiffness and the mass of beam, respectively. The transverse deflection $w(x, \tau)$ can be represented as

$$w(x, \tau) = \sum_{k=1}^{N} w_k(\tau) sin(k\pi x) \tag{91}$$

The equation of motion for the desired number of modes can be derived by substituting Eq. (91) into Eq. (89) and by performing the Galerkin's method. This yields the set of equations

$$\ddot{w}_k + \eta_k \dot{w}_k + k^4 w_k + \lambda w_k(\tau - \tau_d) = w_k a_k \Omega^2 cos(\Omega\tau) \tag{92}$$

where $\eta_k = \eta(k^2\pi)^2$ and $\Lambda_{kmnl} = (m\pi^2)^2 nl \left(\int_0^1 \sin(k\pi x)\sin(m\pi x)dx\right)\left(\int_0^1 \cos(n\pi x)\cos(l\pi x)dx\right)$ are the kth internal damping and the coefficient of the modal interaction, respectively, and $a_k = (k\pi)^2 a$.

We apply the method of direct partition of motion (DPM) [8] to separate between the slow and fast dynamics of the individual oscillation modes. This provides the main autonomous equation governing the slow motion of the considered mode. We introduce two time scales: a fast time $T_0 = \Omega\tau = \epsilon^{-1}\tau$ and a slow time $T_1 = \tau$, and we seek the solution $w_k(T_0, T_1)$ in the uniformly valid expansion to the order ϵ^2 having the form

$$w_k(T_0, T_1) = z_k(T_1) + \epsilon\phi_{1k}(T_0, T_1) + \epsilon^2\phi_{2k}(T_0, T_1) + O(\epsilon^3) \tag{93}$$

The time derivatives is transformed according to $d/d\tau = \epsilon^{-1}D_0 + D_1 \quad \text{and} \quad d^2/d\tau^2 = \epsilon^{-2}D_0^2 + 2\epsilon^{-1}D_0D_1 + D_1^2$ where $D_i^j \equiv \partial^j/\partial T_i^j$. Assume that the coefficient $a_k\Omega$ is the order ϵ^0. The first term of the expansion, $z_k(T_1)$, describes the slow main motion of the considered mode, whereas the ϕ-terms stand for small overlays of fast motion. The fast component $\epsilon\phi_{ik}$ is considered to be

small compared to the slow oscillation. Using the DPM technique we obtain the following main equation governing the slow components $z_k(T_1)$ of $w_k(T_0, T_1)$

$$D_1^2 z_k + \eta_k D_1 z_k + \left(k^4 + \frac{(a_k\Omega)^2}{2}\right) z_k + \lambda z_k(T_1 - \tau_d) = 0 \tag{94}$$

The natural frequencies of the slow motion for the case of undamped undelayed oscillations is [6]

$$\omega_k = k^2\sqrt{1 + \pi^4\frac{(a\Omega)^2}{2}} \tag{95}$$

5.1.1 Modal analysis and stability chart

The linear equation corresponding to Eq. (94) reads

$$\ddot{z_k} + \eta_k \dot{z_k} + \omega_k^2 z_1 + \lambda z_k(T_1 - \tau_d) = 0 \tag{96}$$

The corresponding transcendental characteristic equation is given by

$$s^2 + \eta_k s + \omega_k^2 + \lambda e^{-\tau_d s} = 0 \tag{97}$$

This equation possesses infinitely many finite roots for $\lambda \neq 0$ and $\tau_d \neq 0$. To achieve stability, two dominant roots of Eq. (97) should be placed on the imaginary axis at the desired resonant frequency, while other roots remain in the stable left-half of the complex plane. The imaginary characteristic roots are $s = \pm i\omega_c$, where ω_c is the resonance frequency and $i = \sqrt{-1}$. The subscript c implies the crossing of the root loci on the imaginary axis. Substituting $s = \pm i\omega_c$ into Eq. (97) and solving for the control parameters λ_c and τ_{dc} yields

$$\lambda_c = \sqrt{((\omega_k^2 - \omega_c^2)^2 + (\eta_k\omega_c)^2)} \tag{98}$$

and

$$\tau_{dc} = \frac{1}{\omega_c}\left\{\arctan\left[\frac{\eta_k\omega_c}{\omega_k^2 - \omega_c^2}\right] + 2(\ell - 1)\pi\right\}, \quad \ell = 1, 2, 3... \tag{99}$$

where ℓ corresponds to the ℓth branch.

The natural undelayed frequencies, Eq. (95), and the natural delayed frequencies $\omega_{ck}\pm = \sqrt{k^4(1 + \pi^4\frac{(a\Omega)^2}{2}) \pm \lambda^2}$ of the slow motion are shown in Fig. 33 for the first three modes versus fast excitation force intensity. The critical value of the feedback gain must satisfy the condition $\lambda \leq \sqrt{k^4(1 + \pi^4\frac{(a\Omega)^2}{2})}$ for each kth mode. This figure shows the influence of the time delay on the natural frequencies. It can be seen that each natural frequency spectrum is splited into two branches which come closer to the undelayed natural spectrum (dashed line) for large excitation

force intensity. The splitting is more visible for the low frequencies. This result suggests that the delayed beam may have, for the same excitation, two possible harmonic vibrations. Moreover, by increasing the gain λ, the gap between the two splited branches increases (Fig. 33b).

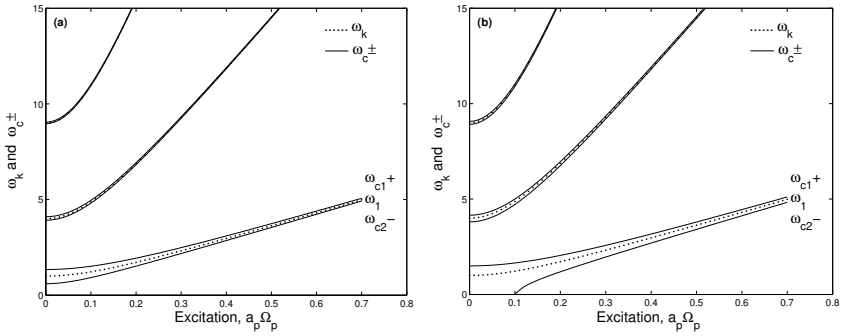

Figure 33: The first three undelayed natural frequencies (dashed line) and the corresponding delayed frequencies (solid line) vs fast excitation force intensity; (a) $\lambda = 0.8$ and (b) $\lambda = 1.24$.

The stability chart is presented in Fig. 34a for fixed $\eta_1 = 0.067$, $a_1 = 0.02$ and $\Omega = 100$. The dashed region corresponds to the stability domain of the trivial equilibrium of the mode beam.

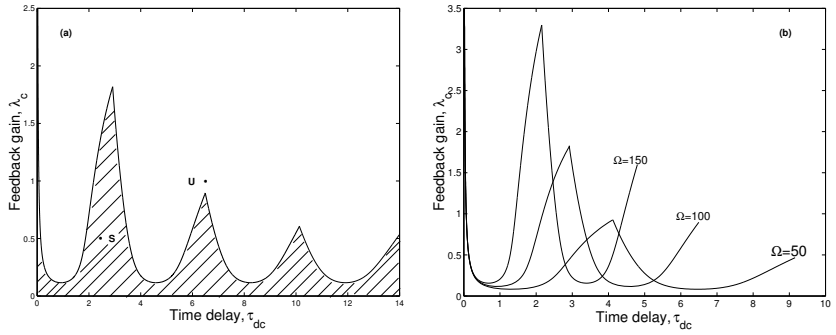

Figure 34: (a) Stability chart of the trivial solution of Eq. (96); $\eta_1 = 0.067$, $a_1 = 0.02$. $\Omega = 100$. (b) Effect of varying Ω on the stability chart.

In Fig. 34b, we show the effect of the high-frequency excitation Ω on the stability chart. As a result, the stability domain increases, the lobes shift right and the peaks maxima increase. Finally, Fig. 35 illustrates numerical time traces integration of Eq. (96) using *dde*23 [9] of the slow component $z_1(\tau)$ for the two operating points S and U selected in the stable and unstable zones in Fig. 34, respectively.

Results show that a fast harmonic excitation can increase and shift the stability domain of the trivial equilibrium (Fig. 34). It was also shown that the delay can cause the natural frequency spectrum to split into two branches offering the possibility for the system to have, for the same

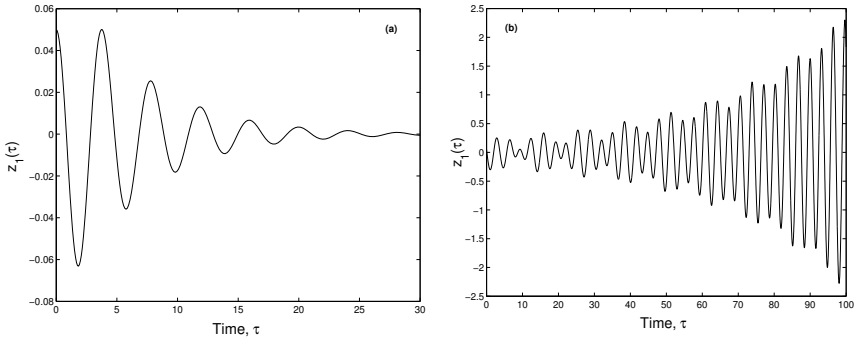

Figure 35: The time trace of slow component $z_1(\tau)$ response corresponding to points S and U in Fig. 34; (a) $\lambda_c = 0.5, \tau_{dc} = 2.4$ and (b) $\lambda_c = 1, \tau_{dc} = 6.6$.

excitation, two harmonic motions (Fig. 33). The gap between the two branches increases by increasing the amplitude of the delay.

5.2 Rapid forcing in a delayed self excited system

5.2.1 Partition of motion and averaging

Vibrations of pendulum with time delay subjected to a horizontal parametric forcing and to a self-excitation can be described in non-dimensional form by the following equation

$$\frac{d^2x}{dt^2} - (\alpha - \beta x^2)\frac{dx}{dt} + \sin\, x = a\Omega^2\, cos\, x \cos\, \Omega t + \lambda x(t-T) \tag{100}$$

where the parameters α and β are assumed to be small, a is the excitation amplitude, Ω is the parametric excitation frequency, and the parameters λ and T are the amplitude of the delay and the delay period, respectively. Eq. (100) has relevance to regenerative effect in high-speed milling.

We focus the analysis on small vibrations around the origin by expanding in Taylor's series up to the third-order terms $sinx \simeq x - \delta x^3$ and $cosx \simeq 1 - \gamma x^2$ where the coefficients $\delta = 1/6$ and $\gamma = 1/2$. Eq. (100) becomes

$$\frac{d^2x}{dt^2} - (\alpha - \beta x^2)\frac{dx}{dt} + (x - \delta x^3) = a\Omega^2(1 - \gamma x^2)\cos\Omega t + \lambda\, x(t-T) \tag{101}$$

To implement the method of DPM, we introduce two different time-scales: a fast time $T_0 \equiv \Omega t$ and a slow time $T_1 \equiv t$, and we split up $x(t)$ into a slow part $z(T_1)$ and a fast part $\epsilon\varphi(T_0, T_1)$ as follows

$$x(t) = z(T_1) + \epsilon\varphi(T_0, T_1) \tag{102}$$

and

$$x(t-T) = z(T_1 - T) + \epsilon\varphi(T_0 - \Omega T, T_1 - T) \tag{103}$$

where z describes slow main motions at time-scale of oscillations of the pendulum, and $\epsilon\varphi$ stands for an overlay of the fast motions. In Eqs. (102) and (103), ϵ indicates that $\epsilon\varphi$ is small compared to z. Since Ω is considered as a large parameter we choose $\epsilon \equiv \Omega^{-1}$, for convenience. The fast part $\epsilon\varphi$ and its derivatives are assumed to have a zero T_0-average, so that $< x(t) >= z(T_1)$ and $< x(t-T) >= z(T_1 - T)$ where $<>\equiv \frac{1}{2\pi}\int_0^{2\pi}()\, dT_0$ defines time-averaging operator over one period of the fast excitation with the slow time T_1 fixed. Inserting (102) and (103) into (101) and introducing $D_i^j \equiv \frac{\partial^j}{\partial^j T_i}$ yields

$$\begin{aligned} D_1^2 z &+ \epsilon D_1^2\varphi + 2D_0D_1\varphi - \alpha(D_1 z + \epsilon D_1\varphi + D_0\varphi) + \beta(z^2 D_1 z + \epsilon z^2 D_1\varphi \\ &+ z^2 D_0\varphi + 2\epsilon z\varphi D_1 z + 2\epsilon z\varphi D_0\varphi) + z + \epsilon\varphi - \delta(z^3 + 3\epsilon z^2\varphi) \\ &= \epsilon^{-1}(a\Omega) z\, cosT_0 - \epsilon^{-1}(a\Omega)\gamma z^2\, cosT_0 - 2(a\Omega)\gamma z\varphi\, cosT_0 - \epsilon(a\Omega)\gamma\varphi^2\, cosT_0 \\ &+ \lambda z(T_1 - T) + \epsilon\lambda\varphi(T_0 - \Omega T, T_1 - T) \end{aligned} \tag{104}$$

Averaging (104) leads to

$$\begin{aligned} D_1^2 z - \alpha D_1 z + \beta z^2 D_1 z + z - \delta z^3 &= -2(a\Omega)\gamma z < \varphi\, cosT_0 > \\ &- \epsilon(a\Omega)\gamma < \varphi^2 cosT_0 > + \lambda z(T_1 - T) \end{aligned} \tag{105}$$

Subtracting (105) from (104), an approximate expression for $\epsilon\varphi$ is obtained by considering only the dominant terms of order ϵ^{-1} as

$$D_0^2\varphi = a\Omega(1 - \gamma z^2) cosT_0 \tag{106}$$

where it is assumed that $a\Omega = O(\epsilon^0)$. The stationary solution to the first order for φ is written as

$$\varphi = -a\Omega(1 - \gamma z^2) cosT_0 \tag{107}$$

Retaining the dominant terms of order ϵ^0 in Eq. (105), inserting φ from (107) and using that $< cos^2 T_0 >= 1/2$ gives

$$D_1^2 z - (\alpha - \beta z^2) D_1 z + (1 - (a\Omega)^2 \gamma) z + ((a\Omega\gamma)^2 - \delta) z^3 = \lambda z(t - T) \tag{108}$$

The autonomous Eq. (108) governing the slow dynamic of the motion can be examined through analytical predictions.
We apply the averaging method [10, 11] by introducing a small parameter μ such that $\alpha = \mu\tilde{\alpha}$, $\beta = \mu\tilde{\beta}$, $\gamma = \mu\tilde{\gamma}$, $\delta = \mu\tilde{\delta}$ and $\lambda = \mu\tilde{\lambda}$. Then, Eq. (108) reads

$$\ddot{z} - \mu(\tilde{\alpha} - \tilde{\beta} z^2)\dot{z} + \omega_0^2 z + (\mu^2 (a\Omega)^2 \tilde{\gamma}^2 - \mu\tilde{\delta}) z^3 = \mu\tilde{\lambda} z(t - T) \tag{109}$$

where $\dot{z} = \frac{dz}{dt}$ and $\omega_0^2 = (1 - (a\Omega)^2 \gamma)$. In the case $\mu = 0$, Eq. (10) reduces to

$$\ddot{z}(t) + \omega_0^2 z(t) = 0 \tag{110}$$

with the solution

$$z(t) = R\, cos(\omega_0 t + \phi), \quad \dot{z}(t) = -R\, \omega_0 sin(\omega_0 t + \phi) \tag{111}$$

For $\mu > 0$, a solution is sought in the form (111) with R and ϕ time dependent. Variations of parameters gives the following equations on $R(t)$ and $\phi(t)$:

$$\begin{aligned} \dot{R}(t) = &-\frac{\mu}{\omega_0} sin(\omega_0 t + \phi)\, F_1(R\, cos(\omega_0 t + \phi), -\omega_0 R\, sin(\omega_0 t + \phi), t) \\ &-\frac{\mu^2}{\omega_0} sin(\omega_0 t + \phi)\, F_2(R\, cos(\omega_0 t + \phi), -\omega_0 R\, sin(\omega_0 t + \phi), t) \end{aligned} \tag{112}$$

$$\begin{aligned} \dot{\phi}(t) = &-\frac{\mu}{\omega_0 R} cos(\omega_0 t + \phi)\, F_1(R\, cos(\omega_0 t + \phi), -\omega_0 R\, sin(\omega_0 t + \phi), t) \\ &-\frac{\mu^2}{\omega_0 R} cos(\omega_0 t + \phi)\, F_2(R\, cos(\omega_0 t + \phi), -\omega_0 R\, sin(\omega_0 t + \phi), t) \end{aligned} \tag{113}$$

where

$$F_1(z,\dot{z},t) = (\tilde{\alpha} - \tilde{\beta}z^2)\dot{z} + \tilde{\delta}z^3 + \tilde{\lambda}z(t-T) \tag{114}$$

and

$$F_2(z,\dot{z},t) = -(a\Omega)^2\tilde{\gamma}^2 z^3 \tag{115}$$

with $z(t)$ is given by (111). Using the averaging method [10, 11] for small μ and replacing the right-hand sides of (112) and (113) by their averages over one 2π period, since Eq. (109) is autonomous, we obtain:

$$\dot{R} \approx -\frac{\mu}{\omega_0}\frac{1}{2\pi}\int_0^{2\pi} sin(\omega_0 t + \phi)F_1.dt - \frac{\mu^2}{\omega_0}\frac{1}{2\pi}\int_0^{2\pi} sin(\omega_0 t + \phi)F_2.dt \tag{116}$$

$$\dot{\phi} \approx -\frac{\mu}{\omega_0 R}\frac{1}{2\pi}\int_0^{2\pi} cos(\omega_0 t + \phi)F_1.dt - \frac{\mu^2}{\omega_0 R}\frac{1}{2\pi}\int_0^{2\pi} cos(\omega_0 t + \phi)F_2.dt \tag{117}$$

in which

$$F_1 = -(\tilde{\alpha} - \tilde{\beta}z^2)\,\omega_0 R\, sin(\omega_0 t + \phi) + \tilde{\delta}R^3\, cos(\omega_0 t + \phi)^3 + \tilde{\lambda}\tilde{R}\, cos(\omega_0 t - \omega_0 T + \tilde{\phi}) \tag{118}$$

and

$$F_2 = -(a\Omega)^2\tilde{\gamma}^2 R^3\, cos(\omega_0 t + \phi)^3 \tag{119}$$

with $\tilde{R} = R(t-T)$ and $\tilde{\phi} = \phi(t-T)$. Evaluating the integrals in (116) and (117) yields

$$\dot{R} = \mu\Big(\frac{\tilde{\alpha}}{2}R - \frac{\tilde{\beta}}{8}R^3 - \frac{\tilde{\lambda}}{2}\frac{\tilde{R}}{\omega_0}\, sin(\omega_0 T - \tilde{\phi} + \phi)\Big) \tag{120}$$

$$\dot{\phi} = \mu\Big(-\frac{3\tilde{\delta}}{8}\frac{R^2}{\omega_0} - \frac{\tilde{\lambda}}{2}\frac{\tilde{R}}{\omega_0 R}\, cos(\omega_0 T - \tilde{\phi} + \phi)\Big) + \mu^2\Big(\frac{3\tilde{\gamma}^2}{8}\frac{(a\Omega)^2R^2}{\omega_0}\Big) \tag{121}$$

Eqs. (120) and (121) show that $\dot{R}$ and $\dot{\phi}$ are $O(\mu)$. We expand in Taylor's series $\tilde{R}$ and $\tilde{\phi}$ as

$$\tilde{R} = R(t-T) = R(t) - T\dot{R}(t) + \frac{1}{2}T^2\ddot{R}(t) + \dots \tag{122}$$

$$\tilde{\phi} = \phi(t-T) = \phi(t) - T\dot{\phi}(t) + \frac{1}{2}T^2\ddot{\phi}(t) + \dots \tag{123}$$

Then, we replace $\tilde{R}$ and $\tilde{\phi}$ by $R(t)$ and $\phi(t)$ in Eqs. (120) and (121) since $\dot{R}$ and $\dot{\phi}$ and $\ddot{R}$ and $\ddot{\phi}$ are of $O(\mu)$ and $O(\mu^2)$, respectively [12]. This approximation reduces the infinite dimensional problem into a finite dimensional one by assuming μT is small.
After substituting the above approximation into (120) and (121), we obtain the following slow flow

$$\dot{R} = (\frac{\alpha}{2} - \frac{\lambda}{2\omega_0}\, sin\, \omega_0 T)\, R - \frac{\beta}{8}\, R^3 \tag{124}$$

$$\dot{\phi} = -\frac{\lambda}{2\omega_0}\, cos\, \omega_0 T + \frac{3}{8\omega_0}\, (\gamma^2 (a\Omega)^2 - \delta)\, R^2 \tag{125}$$

5.2.2 Equilibria and self-excited oscillations

The equilibrium points in Eqs. (124) and (125), corresponding to the periodic motions in the original system (108), are obtained by setting $\dot{R} = \dot{\phi} = 0$. This gives the two equilibria

$$R = 0, \quad R = \sqrt{\frac{8}{\beta}\, (\frac{\alpha}{2} - \frac{\lambda}{2\omega_0}\, sin\, \omega_0 T)} \tag{126}$$

The solution $R = \sqrt{\frac{8}{\beta}\, (\frac{\alpha}{2} - \frac{\lambda}{2\omega_0}\, sin\omega_0 T)}$ corresponding to a periodic motion is real if

$$\frac{\alpha}{2} - \frac{\lambda}{2\omega_0}\, sin\omega_0 T \, \geq \, 0 \tag{127}$$

By setting $\omega_0 = \sqrt{1 - (a\Omega)^2\gamma}$, Eq. (28) becomes

$$sin(\sqrt{1 - (a\Omega)^2\gamma}\, T) \, \leq \, \frac{\alpha}{\lambda}\, \sqrt{1 - (a\Omega)^2\gamma} \tag{128}$$

The above inequality provides the two following conditions, denoted by (CI), corresponding to

the birth of the limit cycle

$$T < \frac{1}{\sqrt{1-(a\Omega)^2\gamma}}\, arcsin(\frac{\alpha}{\lambda}\sqrt{1-(a\Omega)^2\gamma}) \tag{129}$$

and

$$T > \frac{1}{\sqrt{1-(a\Omega)^2\gamma}}\,(\pi - arcsin(\frac{\alpha}{\lambda}\sqrt{1-(a\Omega)^2\gamma})) \tag{130}$$

On the other hand, to find the frequency of the limit cycle, we let $\theta = \omega_0 t + \phi$ denote the argument of the cosine in Eq. (12). Then the frequency of the limit cycle is

$$\omega = \frac{d\theta}{dt} = \omega_0 + \frac{d\phi}{dt} \tag{131}$$

Using Eq. (125) yields

$$\omega = \omega_0 - \frac{\lambda}{2\omega_0}\, cos\,\omega_0 T + \frac{3}{8\omega_0}\,(\gamma^2(a\Omega)^2 - \delta)\, R^2 \tag{132}$$

Eq. (132) gives a relation between the frequency of the limit cycle ω, the excitation frequency Ω, with $\omega_0 = \sqrt{1-(a\Omega)^2\gamma}$, and the delay period T. A condition for the existence of the limit cycle is guaranteed when ω is positive, which means that the following conditions, denoted by (CII), obtained from Eq. (132) must be satisfied

$$T < \frac{-i}{\omega_0}\, ln\Big(\frac{EF - i\sqrt{F^2(G^2+F^2-E^2)}}{F(-G+iF)}\Big) \tag{133}$$

and

$$T > \frac{-i}{\omega_0}\, ln\Big(\frac{EF + i\sqrt{F^2(G^2+F^2-E^2)}}{F(-G+iF)}\Big) \tag{134}$$

where $E = \omega_0^2 + \frac{3\alpha}{2\beta}(\gamma(1-\omega_0^2) - \delta)$, $F = \frac{3\lambda}{2\beta\omega_0}(\gamma(\omega_0^2 - 1) + \delta)$, $G = -\frac{\lambda}{2}$ and $i = \sqrt{-1}$.
A third condition (CIII) obtained from the expression of ω_0 reads

$$\Omega < \frac{1}{a\sqrt{\gamma}} \tag{135}$$

This condition (CIII) as well as the conditions (CI), Eqs. (129) and (130), and (CII), Eqs. (133) and (134), are plotted in Fig. 36. These three combined conditions delimit the region of suppression of limit cycles in the parameter plane (T, Ω). Results obtained by numerical integration (squares) done in Matlab by using the integrating function dde23 [9] are also reported. As it can be seen in Fig. 36, the region (B) where self-excited oscillations are absent increases by increasing the delay amplitude λ. For large values of delay amplitude λ, self-oscillations can be suppressed for moderate values of Ω in the vicinity of $T = \frac{\pi}{2}$. In contrast, the case without delay requires large values of Ω to suppress limit cycle. Indeed, Fig. 36(b) shows that for $T = 0$, the limit cycle disappears for $\Omega = 70.7$ and for $T = \frac{\pi}{2}$ the limit cycle vanishes for $\Omega = 32.8$.
Phase portraits of slow dynamics (Eq. (108), Fig. 37(a-b)) and time histories of the corresponding full motion (Eq. (2), Fig. 2(c-d)) are shown in Fig. 2 for $\lambda = 0.3$, $T = 2.5$ and for different values of Ω. This illustrates the elimination of the limit cycle as we move from region A to region B, in Fig. 1. Similar phase portraits and time histories are shown in Fig. 3 for $\lambda = 0.3$ and $T = 0.5$. Phase portraits and time histories in Figs. 2 and 3 are obtained by numerical integration [9].

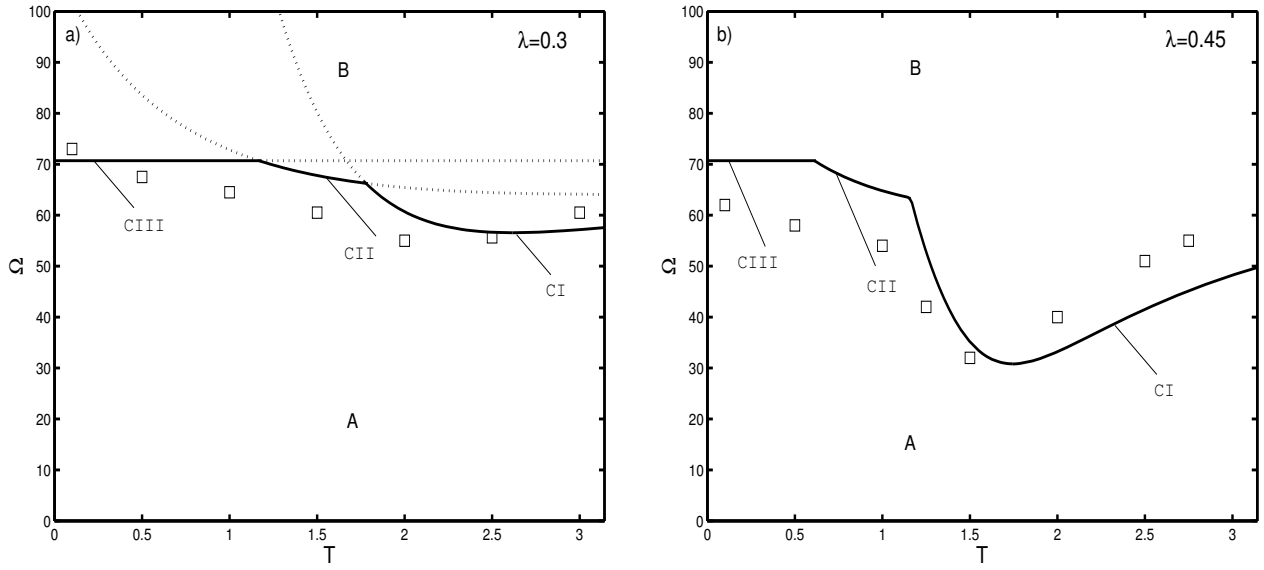

Figure 36: Comparison between analytical results (solid line) based on conditions CI, CII, and CIII and numerical integration (squares) of the original system, Eq. (2), for $a = 0.02$, $\alpha = \beta = \gamma = 0.5$, $\delta = 1/6$. Region A : limit cycle exists. Region B : no limit cycle.

We have shown that adding delay in the horizontal fast harmonic (FH) excitation case increases significantly the region in the (T,Ω) plane where undesirable self-excited vibration can be eliminated. In contrast to the case without delay that requires large values of Ω to eliminate self-excited vibration, the elimination here can be achieved for moderate values of Ω.

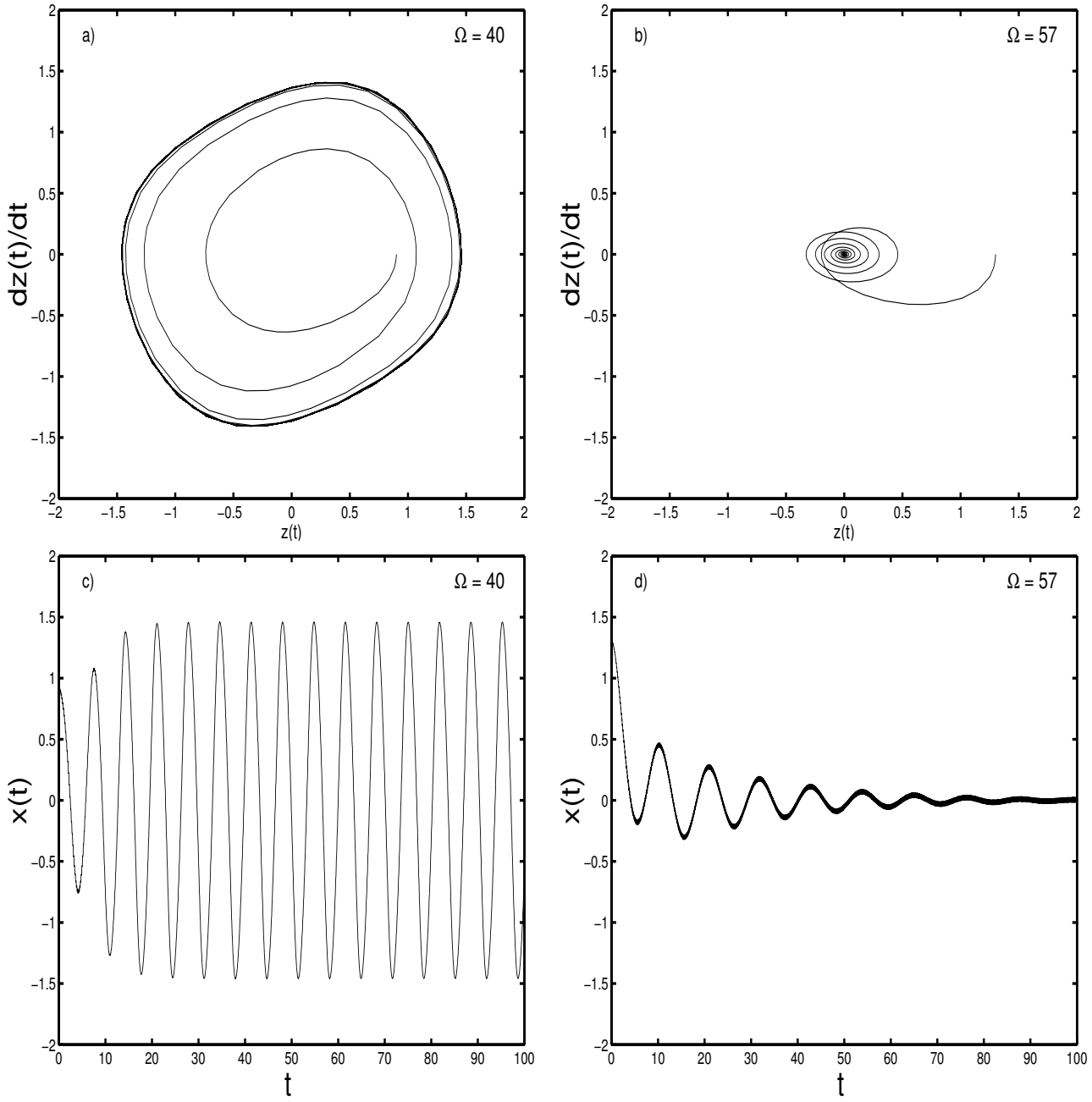

Figure 37: Phase portraits of slow dynamics of $z(t)$, Eq. (9), and time histories of the full motion $x(t)$, Eq. (2), with parameter values as for Fig. 1(a) and $T = 2.5$. Fig. 2(a-c) and Fig. 2(b-d) correspond to regions A and B in Fig. 1(a), respectively.

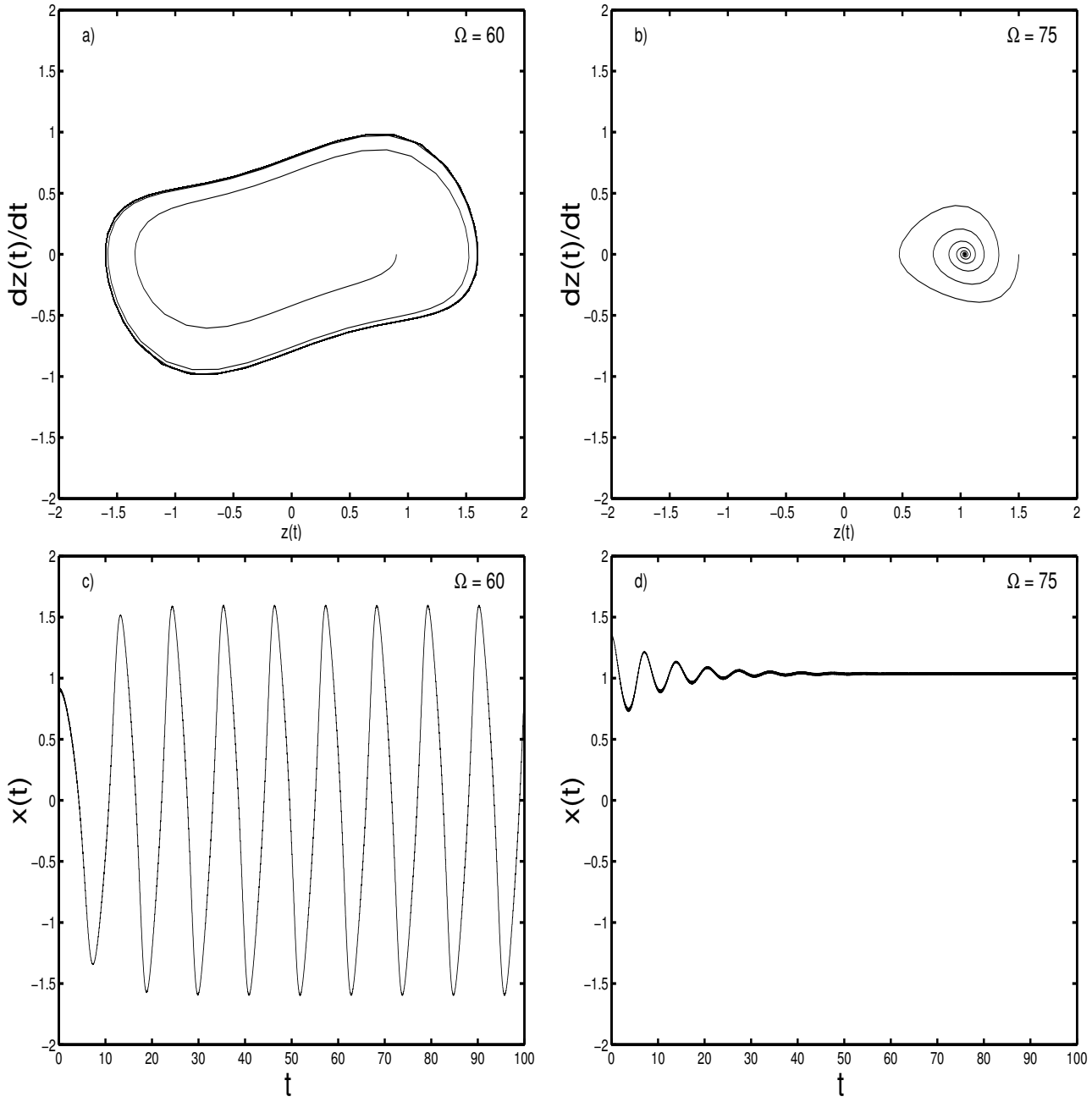

Figure 38: Phase portraits of slow dynamics of $z(t)$, Eq. (9), and time histories of the full motion $x(t)$, Eq. (2), with parameter values as for Fig. 1(a) and $T = 0.5$. Fig. 3(a-c), and Fig. 3(b-d) correspond to regions A and B in Fig. 1(a), respectively.

5.3 Effect of rapid forcing on frequency-locking in a nonlinear self-excited system

In this section we investigate the effect of high-frequency excitation on a van der Pol-Mathieu-Duffing oscillator. We focus attention on the frequency-locking area in the neighborhood of the 2:1 resonance.

5.3.1 Slow motion

Consider the following van der Pol-Mathieu-Duffing oscillator subjected to a horizontal FH excitation

$$\ddot{x} + (1 - h\cos\,\omega t)x - (\alpha - \beta x^2)\dot{x} - \gamma x^3 = a\Omega^2 \cos x \cos\,\Omega t \tag{136}$$

where damping α, β, nonlinearity γ and excitation amplitudes h and a are small. An overdot denotes differentiation with respect to time t. We assume that the frequency Ω is large comparing to ω such that resonance phenomena with the frequency Ω is avoided. This oscillator can model, for instance, optically driven MEMS resonators. It is known that these devices can self-oscillate in the absence of external forcing, when illiminated by a DC laser of sufficient amplitude. The parametric excitation in eq. (136) can be induced by modulating the incident laser.

To analyze the influence of high-frequency excitation on the slow dynamic of system (136), it is convenient to use as before the method of DPM. We find the approximate equation for slow motions

$$D_1^2 z + (1 - h\cos\,\omega T_1)z - (\alpha - \beta z^2)D_1 z - \gamma z^3 = \frac{1}{2}(a\Omega)^2 \cos z \sin z \tag{137}$$

This equation is similar to the original equation (136) in which the non-autonomous term $a\Omega^2 \cos x \cos \Omega t$ is replaced by the autonomous one $\frac{1}{2}(a\Omega)^2 \cos z \sin z$. We focus the analysis on small vibrations around the origin by expanding in Taylor's series the terms $\sin z \simeq z - z^3/6$ and $\cos z \simeq 1 - z^2/2$. Keeping only terms up to order three in z, Eq. (137) becomes

$$D_1^2 z + (1 - \frac{1}{2}(a\Omega)^2 - h\cos\omega T_1)z - (\alpha - \beta z^2)D_1 z - (\gamma - \frac{1}{3}(a\Omega)^2)z^3 = 0 \tag{138}$$

Note that in Eq. (138) the influence of frequency Ω is introduced in the natural frequency of the system and in the nonlinear stiffness coefficient.

5.3.2 Slow flow and entrainment

We rewrite Eq. (138) in the following form

$$\ddot{z} + \omega_0^2 z = (\alpha - \beta z^2)\dot{z} + \xi z^3 + hz\cos\omega t \tag{139}$$

where $\omega_0^2 = 1 - \frac{1}{2}(a\Omega)^2$, $\xi = \gamma - \frac{1}{3}(a\Omega)^2$. We express the main resonant condition by introducing a detuning parameter σ according to

$$\omega_0^2 = \frac{\omega^2}{4} + \sigma \tag{140}$$

We apply a double perturbation technique [13,14] by introducing two bookkeeping parameters μ and η, which will be set equal to unity in the final analysis. To implement the first perturbation we use the parameter μ and for the second step perturbation we introduce the other parameter η. Hence, Eq. (139) is rewritten as

$$\ddot{z} + \frac{\omega^2}{4} z = \mu\{-\sigma z + (\alpha - \beta z^2)\dot{z} + \xi z^3 + hz\cos\omega t\} \tag{141}$$

Using the multiple scales technique [7], we seek a solution to Eq. (141) in the form

$$z(t) = z_0(T_1, T_2) + \mu z_1(T_1, T_2) + O(\mu^2) \tag{142}$$

where $T_1 = t$ and $T_2 = \mu t$. In terms of the variables T_i, the time derivatives become $\frac{d}{dt} = D_1 + \mu D_2 + O(\mu^2)$ and $\frac{d^2}{dt^2} = D_1^2 + 2\mu D_1 D_2 + O(\mu^2)$ where $D_i^j = \frac{\partial^j}{\partial^j T_i}$. Substituting Eq. (142) into Eq. (141) and equating coefficients of like powers of μ, we obtain

- Order μ^0:

$$D_1^2 z_0 + \frac{\omega^2}{4} z_0 = 0 \tag{143}$$

- Order μ^1:

$$D_1^2 z_1 + \frac{\omega^2}{4} z_1 = -2D_1 D_2 z_0 - \sigma z_0 + (\alpha - \beta z_0^2) D_1 z_0 + \xi z_0^3 + h z_0 \cos\omega T_1 \tag{144}$$

The solution to the first order is given by

$$z_0(T_1, T_2) = r(T_2)\cos(\frac{\omega}{2} T_1 + \theta(T_2)) \tag{145}$$

Substituting Eq. (145) into Eq. (144) and removing secular terms, we obtain the slow flow modulation equations of amplitude and phase

$$\begin{aligned} \frac{dr}{dT_2} &= \frac{\alpha}{2} r - \frac{\beta}{8} r^3 - \frac{h}{2\omega} r \sin(2\theta) \\ \frac{d\theta}{dT_2} &= \frac{\sigma}{\omega} - \frac{3\xi}{4\omega} r^2 - \frac{h}{2\omega}\cos(2\theta) \end{aligned} \tag{146}$$

Note that the system (146) is invariant under the transformation $\theta \to -\theta + \frac{\pi}{2}$, $\sigma \to -\sigma$ and $\xi \to -\xi$. This allows us to replace in Eq. (146) σ by $s\sigma$ and ξ by $s\xi$ with $s = \pm 1$. Thus system (146) reads

$$\begin{aligned} \frac{dr}{dT_2} &= \frac{\alpha}{2} r - \frac{\beta}{8} r^3 - \frac{h}{2\omega} r \sin(2\theta) \\ \frac{d\theta}{dT_2} &= \frac{s\sigma}{\omega} - \frac{3s\xi}{4\omega} r^2 - \frac{h}{2\omega} \cos(2\theta) \end{aligned} \tag{147}$$

Equilibrium points of the slow flow (147), corresponding to periodic oscillations of Eq. (139), are determined by setting $\frac{dr}{dT_2} = \frac{d\theta}{dT_2} = 0$. Using the trigonometric identity $\cos^2\theta + \sin^2\theta = 1$ and we define $\rho = r^2$, we obtain the following quadratic equation on ρ

$$(\frac{\beta^2}{64} + \frac{9\xi^2}{16\omega^2})\rho^2 - (\frac{\alpha\beta}{8} + \frac{3\sigma\xi}{2\omega^2})\rho + \frac{\alpha^2}{4} + \frac{\sigma^2}{\omega^2} - \frac{h^2}{4\omega^2} = 0 \tag{148}$$

Eq. (148) has two real roots if the discriminant Δ is nonnegative. This gives the condition

$$\Delta = (\frac{\alpha\beta}{16} + \frac{3\sigma\xi}{4\omega^2})^2 - (\frac{\beta^2}{64} + \frac{9\xi^2}{16\omega^2})(\frac{\alpha^2}{4} + \frac{\sigma^2}{\omega^2} - \frac{h^2}{4\omega^2}) > 0 \tag{149}$$

These two solutions are positive if the two following conditions are held

$$C = \frac{\alpha^2}{4} + \frac{\sigma^2}{\omega^2} - \frac{h^2}{4\omega^2} > 0, \qquad B = \frac{\alpha\beta}{4} + \frac{3\sigma\xi}{\omega^2} > 0 \tag{150}$$

Furthermore, Eq. (148) has only one positive root if

$$C = \frac{\alpha^2}{4} + \frac{\sigma^2}{\omega^2} - \frac{h^2}{4\omega^2} < 0 \tag{151}$$

In what follows we fixe the parameters $\alpha = 0.01$, $\beta = 0.05$, $\gamma = 0.1$, $h = 0.1$, and $a = 0.02$.
In Fig. 1a the frequency response curve, as given by Eq.(148), is presented for $\Omega = 0$ exhibiting stable entrainment oscillations. The effect of the excitation frequency Ω on the frequency-locking area is illustrated in Fig. 1b,c,d for the values $\Omega = 25$, $\Omega = 40$ and $\Omega = 50$. It can be seen that as the frequency Ω increases, the entrainment area shifts left and the nonlinear characteristic stiffness changes causing the system to switch from softening to hardening behavior. Analytical approximations (solid line for stable oscillations and dashed line for unstable one) are compared to numerical integration (circles) using a Runge-Kutta method.
Fig. 2a illustrates the bifurcation curves of periodic solutions of the slow dynamic (139) for $\Omega = 0$. We can distinct three regions. In region I, where conditions (149) and (151) are satisfied, there are two possible solutions: an unstable trivial solution and a larger stable one. Within region II, where conditions (149) and (150) are satisfied, there are three possible solutions: one

unstable, a larger stable one and the trivial unstable solution. Within the regions III only an unstable trivial solution exists. In this region a limit cycle exists and it is stable. Fig. 2b is plotted for $\Omega = 40$ showing the effect of Ω on the bifurcation curves. It can be seen that, as Ω increases, the region I switches from the right branche of the curve $\Delta = 0$ to the left one causing an exchange between regions II and III inside the curve $\Delta = 0$. This behavior is consistent with the spring characteristic change of the backbone curve in Fig. 1.

5.3.3 Slow slow flow and limit cycle

In this section we construct analytical approximations of the limit cycle of the slow flow (147) corresponding to quasi-periodic motion of the slow dynamics (139).
We transform the polar form (147) using the variable change

$$u = r\cos\theta, \quad v = -r\sin\theta \tag{152}$$

to the Cartesian system

$$\begin{aligned} \frac{du}{dT_2} &= (\frac{s\sigma}{\omega} + \frac{h}{2\omega})v + \eta\{\frac{\alpha}{2}u - (\frac{\beta}{8}u + \frac{3s\xi}{4\omega}v)(u^2+v^2)\} \\ \frac{dv}{dT_2} &= -(\frac{s\sigma}{\omega} - \frac{h}{2\omega})u + \eta\{\frac{\alpha}{2}v - (\frac{\beta}{8}v - \frac{3s\xi}{4\omega}u)(u^2+v^2)\} \end{aligned} \tag{153}$$

To implement the second perturbation step, η is introduced in damping and nonlinearity. Following [13,14], we approximate periodic solution of the slow flow (153) by using a multiple scales perturbation expansion. We expand

$$\begin{aligned} u(T_2,T_3) &= u_0(T_2,T_3) + \eta u_1(T_2,T_3) + O(\eta^2) \\ v(T_2,T_3) &= v_0(T_2,T_3) + \eta v_1(T_2,T_3) + O(\eta^2) \end{aligned} \tag{154}$$

where $T_2 = \mu t$ and $T_3 = \eta T_2 = \eta\mu t$. Introducing $D_i = \frac{\partial}{\partial T_i}$ yields $\frac{d}{dT_2} = D_2 + \eta D_3 + O(\eta^2)$.
Substituting Eqs. (154) into Eqs. (153) and collecting terms, we get
- Order η^0:

$$\begin{aligned} D_2^2 u_0 + \nu^2 u_0 &= 0, \\ (\frac{s\sigma}{\omega} + \frac{h}{2\omega})v_0 &= D_2 u_0 \end{aligned} \tag{155}$$

- Order η^1:

$$\begin{aligned} D_2^2 u_1 + \nu^2 u_1 &= (\frac{s\sigma}{\omega} + \frac{h}{2\omega})[-D_3 v_0 + \frac{\alpha}{2}v_0 - (\frac{\beta}{8}v_0 - \frac{3s\xi}{4\omega}u_0)(u_0^2+v_0^2)] \\ &- D_2 D_3 u_0 + \frac{\alpha}{2}D_2 u_0 - D_2[(\frac{\beta}{8}u_0 + \frac{3s\xi}{4\omega}v_0)(u_0^2+v_0^2)] \\ (\frac{s\sigma}{\omega} + \frac{h}{2\omega})v_1 &= D_2 u_1 + D_3 u_0 - \frac{\alpha}{2}u_0 + (\frac{\beta}{8}u_0 + \frac{3s\xi}{4\omega}v_0)(u_0^2+v_0^2) \end{aligned} \tag{156}$$

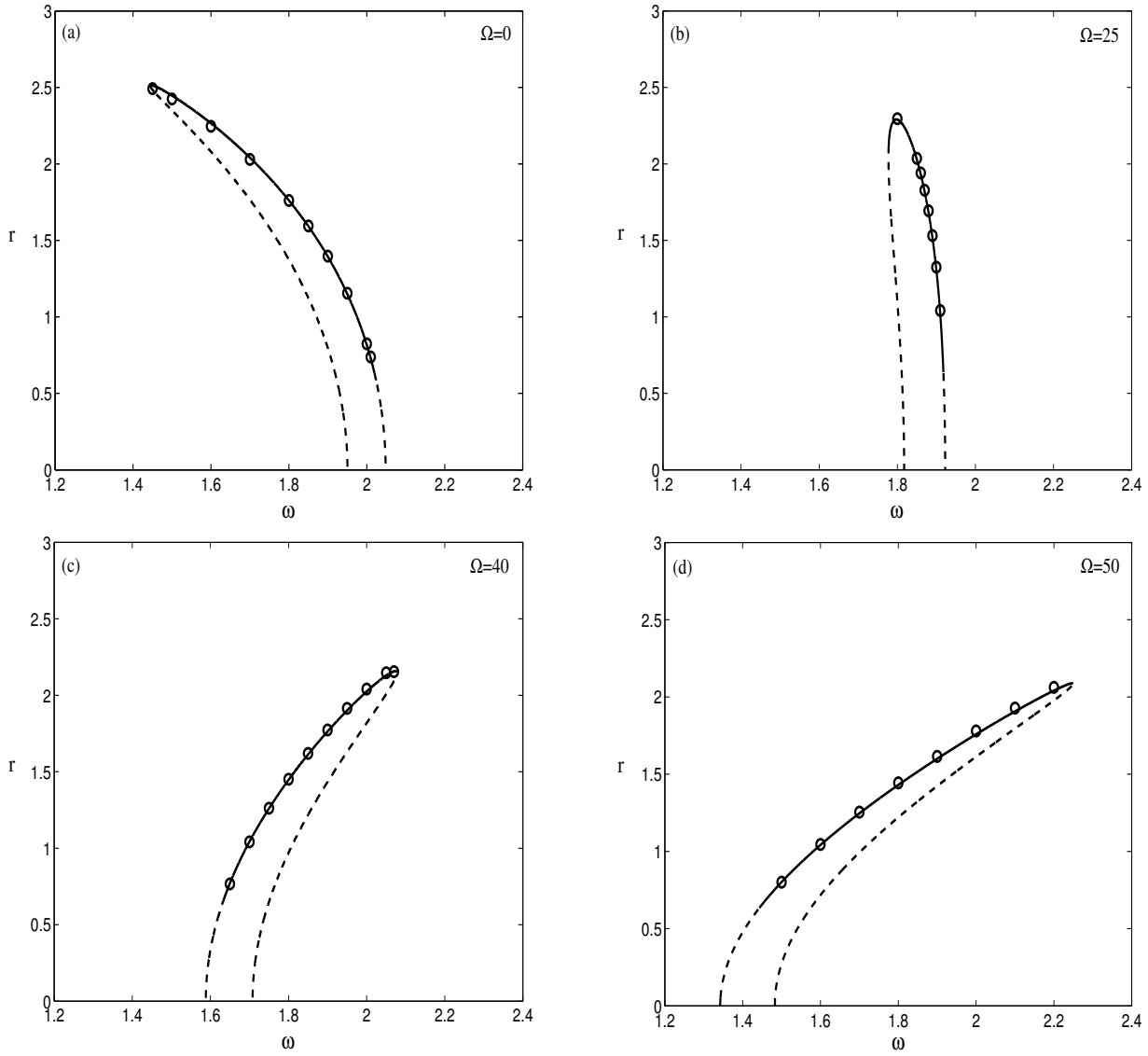

Figure 39: Amplitude frequency response near 2:1 resonance. Analytical approximation: Solid (for stable) and dashed for (instable). Numerical simulation: circles.

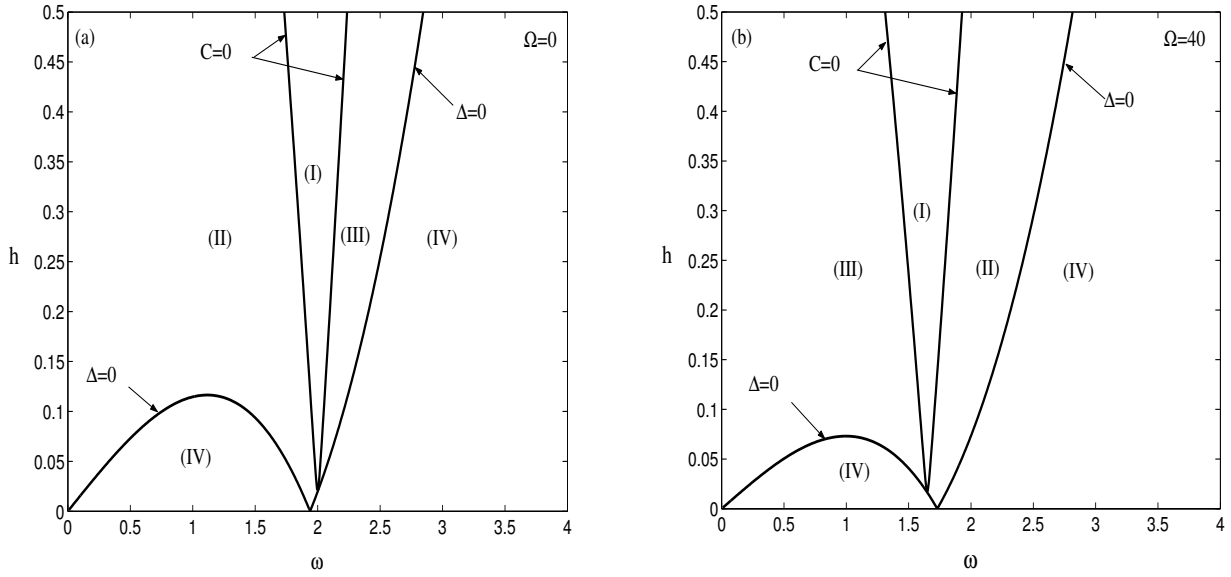

Figure 40: Bifurcation curves of periodic solutions of the slow dynamic (139) near 2:1 resonance.

where $\nu = \sqrt{(\frac{\sigma}{\omega})^2 - (\frac{h}{2\omega})^2}$ is the proper frequency of system (153) corresponding to the frequency of slow flow limit cycle.

The solution to the first order system (155) is given by

$$\begin{aligned} u_0(T_2, T_3) &= R(T_3)\cos(\nu T_2 + \varphi(T_3)) \\ v_0(T_2, T_3) &= -\frac{\nu}{(\frac{s\sigma}{\omega} + \frac{h}{2\omega})} R(T_3)\sin(\nu T_2 + \varphi(T_3)) \end{aligned} \tag{157}$$

Here $R(T_3)$ and $\varphi(T_3)$ are functions of $T_3 = \eta T_2$. Since $T_2 = \mu t$ is slow time, and since we have assumed η to be small, we shall refer to T_3 as "*slow slow* time" or "s.s. time" for brevity [15]. Substituting (157) into (156) and removing secular terms gives the following autonomous s.s. flow system on R and φ

$$\begin{aligned} \frac{dR}{dT_3} &= \frac{\alpha}{2}R - \frac{s\beta\sigma}{8s\sigma + 4h}R^3 \\ \frac{d\varphi}{dT_3} &= -\frac{3s\xi(8\sigma^2 + h^2)}{8\omega(2s\sigma + h)\sqrt{4\sigma^2 - h^2}}R^2 \end{aligned} \tag{158}$$

Equilibria in Eqs. (158) are obtained by setting $\frac{dR}{dT_3} = 0$ and given by

$$R = 0, \quad R = \sqrt{\frac{2\alpha(2s\sigma + h)}{s\beta\sigma}} \tag{159}$$

The non-trivial equilibrium in Eq. (159) will correspond to the amplitude of the limit cycle of the slow flow (153) and to quasi-periodic oscillations in the slow dynamic (139). In Figs. 42

a,b we draw for the two different values $\Omega = 0$ and $\Omega = 40$ the analytical amplitude of the slow flow limit cycle, Eq.(159), and the entrainment area as given by Eq. (148). The curves labelled L^+ correspond to $s = +1$ in Eq.(159) and the curves labelled L^- correspond to $s = -1$. The shift of the entrainment area can be clearly seen. The numerical modulation amplitude vibrations (quasi-periodic oscillations) are marked with double circles connected with a vertical line. Comparison of analytical results and numerical integration of the modulation amplitude motion shows a good agreement.

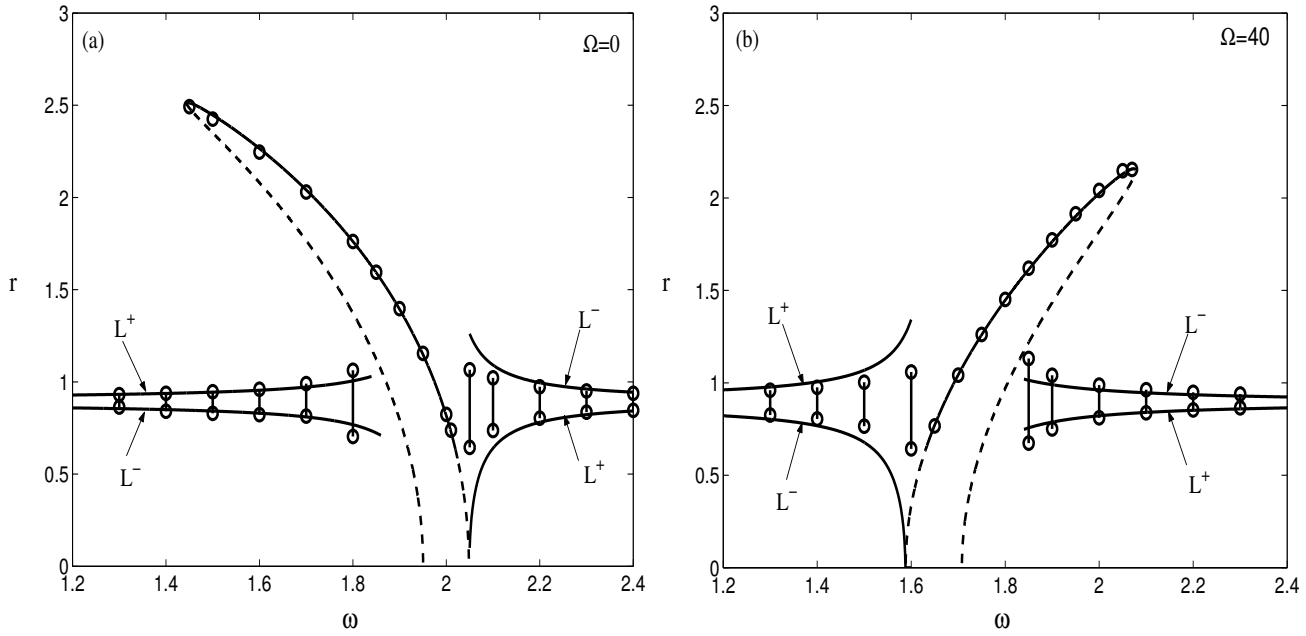

Figure 41: Effect of the frequency Ω on the entrainment area and on the modulation amplitude vibration.

The approximate periodic solution is given by

$$\begin{aligned} u(T_2) &= R\cos(\nu T_2 + \varphi) \\ v(T_2) &= -\frac{2\nu\omega}{(2s\sigma + h)} R\sin(\nu T_2 + \varphi) \end{aligned} \tag{160}$$

where

$$\varphi = -\frac{3s\xi(8\sigma^2 + h^2)}{8\omega(2s\sigma + h)\sqrt{4\sigma^2 - h^2}} R^2 T_3 \tag{161}$$

and the quasi-periodic oscillation of the slow dynamic system (139) is written as

$$z(t) = u(T_2)\cos(\frac{\omega}{2}t) + v(T_2)\sin(\frac{\omega}{2}t) \tag{162}$$

Finally, the *quasi* quasi-periodic response of the original system (136) is given by Eqs. (160), (161) and (162). To validate the analytical finding, we show in Fig. 42 the comparison between

the approximate periodic solution (160) and the numerical integration of the slow flow (153) using Runge-Kutta method. Fig. 42 (a),(c) are plotted for $s = +1$ and Fig. 42 (b), (d) are plotted for $s = -1$.

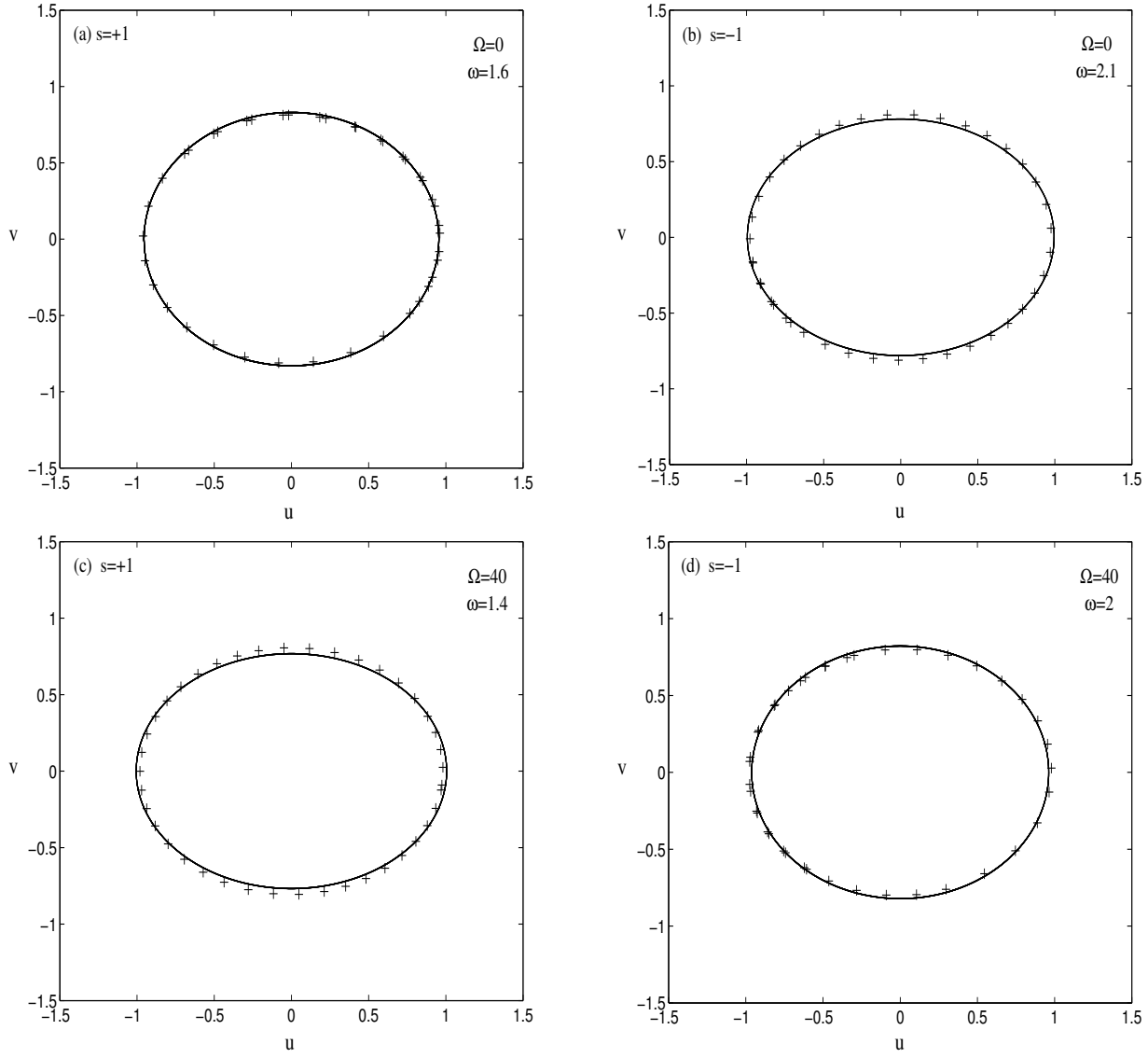

Figure 42: Comparison between analytical approximation (solid line) of periodic solution, Eq. (160), and numerical integration (crossed line) of the slow flow (153).

In Fig. 43 we present examples of time histories of the slow dynamic $z(t)$ obtained by numerical simulation. Results show that FH excitation can change the nonlinear characteristic spring behavior of the system from softening to hardening or vice versa and cause the entrainment area to shift. In contrast, no significant effect on the amplitudes of both entrained and quasi-periodic

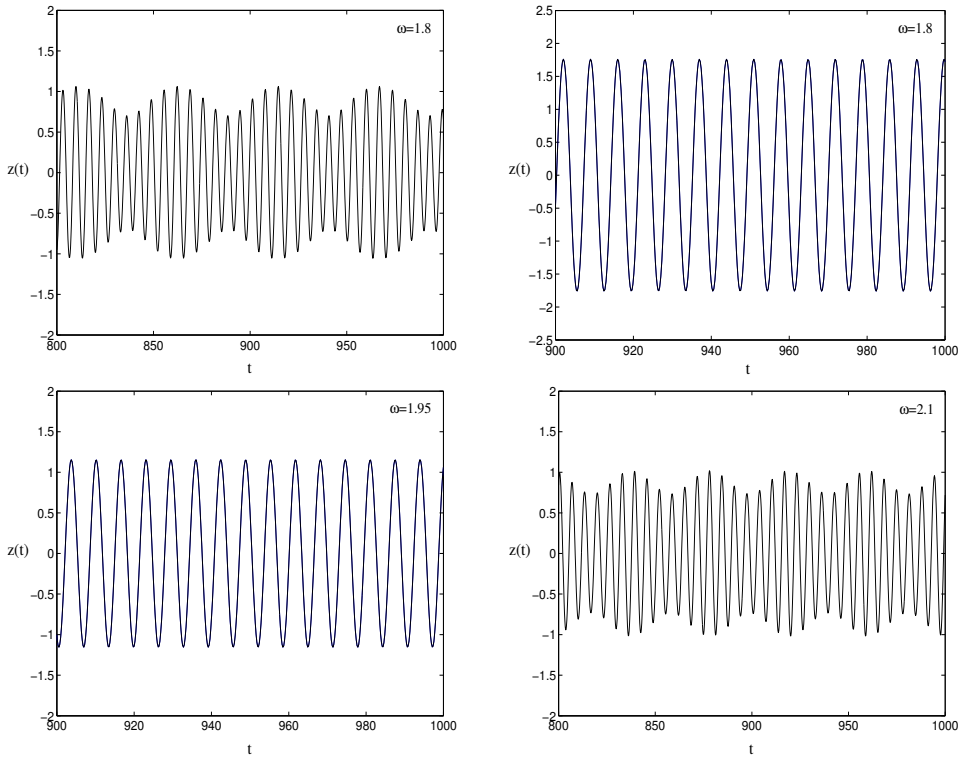

Figure 43: Examples of time histories of the slow dynamic $z(t)$ by numerical integration for $\Omega = 0$.

responses is noticed. The control and adjustment of the entrainment area to a desired frequency range in the vicinity of the considered resonance may be achieved by acting only on the frequency Ω. This result is of interest from engineering applications point of view.

6 Homoclinic functions and homoclinic bifurcation

Our efforts have aimed at

1. the inhibition of homoclinic chaos in an asymmetric oscillator driven by an external excitation,

2. homoclinic bifurcations in planar polynomial systems perturbed by an arbitrary analytic autonomous functions,

3. approximation of homoclinic or heteroclinic bifurcations in three-dimensional ordinary differential equations.

The first two parts constitute the core of the Ph.D. dissertation by [A. Azouani, "Suppression of chaos in an asymmetrical mechanical system and computation of Melnikov functions of second order autonomous equations" Ph.D. University Hassan II-Ain Chock (November 2004)].
The first part of this work deals with the suppression of chaos in a driven nonlinear system corresponding to an asymmetric two-well potential energy with two kinds of nonlinearities: quadratic and cubic

$$\ddot{x} + \delta\dot{x} + \alpha x + \beta x^2 + \gamma x^3 = P\cos(\omega t) \tag{163}$$

The cases of symmetric two-well potential and single well potential were studied separately in the last two decades. Melnikov analysis is used to detect parameter regions with homoclinic chaos. It was shown that different nonlinear resonant parametric perturbations lead to suppression of chaotic motions. Numerical support was performed to confirm the analytical prediction using Lyapunov exponents. The resonances that may suppress chaos in the system were depicted. For instance, it was shown that the fundamental resonance 1:1 and the subharmonic resonance 1:2 do not suppress chaos in the nonlinear cubic case.

ln the second part of this work, we have considered the homoclinic bifurcations in planar polynomial systems perturbed by arbitrary analytic autonomous functions. The purpose here is to give an explicit computation of the Melnikov function which plays a fundamental role in the theory of homoclinic bifurcation. This Melnikov method gives us an excellent tool for studying global bifurcations that occur at homoclinic (heteroclinic) loops or in one-parameter families of perturbed dynamical systems.
ln the classical case where the degree of the potential energy is less than three, the Melnikov function is related to the elementary functions which are connected with circular functions. ln

the case of degree four or five, the Melnikov function is related to elliptic functions. If we consider for example the polynomial function of order 5, local analysis tells us that the movable singularities are square root branch points and the corresponding quadrature becomes the hyperelliptic integral. Explicit integration becomes much more complicated, the complex time extension is necessary and many deep results from algebraic geometry come into play.

Concerning the approximation of homoclinic or heteroclinic bifurcations in three-dimensional ordinary differential equations, we have investigated the system

$$\begin{aligned} \dot{x} &= y \\ \dot{y} &= z \\ \dot{z} &= -z - \mu_1 y + \mu_2 x - x^2 \end{aligned} \tag{164}$$

We have shown that using the collision [17] criterion between the hyperbolic fixed point and the limit cycle involved in the bifurcation, we can determine an analytical expression for the homoclinic connection. The strategy is mainly based on the construction of analytical approximations of the periodic solution. Then the collision criterion is applied and analytical approximations for homoclinicity are given. The result is summarized in [16].

7 Development relevance

One of the main purpose of the current DFG/BMZ program, devoted to research institutions in developing countries, is focused on *strengthening the research capacity and the scientific efficiency of participating scientists in the countries in question in order to solve developmental problems in these countries.* The current program has largely contributed to this goal.

For the first time, experimental research on vibration problems in mechanics has been established in the Prof. Belhaq laboratory in Casablanca through this bilateral cooperation project. To our knowledge, this important realization constitutes the first achievement of experimental research in vibration mechanics in any Moroccan university. As an ultimate objective, this realization will contribute to generate links with the socio-economic environment in Morocco and will initiate specific joint research projects with industrial partners. Such cooperation has been deeply missing in Moroccan universities so far. The establishment of the experimental set-up (see in the CD-ROM : "key_elements/vue_exp.JPG") in Casablanca will focus Prof. Belhaq's research activity

essentially towards experimental work. Future graduate students in the group will be guided to experimental projects when preparing their Ph.D. thesis.

As a direct result of our experimental environment, the head of the Casablanca Polytechnic Institute, a branch of the Canadian based Laval University, has expressed his great interest to collaborate in the experiment and proposed to involve the department of mechanical engineering of his institute into the project. As a first step, he offered laboratory space and provided some equipment and facilities for our graduate students in his institute.

Also, two assistant professors from his institute will be involved in the experiment works, namely:
1- Dr. Faouzi Lakrad, former Ph.D. student of Prof. Belhaq (2001), PostDoc of Prof. Fiedler in Berlin (2001-2003) and Humboldt research fellow with Prof Schiehlen in Stuttgart (2003-2004) and now Director of Research in the Casablanca Polytechnic Institute.
2- Dr. Mustafa Charafi, graduate of the Department of physics in Casablanca and now Director of Alumni Affairs in the Casablanca Polytechnic Institute.

Since 2006, the laboratory in this institute became operational. Many students from the institute and from the university prepared their project in working on practical vibrational problems. A student can conceive and realize the plan under the supervision of Dr. Lakrad, responsible of the laboratory, member of the current program. Each year the institute organizes a scientific meeting. Industrials from different area are invited to visit the lab and to see some demonstrations on vibrational problems from our experiments. Very positive reactions were provided by the industrial leaders and some possible connections in terms of academic education and research will be concretized.

Another interesting link has been initiated recently. Indeed, encouraged by the emerging experimental environment in Casablanca, an important Moroccan company (Laraki Automobiles Company) involved in the construction of Moroccan cars (Laraki Fulgura and Laraki Borac) has contacted the Casablanca group to discuss the possibility of collaboration on vibrations and noise testing in industrial vehicles. By the lack of vibration laboratories in Morocco, the company is now planning to collaborate with Prof. Belhaq's research group in terms of research, tests, control and measurement.
As a first step, the Laraki automobiles company plans to organize in Casablanca in collaboration with Prof. Belhaq's research group a Symposium on vibrations and noise in vehicles. This Symposium will be an opportunity for industrials and researchers to meet and discuss possible collaborations. To reinforce our bilateral collaboration with our German colleagues, two German

experts in vibrations will be invited by Prof. Belhaq to attend the Symposium.

Recently very interesting possibilities in terms of industrial cooperation and experimental research are opening. This project indeed helps to accelerate the establishment of a far-reaching research-development process in Morocco in very specific terms. Keeping this cooperation going on will significantly strengthen the research capacity and the scientific efficiency of the participating Moroccan scientists and will help solving developmental problems in Morocco – which is the principal purpose of this program.

Regarding academic collaboration, the group is successfully developing international connection. Indeed, a new international cooperation is established between Prof. Belhaq, Prof. B. Blyukher, Indiana State University (USA) and Dr. T. Niezgoda, Military University of Technology, Warsaw, Poland. Prof. Blyukher visited the Prof. Belhaq lab in March 2005 and set up cooperation between the three partners. The experimental laboratory available in Casablanca will be used to perform experimental analysis of the dynamics of elastic shell structures to be considered in the project on Oil and Gas pipeline security in the framework of the NATO-Mediterranean Dialogue project.

During the congress of Mechanics held in Casablanca in April 2007, some colleagues have been interested in the Belhaq experimental laboratory. Many of them have visited the lab and possibilities for performing some experimental work in Casablanca have been discussed.

Recently, a graduate student from the casablanca group, M. Sah, has been granted the Fulbright award for a co-supervisor doctorate. He is now for one year in Cornell University, at the Department of Theoretical and Applied Mechanics, working under the co-supervising of Prof. R. Rand.

During the period of this programm, the Belhaq group has been very active and productive in terms of scientific publications and in terms of participation in international conferences. See the list of publications in section 1.8.

During the period of the programme, three Moroccan students have defended their Ph.D. Two of them under the direction by Prof. Belhaq (Dr. K. Guennoun and Dr. N. Abouhazim) and Dr. A. Azouani under the co-direction of Prof. Belhaq and Prof. Fiedler. Dr. Azouani has ben-

efited from the DAAD Sandwich Programme established between Prof. Belhaq and Prof. Fiedler.

Other Moroccan students (M. Hamdi, S.M. Sah and R. Bourkha) are now finishing their Ph.D. dissertation in Casablanca. One of them, S.M. Sah, is starting his co-supervisor doctorate at Cornell university under a Fulbright grant. Also, an Assistant Professor, A. Fahsi, working in the Casablanca group will defend his Habilitation diploma this academic year. See the dissertation list in section 1.8.2.

8 Summary

The project addressed the chaotic and nonchaotic dynamics of a vibrating elastic blade in the presence of single-well and double-well magnetic fields. The experimental set-up involved a frequency controlled shaker for the mounted blade, adjustable magnets, electronic tracking of accelerometer data, and video documentation of the resulting dynamics. Theoretical methods included direct numerical simulation of the properly damped beam equation with cubic nonlinearities, as well as in-depth analysis based on multiple scales expansions, mode interactions and homoclinic bifurcation theory. One visually striking phenomenon was the observed energy transfer from high-frequency low-amplitude vibrational modes to high amplitude low-frequency modes, which could even lead to the destruction of the unbreakable blades.

Going beyond the original scope of the project, preliminary results on the combined effects of rapid forcing and time-delayed control on the resulting global diagrams have also been obtained. Specifically this led to a strategy for the suppression of hysteresis between 1:2 frequency locking and quasiperiodic modes. Such hysteresis is often undesirable in mechanics, in general, and in applications to microelectromechanical systems (MEMS) and to material cutting processes, specially. In the framework of this project the first experimental research in Morocco on vibration problems in mechanics has been established in the lab of Prof. Belhaq, Casablanca. The project has drawn substantial interest, both from academic and industriel partners. Theoretical results have been presented in 24 publications.

A total of six PhD students have been partially supported by the project, as well as one Habilitation candidate. Dr. Lakrad, a previous graduate from Belhaq group who was significantly involved in the project, has been hired as Full Professor at the Univesity Hassan II, Casablanca, in January 2008.

References

[1] S.S. Antman, *Nonlinear Problems of Elasticity*. Spring Verlag, New York, 1995.

[2] A. Azouani, M. Belhaq: *Effects of different nonlinear Parametric Resonant Perturbations on suppression of chaos*, Progress in Analysis, Proceedings of the 3rd International ISAAC Congress, World Scientific, Vol. 1, p. 519-524 (2003)

[3] J. L. Humar, "*Dynamics of structures*", Prentice Hall International Series in Civil Engineering and Engineering Mechanics, Prentice Hall, Englewood Cliffs. New Jersey 07632. pp. 728-761, 1990.

[4] G. Chen and D.L. Russell, "*A mathematical model for linear elastic systems with structural damping*", Quart. Appl. Math., **39**, 433-454, 1982.

[5] M.A. Zarubinskaya and W.T. Van Horssen, *On an improved elastic dissipation model for a cantilevered beam*, Quart. Appl. Math., **63**, 681-690, 2005.

[6] D. Tcherniak, The influence of fast excitation on a continuous system, *Journal of Sound and Vibration* 227 (1999) 343-360.

[7] A. H. Nayfeh and D. T. Mook, Perturbation Methods, Wiley, New York (1979)

[8] I. I. Blekhman, *Vibrational Mechanics-Nonlinear Dynamic Effects, General Approach, Application*, World Scientific, Singapore, 2000.

[9] L. F. Shampine, S. Thompson, Solving delay differential equations with dde23, 2000, PDF available on-line at http://www.radford.edu/~thompson/webddes/tutorial.pdf.

[10] Rand RH, Lecture Notes on Nonlinear Vibrations (version52). Available from: http://www.tam.cornell.edu/randdocs/nlvibe52.pdf (2005).

[11] Nayfeh AH, Mook DT. Nonlinear Oscillations. Wiley, New York; 1979.

[12] Wirkus S, Rand RH. Dynamics of two coupled van der Pol oscillators with delay coupling. Nonlinear Dynamics 2002;30:205-21.

[13] Belhaq M, Houssni M. Quasi-periodic oscillations, chaos and suppression of chaos in a nonlinear oscillator driven by parametric and external excitations. Nonlinear Dynamics 1999;18:1-24.

[14] Rand RH, Guennoun K, Belhaq M. 2:2:1 Resonance in the quasi-periodic Mathieu equation. Nonlinear Dynamics 2003;31:187-93.

[15] Abouhazim N, Rand RH, Belhaq M. The damped nonlinear quasi-periodic Mathieu equation near 2:2:1 resonance. Nonlinear Dynamics 2006;45:237-47.

[16] M. Belhaq and F. Lakrad, Analytics of homoclinic bifurcations in three-dimensional systems, Int J Bifurcation Chaos, vol. 12 (11), p. 2479-2486, 2002.

[17] M. Belhaq, B. Fiedler and F. Lakrad, Homoclinic connections in strongly self-excited nonlinear oscillators: The Melnikov function and the elliptic Lindstedt-Poincare method, Nonlinear Dynamics , vol. 23, p. 67-86, 2000.